Journal of Photochemistry and Photobiology C: Photochemistry Reviews 47 (2021) 100402

Contents lists available at ScienceDirect

Journal of Photochemistry and Photobiology C: Photochemistry Reviews

journal homepage: www.elsevier.com/locate/jphotochemrev

Review

Recent advances in wireless photofixation of dinitrogen to ammonia under the ambient condition: A review

Sriram Mansingh, Kundan Kumar Das, Sabiha Sultana, Kulamani Parida*

Centre for Nano Science and Nano Technology Institute of Technical Education & Research Siksha 'O' Anusandhan (Deemed to Be University), Bhubaneswar, 751030, India

ARTICLE INFO

Article history:
Received 22 October 2020
Received in revised form 27 January 2021
Accepted 1 February 2021
Available online 12 February 2021

Keywords:
Photocatalytic dinitrogen fixation
Detection technique
Associative/dissociative mechanism
Computational study

ABSTRACT

Ammonia is the most necessitate and second largely produces chemical reagent worldwide to address the need of the fertilizer industry, as a precursor for many value-added chemicals and a competing source (17.6 wt% H_2) for the blooming hydrogen economy. Although N_2 constitutes 78.09 % of the earth's atmosphere, however, its conversion to ammonia is strenuous because of its non-polar and triple bond character. To address the burgeoning demand, ammonia is typically synthesized via the conventional energy and capital intensive Haber-Bosch technique utilizing natural gas and releasing tons of (CO_2) to the environment. On this basis, cost-effective photon-driven dinitrogen reduction reaction (NRR) is aroused thriving attention as a sustainable and eco-friendly process for ammonia production under ambient conditions. Yet, the photocatalytic ammonia production is not up to the mark for industrial application due to low conversion rate, less catalytic selectivity, ambiguous mechanism, and limited faradic or solar-to-chemical efficiency. Further, the NRR activity of a catalyst essentially depends upon its electronic and surface texture; hence the fabrication of advanced materials is of paramount interest to enhance the performance. The present review covers the underlying mechanism of N_2 photoreduction, prevailing theories, different catalytic engineering techniques, various detection methods, and critical challenges encountered in the theme of photofixation of dinitrogen to ammonia. Additionally, the overarching goal of this review is to bestow an outline of recent research articles in earmarking high-caliber photocatalytic systems and hence planting a strong foundation to ensure the succeeding improvement in this promising and hastily stretching field of dinitrogen photofixation research.

Contents

* Corresponding author.
E-mail addresses: kulamaniparida@soa.ac.in, paridakulamani@yahoo.com (K. Parida).

https://doi.org/10.1016/j.jphotochemrev.2021.100402
1389-5567/

Dr. Sriram Mansingh received his B.Sc (2nd Rank), M.Sc, and M.Phil (1st Rank) from Utkal University, India. Then, he completed his Ph.D. degree from the Siksha 'O' Anusandhan (Deemed to be University) Bhubaneswar, India under the guidance of Prof. Kulamani Parida. His current research mainly focuses on the development of nanostructured materials such as metal oxides, metal sulfides, phosphides, and their application towards water splitting, N_2 fixation, and organic/inorganic pollutant detoxification. He has published 24 research articles in various international journals and one patent.

Mr. Kundan Kumar Das obtained his M.Sc and M.Tech in Environmental Science from Fakir Mohan University, Balesore, and Siksha 'O' Anusandhan (Deemed to be University) Bhubaneswar respectively. Then he joined as a Ph.D. scholar under the supervision of Prof. Kulamani Parida at the Centre for Nano Science and Nano Technology, S'O'A Deemed to be University in the 2017 and continuing. His present research includes the design and development of conducting polymer sensitized ferrite based material for energy generation, environmental pollutant degradation, and antibacterial studies. He has published 9 research articles in various high impact international journals and one patent.

Dr. Sabiha Sultana received her Bachelor's degree (1st Rank) from Utkal University, Bhubaneswar in the year 2012, and M.Sc. Chemistry from Ravenshaw University, Cuttack in the year 2014. Then, she joined as a Ph.D. student under the supervision of Prof. Kulamani Parida at the Centre for Nano Science and Nano Technology, S'O'A Deemed to be University and recently completed her Ph.D. degree. Her research area focuses on the development of nanostructured materials such as metal oxides, metal sulfides, phosphides, and their application towards water splitting, N_2, CO_2 reduction, and pollutant abatement. She has published 14 research articles in various international journals.

Prof. Kulamani Parida is a globally distinguished scientist in the area of Materials Science, Catalysis, and Nanotechnology. He was superannuated as a Chief Scientist and a Professor of Academy of Scientific and Innovative Research (AcSIR) from CSIR-IMMT, Bhubaneswar in 2014. His adoration for Chemistry and passion for research couldn't let Prof. Parida sit idle after retirement. With the same devotion and dedication, Prof. Parida (Director) started the 'Centre for Nano Science and Nano Technology' a research unit of Siksha 'O' Anusandhan (Deemed to be University), Bhubaneswar. His research interests include the design and development of advanced materials encompassing a wide variety such as metal oxides/phosphates/sulfates, cationic and anionic clays, perovskites, MOF, carbon-based materials including graphene, g-C_3N_4, and naturally occurring materials such as manganese nodules, manganese nodule leached residues, and manganese oxides of natural origin for the fine chemical, energy, and environmental applications. He has published more than 500 research articles and 10 review articles in renowned international journals. He bags a citation of 20156 to his credit with an h-index of 74 and an i10-index of 326. He has 27 national and international patents to his credit and is the author of four book chapters. For more details: https://kmparidaimmt.weebly.com/

1. Introduction

Undoubtedly, nitrogen (N) is an indispensable element in the periodic table which in the form of N_2 constitutes 78 % of the blue planet atmosphere and more importantly lay the foundation for the development of different bio-macromolecules (proteins and nucleic acids) and nitrogenated compounds from industries bridging agriculture and food cycle [1–4]. But is of no direct use due to its energetically non-polar strong N≡N triple bond which is arduous to break and hydrogenate to produces some essential organic and inorganic compounds [5–8]. Therefore, the entire community of living organisms including plant, animal, and microbial realms relies on the substantial form of N_2 molecules like ammonia and nitrate for fulfilling their requirements [2,7–9]. Henceforth, the conversion of nitrogen to its complete hydrogenated form i.e. ammonia and other nitrate-based products, has gained much more importance and attention from the scientific forum. In addition to its agricultural application towards the preparation of nitrogenous fertilizer to satisfy the food requirement of the booming population, ammonia is considered as one of the most important assets in the aspect of the economy and carbon-free fuel like H_2 (18 % H_2 and easily liquefied at 10 atm and ambient temperature), that drives the world to a new age of prosperity and sustainability [10–13]. Because of its high energy potential (15.3 MJ/L), easy handling, transportation, and storage facility, ammonia can be regarded as a promising renewable replacement of non-renewable fuels to meet the energy demand of the future civilized society [14,15]. Natural nitrogen fixation was brought about by biological (nitrogenase enzyme) and geochemical process (lightning flash) but the conversion ratio is very less and so unable to satisfy the requirements of the human community to uplift the crop production [2,16,17]. In short, Scheme 1 displays the nitrogen cycle and various processes by which dinitrogen fixation is brought about. However, the discovery of the energy-intensive human-led Haber-Bosch (HB) process for ammonia synthesis in the 19th century brings out a revolution in the agricultural sector by multiplying the crop yield many times along with the world economy [11,12,13,17,18]. Further, the development of the HB process makes the commercialization of ammonia possible which contributes about 150 ton of NH_3 per year out of which 80 % is in agricultural production and even have the potential to meet the demand of the booming population [11,15,19]. To date, industrial-scale production or the global market of ammonia is mainly steered by the traditionally Haber-Bosch process. And ammonia synthesis is a reversible and exothermic process, hence, the process will be more favorable under the low-temperature condition as per Le Chatelier's principle but surprisingly in a practical manner, the rate of production is extremely slow that challenge industrial requirement [11,20,21]. However, in the HB process ultra-pure streams of nitrogen and hydrogen are allowed to react with each other at high temperature (400−500 °C) and pressure (100−200 atm) over iron (i.e., Fe_3O_4 (94.3 %), K_2O (0.8 %), Al_2O_3 (2.3 %), CaO (1.7 %)) or ruthenium-based catalysts that generate nearly 97 % by recycling the preparation method multiple times [11,13,22]. But more importantly, the amount of hydrogen utilized to produce one ton of ammonia in the HB process is largely obtained from the steamed reforming of natural gas from fossils, which releases about 1.87 ton of heat trappers (CO_2) into the earth's atmosphere which triggers greenhouse effect leading to serious environmental catastrophes. Apart from air pollution, the HB process also accounts for 1–2 % of global annual energy consumption. Statistically, 3–5% of the world's natural gas and 1–3% of global electrical energy are utilized to run the Haber– Bosch process [11,13,21,23]. Even knowing that the process largely relies on fossil fuel (non-renewable) and its adverse effect on the environment and living community, still this HB pathway is the dominant or widely used method towards ammonia preparation. Therefore, it is very much essential and emboldens to develop a green, sustainable, and cost-effective stratagem for ammonia production to meet the growing demand, which is quite a challenging task for the scientific community. In this direction, various tactics were contrived that include electrocatalysis, bio-catalysis, photocatalysis, and photo (electro) catalysis but are confined to laboratory scale production only and are not able to match the global need [11,20–22]. Further, it is commonly known that around 3.5×10^4–5×10^4 J of energy is utilized for 1 g of ammonia formation via the industrial process and at the cost of environmental safety. Similarly, if we can achieve a Faradic efficiency over 50 % via electrocatalytic and solar to the chemical conversion efficiency of 10 % through photocatalytic, then the energy consumption for a gram of NH_3 formation using water will be 1.9×10^5 J and 2×10^5 J respectively without hampering the ecosystem [24]. Yet these methods run far behind in ammonia pro-

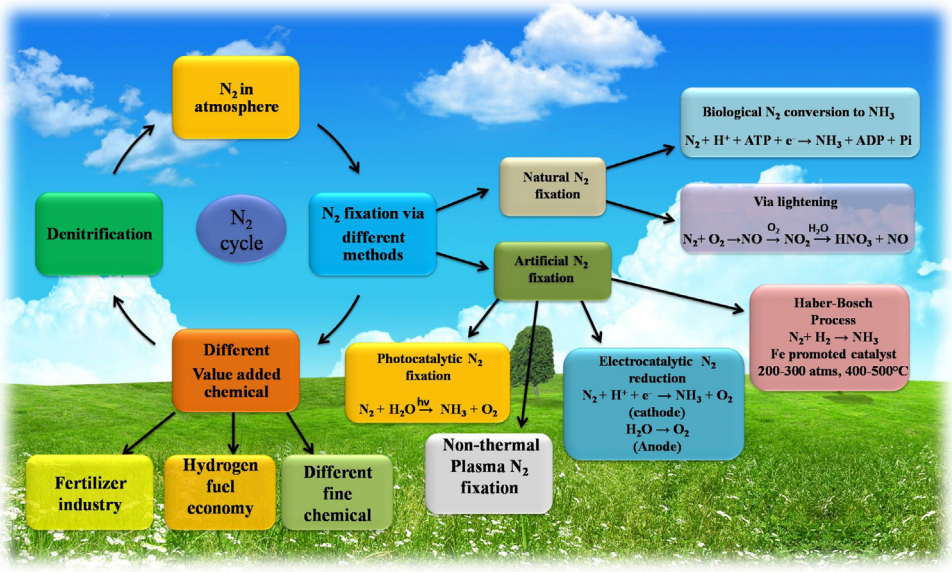

Scheme 1. The nitrogen cycle, different methods for ammonia synthesis, and various applications of NH_3.

duction efficiency as per published literature to meet the industrial specification, but the hunt is on to reach the target and, in this respect, many catalyst modification strategies were implemented both in photocatalytic and electrocatalytic N_2 fixation technique [24].

Naturally, the nitrogenase enzyme (FeCo, FeFe, or FeV co-factor) present in azotobacter carries out ammonia production via shipment of multiple protons and electrons in the presence of an energy transporter (ATP) [11,25].

$$N_2 + 16ATP + 8H^+ + 8e^- \longrightarrow 2NH_3 + H_2 + 16ADP + 16Pi \quad (\Delta G_0 = -248\ kJ/mol\ at\ pH\ 7.0\ and\ 310\ K)$$

Enlightened by this beautiful concept from the natural phenomenon, photocatalytic reduction of nitrogen using an electron-proton coupled mechanism has a great potential for CO_2 free ammonia synthesis at ambient conditions under renewable sources (solar and water). In the photocatalytic N_2 fixation, nitrogen molecules from the atmosphere are used as nitrogen sources while water is the source for proton, and hence nitrogen fixation takes place in normal conditions and hence termed as green synthesis [17,21,22]. This process is a highly promising method for achieving clean, carbon-free, and sustainable ammonia from dinitrogen reduction but formed NH_3 may get oxidized to its corresponding nitrate form and results in low yield [12]. The photocatalytic ammonia synthesis in a sustainable way has begun several decades ago [26]. In this regard, catalysts such as biomimetic, inorganic hybrids/semiconductors, black silicon, and hydrogenated diamond are used to drive photocatalytic N_2 conversion to NH_3 under normal conditions [15]. History speaks that, in the 1970′s Schrauzer and Guth successfully performed di-nitrogen molecules photo-reduction to NH_3 using water molecules and UV light source over TiO_2 (containing both rutile and anatase phase) catalyst and found that rutile is responsible for this reduction [15,17,26]. Likewise, Augugliaro et al. reported that TiO_2 customized Fe metal that plays a crucial role in the HB method can also be utilized as a propitious photocatalyst towards ammonia production [15]. In this domain, a good number of NRR photocatalysts were investigated and further modified by various advanced techniques to exhibit remarkably robust catalytic activity. Here are few budding/propitious NRR catalytic systems such as $FeTiO_3$ [27], TiO_2 [28] CdS:MoFe protein biohybrid [29], g-C_3N_4 [30], CdS [31], ZnO [32,33], GaP [33], black platinum [33] black phosphorus [34], Ga_2O_3-DBD/g-C_3N_4 [35], BiOCl [36], MoS_2 [37], FeOOH [38], $Mo_2Fe_6S_8$–Sn_2S_6(FeMoS) [39], Ru@n-GaN [40], $Sm_2O_3{\cdot}nH_2O/V_2O_3{\cdot}nH_2O$ [41], Sb/TiO_2 [42] Au/$(BiO)_2CO_3$ [43], 2D Sb nanosheets [44], Fe@3Dgraphene [45], Au–Ag_2O nanocages [46] and SiW_{12}/K-C_3N_4 [47] have been successfully fabricated and found to display robust photocatalytic NRR activity under ambient condition. In brief, Ye et al. induced oxygen vacancy in Bi_5O_7Br nanotube via light irradiation and report an ammonia production rate of 1380 μmol/g/h which is 13 times higher than chemically created oxygen vacancy oriented BiOBr prepared by Li and coworker under visible light irradiation [48,49]. Zhang and team doped Mo to defect rich $W_{18}O_{49}$ ultrathin nanowire forming a Mo-W bimetallic center that polarizes N_2 and induce multi-synergetic effect resulting and AQE of 0.33 % at 400 nm and solar-to-ammonia (STA) efficiency of 0.028 % [50]. Sun and group fabricated carbon modified tungstic acid (C-WO_3-H_2O) where carbon supports the migration and separation of excitons leading to an enhanced NH_3 yield of 205 μmol/g/h [51]. Shen et al. made further advancements by employing a few layers of black phosphorus nanosheet for photocatalytic nitrogen reduction under ambient conditions and reported improved results. In another case, Goddard III and partner reported a notable dinitrogen photoconversion to ammonia over BiO quantum dot (1226 μmol/g/h) by stimulated solar light without the assistance of any co-catalyst and sacrificial agent [52]. Lui et al. prepared visible light absorbing MXene derived TiO_2@C/g-C_3N_4 heterojunction based photocatalyst with effective surface defects and charge carrier separation efficiency that results in an ammonia production velocity of 250.6 μmol/g/h [53]. Likewise, designed conducting polymer/TiO_2 heterojunction (P_3MeT/TiO_2) by Hoshino et al. depicts encouraging NRR photocatalytic behavior [54]. Additionally, Zhang and his colleagues showed visible driven photocatalytic dinitrogen reduction in absence of sacrificial reagent over disorder structured and strain framed defective CuCr LDH ultrathin sheet [55]. Further, the Haung research group synthesized Ni_2P decorated $Cd_{0.5}Zn_{0.5}S$ photocatalyst and showed an ammonia production of 253.8 μmol/g/h and quantum efficiency of 4.32 % at 420 nm under visible photon agitation [56]. Based on the concept of 'working in tandem' of nitrogenase, Yang et al. developed an oxygen defective Au-TiO_2 dinitrogen photo-reducing catalyst that exhibits an ammonia formation of 130.5 mmol/g/h and an AQE of 0.82 % at

550 nm [57]. Interestingly, amorphous engineered defective SmOCl NSs prepared by Wang and the team display impressive dinitrogen photoreduction to ammonia i.e. 426 μmol h^{-1} $g^{-1}$and AQE of 0.32 % at 420 nm [58]. Viswanathan et al. and Rao group separately investigated the aftereffect of noble metal and metal loading over TiO_2 toward photocatalytic N_2 reduction [59,60]. Making a strong literature survey on this topic, our research team have also made tremendous advancement by employing several semiconducting materials like 2D-CeO_2, non-metals doped TiO_2, and 1T-MoS_2 as photocatalyst for the reduction of dinitrogen to ammonia under visible light without the assistance of any co-catalyst or precious metal and achieved remarkable activity [61–64]. However, the yield and efficiency of ammonia synthesis is unsatisfactory and is far away from replacing the industrial based HB process. The weak adsorption, difficulty in N_2 activation on the catalyst surface, hydrogen evolution (HER), the involvement of high-energy intermediates, and complicated electron transfer pathway are some of the lacunas responsible for insufficient nitrogen reduction reaction in these heterogeneous photocatalysts [2,15]. In addition to, side reactions like oxidation of NH_3, quick recombination of photo-generated electron-hole pairs are an important parameter for low photocatalytic reduction efficiency [12]. Hence, the urgency towards the fabrication of efficient, cost-effective, and durable photocatalyst is of top priority to surmount the above-highlighted shortcomings. In this subject, the current review projects the fundamentals of NRR, various proposed mechanistic pathways towards dinitrogen photofixation, different experimental detection/quantification methods, associated shortcoming, adopted modification techniques to tune the catalyst efficiency, and an outline of advanced materials examined in the context of photo-NRR. In brief, this review will furnish the trendy breakthrough in the experimental procedure and basic understanding or mechanism of photocatalytic ammonia synthesis with smart materials. The text also narrates the important outcomes of performed computation calculations made on various NRR catalysts. Lastly, the conclusion describes upcoming scientific master plans towards the construction of promising NRR photocatalysts which will encourage and pave new routes for academia and industry working in this research stream to make photon driven dinitrogen reduction reaction (NRR) commercialization a reality.

2. Fundamental and mechanistic aspects of N_2 fixation to NH_3

Dinitrogen fixation is thermodynamically feasible but under the ambient condition not spontaneous or in other words ammonia formation from atmospheric N_2 is chemically an uphill process. This is because of (i) short (109 pm) and sturdy N≡N, (ii) high bond energy (945.33 kJ/mole), (iii) high ionization value (15.85 eV), (iv) low proton affinity (1.90 eV), (v) absence of dipole moment or non-polarity character,(vi) negative electron affinity (-1.8 eV) and wide HOMO(σ_g2p)-LUMO($^*\Pi_g$2p) gap (22.9 eV) [1,2,12,24].

$$N_2(g) + 3H_2(g) \rightarrow 2NH_3(g),\ \Delta H^0 = -92.22\ \text{kJ/mole},\ \Delta S^0 = -99\ \text{J/mole} * \text{K} \quad (1)$$

$$N_2(g) + 6e^- + 6H^+ \rightarrow 2NH_3,\ E^0 = -0.148\ \text{VvsRHE} \quad (2)$$

Equation-1 is the general thermodynamic equation and Eqn-2 represents the ionic equation of NH_3 formation in an aqueous medium. Additionally, the formation of these high energy intermediates like diazene (ΔH_f° = +212.9 kJ/mole) and hydrazine (ΔH_f° = +95.35 kJ/mole) in a water medium further restrict the NRR process. Again, the bond dissociation entropy of N_2 is nearly the same as that of acetylene. As we know, N_2 is inert which can be further explained by considering the first dissociation energy of N≡N i.e. 410 kJ/mole whereas that of HC≡CH is about 222 kJ/mole. The large forbidden zone/energy gap between HOMO and LUMO makes the electron transfer process sluggish/arduous. Again, the hydrogenation of N_2 is very tough compared to CO_2, HC≡CH, and CH_4 reduction under ambient conditions in an acidic medium [1,24]. N_2 fixation involves the following stages, (i) adsorption of nitrogen on the catalytic surface, (ii) hydrogenation followed by cleavage or cleavage followed by hydrogenation/vice-versa, and (iii) desorption of formed NH_3 from catalyst horizon [24]. In short, chemisorptions of N_2 on the reactive site followed by activation by gaining electrons from the catalyst are taken as the proviso stages towards N_2 reduction to NH_3. And in this respect, transition metal-based catalysts are considered to commanding due to their empty and filled d-orbital that helps in the strong bind of nitrogen and metal center [1,13,15]. In this process, the vacant orbital of metal receives lone-pair electrons of N_2 and donates its electrons to the π-antibonding orbital of nitrogen known as π back-donation resulting in enfeebling of triple bond of dinitrogen [12,21]. However, this back-donation concept is very knotty for main group compounds but quite advantageous in the case of p-block sp^2 and sp^3 compounds (as shown in Fig. 1) [12].

Further, the computation study provides ideas for experimental investigation while practical outcomes portray the standardization of the reaction process and design of the theoretical model. Additionally, a computational calculation helps in filtering out the potential catalytic systems with high efficiency, high selectivity, and budget-friendly features. This computational tool needs a supercomputer, upgraded simulation software, and a skilled programmer. DFT study commonly gives information regarding the characteristic of samples and also the job of different constituents in the reaction mechanism, besides theoretical stimulation describes the whole catalysis process in a structural manner both on the mesoscopic and microscopic state [65,66]. Hence, these computational studies work as a handy guide for the experimentalists in developing top-quality nitrogen-fixing catalysts and it also supervises in elaborating the NRR mechanism over the catalyst surface [2,67,68]. NRR is generally a proton-coupled electron transfer process, where the adsorbed N_2 gets hydrogenated by gaining a proton from the reaction medium and get reduced by absorbing one photo-excited electron from the conduction band of the photocatalyst to produce N=NH-catalyst and get transfer to NH_3 which finally get desorbed from the catalyst surface [11–13,17]. As per the DFT study made by Azofra and group, 5 proton-coupled electron transfer pathways were proposed (shown in Fig. 2), from which two are the most followed and verified mechanistic route towards N_2 reduction to NH_3 [17,69].

These are classified as dissociative and associative mechanisms as shown in the Scheme 2, via the dissociative route, the breaking of the N≡N bond occurs first on the catalyst surface followed by independent hydrogenation before NH_3 formation [20,68]. The 100 years old industrial Haber-Bosch NH_3 synthesis goes via this dissociative mechanism which is still a topic of controversy [2,11,70]. However, a general dissociative mechanistic pathway is there for this thermocatalytic N_2 reduction reaction (HB process) which is equated as follow (Eqn.3–8):

$$H_2 + 2\ Cat \longrightarrow 2\ Cat{-}H \quad (3)$$

$$N_2 + 2\ Cat \longrightarrow 2\ Cat{-}N \quad (4)$$

$$Cat{-}H + Cat{-}N \longrightarrow Cat{-}NH + Cat \quad (5)$$

$$Cat{-}NH + Cat{-}H \longrightarrow Cat{-}NH_2 + Cat \quad (6)$$

$$Cat{-}NH_2 + Cat{-}H \longrightarrow Cat{-}NH_3 + Cat \quad (7)$$

$$Cat{-}NH_3 \longrightarrow NH_3 + 2\ Cat \quad (8)$$

* Cat = Active site of catalyst

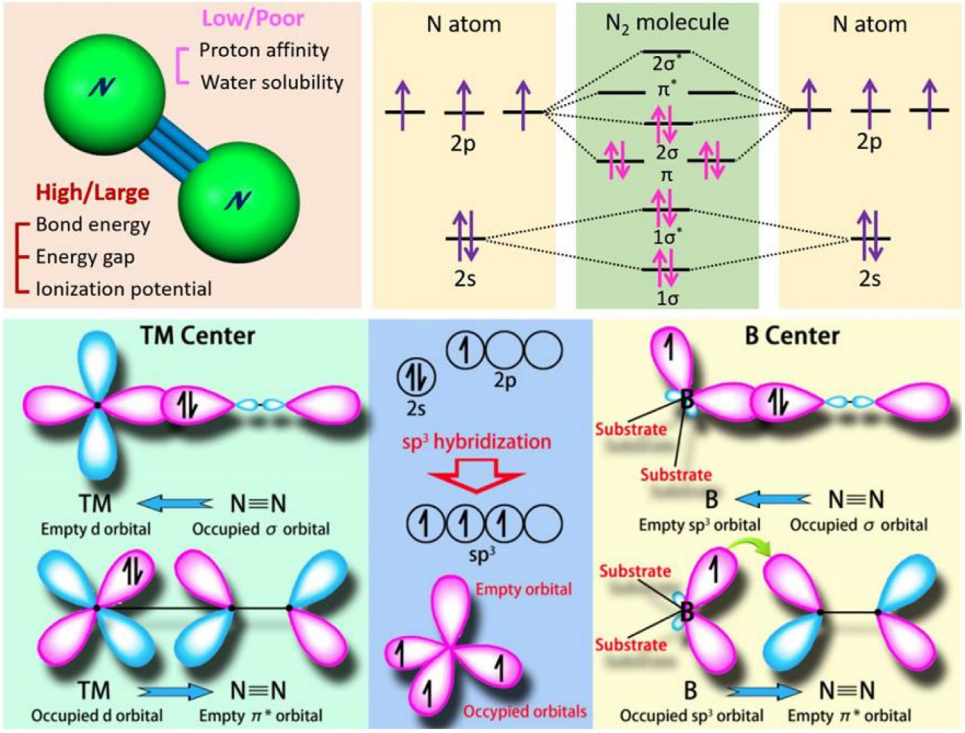

Fig. 1. Represents the molecular orbital diagram N_2 along with transition metal and dinitrogen orbital interaction via the back donation concept. Reproduced with permission from reference [12].

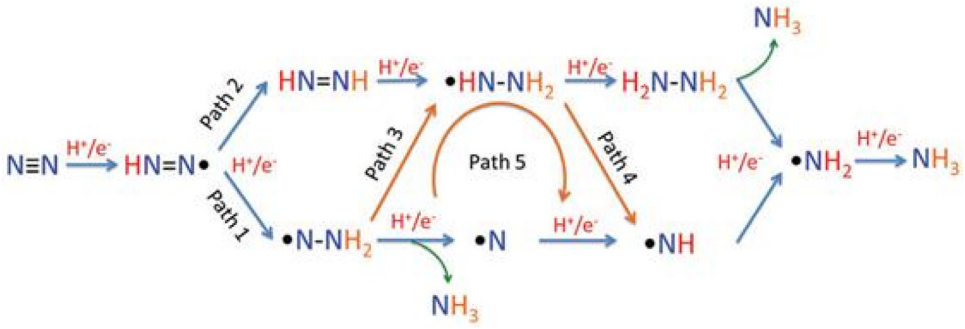

Fig. 2. The possible pathway of dinitrogen conversion to ammonia. Reproduced with permission from reference [69].

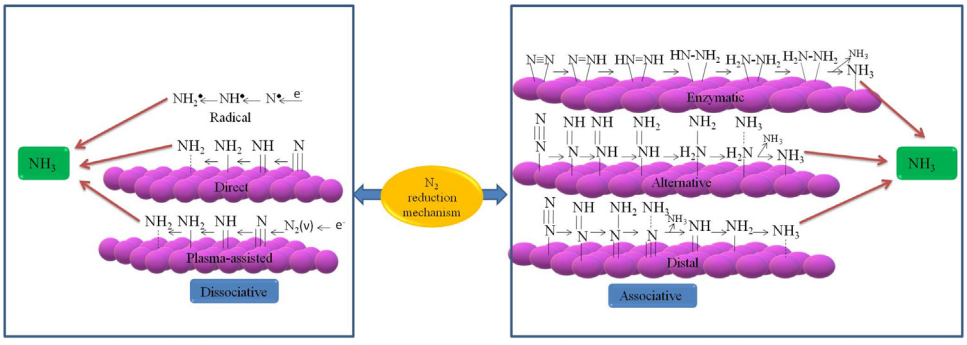

Scheme 2. Dissociative and associative proton-electron coupled mechanistic pathway towards N_2 fixation to ammonia.

Moreover, in this dissociative pathway, N_2 adsorption over the catalyst surface is the rate-determining step and the cleavage of the N_2 and H_2 bond is achieved by the donation of electrons from the metal side to the anti-bonding molecular orbital of the adsorbed molecule. Further, this electron transfer process is modulated by the presence of alkali and alkaline earth metal/metal oxide promoters, which ultimately increases the thermocatalytic ammonia synthesis rate. To figure out the best catalytic material with desired properties for effective N_2 hydrogenation: volcano plot, Bronsted-Evans-Polanyi (BEP) relationship, and d-band theory are frequently

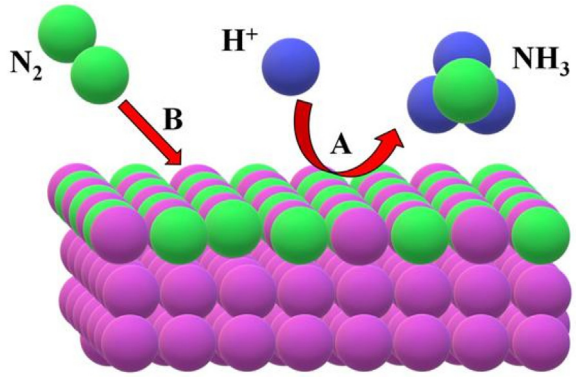

Scheme 3. Schematic representation of Mars-van Krevelen reaction mechanism for N_2 reduction over transition metal nitrides (TMN) surface (* A: the surface of TMN reduced to ammonia and B: Regeneration of the vacancy by gaseous N_2).

followed [11]. Whereas in the associative path the dinitrogen gets adsorbed on the catalyst surface by 'end-on' or 'side-on' fashion i.e. via end-on mode, one N-atom of N_2 binds on the catalyst horizon. Further, based on the protonation sequence of N_2, it is divided as an alternative and distal. In the distal or asymmetric pathway, the remote or farthest N-atom is hydrogenated first resulting in NH_3 release, and then the process continues to generate the next ammonia molecule [2,20,24]. Adding more to this, the alternative or symmetric route as observed in case of natural nitrogen fixation by nitrogenase enzyme, where both the nitrogen atoms get hydrogenated synchronously or in other words protonation of both N-atoms occurs in a single step reaction and the formed NH_3 get detached from the material surface successively [20,22]. Again, in the 'side-on' mode both nitrogen atoms get co-ordinated to the catalyst site followed by hydrogenation of both the N-atom with the dissociation of N≡N resulting NH_3 molecule [20].

In addition to the above-narrated mechanism towards NH_3 generation, Mars-van Krevelen (Mvk) N_2 reduction pathway over transition metal nitride (TMN) is another highly acceptable mechanistic route towards NH_3 generation (depicted in Scheme 3) [11]. In this case, the nitrogen atom of TMN gets reduces to NH_3 and the N-vacancy at once gets refilled by the supplied N_2 gas to restore the catalyst [71]. As per computational calculation, the Mvk pathway for N_2 fixation over TMNs is more feasible than the stereotypical associative and dissociative pathway because (i) N_2 isolation from TMNs catalyst surface via dissociative route is quite frustrating because of large activation energy barrier and endothermic nature, and (ii) high overpotential value for N_2 reduction in the associative mechanism [15,72]. Li. et al. reported Mvk type mechanism for N_2 reduction over KOH etched g-C_3N_4 [11].

Further, by performing SEIRS (surface-enhanced infrared absorption spectroscopy) characterization, Yao and the team proposed the associative pathway towards di-nitrogen reduction over the Au surface. In detail, the N_2H_y species formed during NRR shows trademark IR bands at wavenumber 1453 cm^{-1}, 1298 cm^{-1}, and 1109 cm^{-1} corresponding to N—H bending, -NH_2 wagging, and N—N stretching vibration respectively which indicates the above associative route [73]. Further, *in situ* FTIR is another handy characterization technique frequently used to understand the adsorption, activation, and reaction pathway of dinitrogen reduction (when the reaction is carried out in presence of N_2 gas and water vapor). In brief, the IR band visualized at 1655 cm^{-1} is ascribed to chemisorbed N_2, and with an increase in time, this peak intensity gradually increases. When the system is irradiated with light, two strong and intense IR peaks are observed at wavenumber 1460 and 1740 cm^{-1} which corresponds to the H-*N*-H bending mode of vibration indicating the generation of ammonia or ammonium ion. The asymmetric deformation vibrational band of NH_4^+ is visualized at 1648 cm^{-1} and the two asymmetric stretching modes of the N—H bond are observed at 3246 and 3555 cm^{-1} respectively [11,13,15]. Also low-temperature Fourier-transform infrared spectroscopy technique is utilized to find out the adsorption mechanism of N_2 over catalyst surface [50]. Additionally, *in situ* diffuse reflectance, infrared Fourier-transform spectroscopy (DRIFTS) is another sensitive analysis method used to figure out the N_2 photoreduction mechanism. As we know, NH_3 formation involves a multistep proton-coupled electron migration process, so several intermediates with N—H bonds such as N_2Hy and NH_z may appear in the DRIFTS spectra. The peaks located at 3205 or 3164 and 3412 cm^{-1} represent N—H stretching vibration of intermediates and NH_3 molecule respectively. Whereas the bending mode of vibration is seen within the 1200–1800 cm^{-1} range i.e. the peaks observed about 1457, 1554, and 1620 cm^{-1} are ascribed to N—H bending motion of intermediates and NH_3 species. The wagging mode of -NH_2 is represented by the band seen at 1268 cm^{-1}, all these peaks in the DRIFTS spectra ascertain the N_2 fixation reaction [50]. Adding more to the text, quasi *in situ* XPS, XAS, *in situ* XRD, and high-resolution electron energy loss spectroscopy (HREELS) are few other operando characterization techniques employed to monitor the formed intermediates and hence gather more information and deep understanding about the NRR mechanism [2,12,17]. Moreover, the pH of the reaction medium plays an inherent part in regulating the catalytic execution of the material towards N_2 fixation. From the conducted investigation it was surmised that NH_3 production is usually high in low pH or acidic medium compared to neutral solution. The report by Wang et al. manifests that the NH_3 generation rate at pH = 3.5 is 6 fold higher than observed in neutral solution and a similar trend is also noticed by Goddard III et al. over BiO quantum dots [37,52]. This increment in the rate of NH_3 generation is accredited to a plethora of H^+ ions near the catalyst surrounding to drive the protonation of adsorbate (N_2) and also reduces the kinetic energy hump of nitrogen reduction. However sometimes this acidic medium work in the wrong direction and decrease the ammonia yield because several unstable catalysts are there, which crumbles swiftly in the acidic medium [2]. A surprising observation was reported by Bian and the team, where the group found a 2.5 times more dinitrogen reduction rate at pH 9 over a Mxene derived photocatalytic system. The cause of such anomalous remark accompanies to increase in negative charge of catalyst surface which draws more number of photoinduced holes and speeds up the rate-limiting oxidation half-reaction [74].

2.1. Mechanism of photocatalytic N_2 to NH_3

The pioneering work of Schrauzer and Guth over TiO_2 (the classical photocatalyst) led to the foundation of N_2 photo-fixation which later on taken further by Bourgeois *el at*., Augugliaro-team, Zhao et al., and many other eminent research groups [26,75–78]. However, photocatalytic N_2 fixation in the aqueous medium is very tedious due to the requirement of 6 electrons and 6 protons to reduce N_2 to NH_3 addition to the adsorption of inert N_2 to the catalytic site and selectivity between N_2 reduction and proton reduction reaction issue [15,17,20]. The symmetric and asymmetric proton-electron couple transfer mechanism is the most commonly encountered reaction pathway towards photocatalytic NRR. Fundamentally, the photocatalytic NRR involves the following steps, (i) absorption of an irradiated photon with energy ≥ bandgap, (ii) generation and separation of exciton pairs (e^- - h^+), (iii) diffusion of photo-excited electron-hole pairs from bulk to surface to carry out the redox process, (iv) desorption of formed products from the catalyst surface and (v) recombination of some charge carriers either at the bulk or surface releasing energy that reduces the reaction turnover [2,12]. So, a promising NRR catalyst is the one that

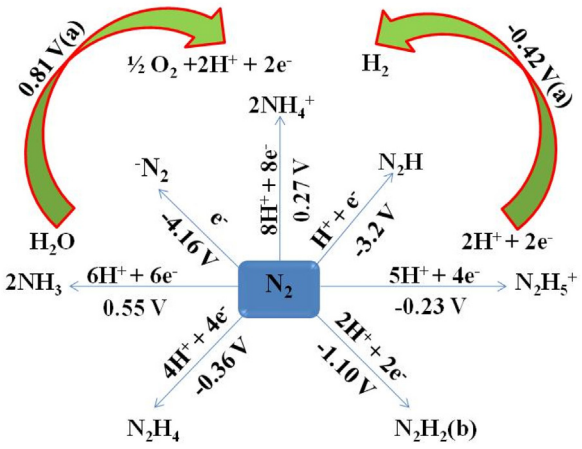

Scheme 4. Typical hydrogenation reactions related to the reduction of N_2 to NH_3 with corresponding standard reduction potential vs. NHE scale at pH 0 (* a vs. NHE at pH 7 and b vs. RHE scale) [17].

possesses a wide light absorption range, a large number of active sites, and surface effective excitons separation. Adding more to it, adsorption of N_2 (adsorbate) on the reactive center and its successive photoreduction on the catalyst platform are the primary stages in the photocatalytic nitrogen fixation process. But the non-polar nature of N_2 makes the former step onerous i.e. the adsorption step. As a substitute, the 'solvated electron' chemistry by Zhu et al. and Bandy co-worker over hydrogen-terminated diamond is proved to be a very fascinating science towards photocatalytic NRR [79,80]. In this process, the emitted electrons from the H-terminated diamond interacts with the solvent resulting in the generation of solvated electrons that directly reacts with N_2 molecules and brought about the reduction process i.e. N_2 to NH_3. Interestingly the whole reaction does not require the adsorption of nitrogen on the catalyst surface and this concept is also applicable to various other traditional/popular photocatalytic reactions. Further, headway in this NRR via solvent electron mechanism made by the Christianson group suggests that proton addition is the first step followed by successive reduction and protonation [81]. The below given thermodynamic equation in Scheme 4 with their respective standard reduction potential, further clarifies why the reduction of N_2 to NH_3 is a challenging task [17].

Therefore, the photoexcited electrons in the CB of the semiconductor need to be highly negative compared to the reduction potential required for N_2 reduction (0.092 V vs NHE) to successfully carry out the reaction. Similarly, the holes in the VB should be either more positive for water oxidation or oxidation of used sacrificial agents [17]. Further, it was found from the theoretical calculation that the reduction potential of N_2 to NH_3 is nearly comparable to that of the hydrogen reduction reaction. Thermodynamically, NRR is more feasible but from a kinetic perspective, HER gets the advantage, as the latter requires only two electrons compared to the former which proceeds via six electrons [11,82]. HER somehow becomes an integral part of artificial NRR as water is used from a proton source. Again, proton gets easily attached to the catalyst surface and blocks the active sites for N_2 adsorption and hence, hinders the NRR process. The detailed dinitrogen photofixation to ammonia with associated side reaction is depicted in scheme 5 .

Even in nature, HER competes with the NRR process i.e. for enzyme-catalyzed dinitrogen fixation selectivity is a big challenge [21]. Further, an experiment by Schubert et al. over nitrogenase reveals that 40–60 % electron moves from the enzyme to nitrogen to carry out the NRR process while the rest is used for proton reduction [83]. Additionally, because of the large activation energy hump, the energy loss of the photoelectrons, overpotential, and 6 electron-coupled reactions, the nitrogen reduction practically occurs at higher –ve potential (N_2(solvated) + $e^- \rightarrow {}^{-}N_2$, −4.2 V vs. NHE) compared to hydrogen [2,12]. These observations suggest that NRR is a kinetically sluggish type process. Sometimes noble metals (Pt, Rh, Ru, and Pd) are loaded over catalysts to improve the activity of the material but in the case of NRR these noble metal co-catalysts act differently and decreased the efficiency (supports HER response). The rate of NH_3 formation is directly related to the bond potential between H-atom and metal. Co-catalyst generally acts as an electron sink and hence boost the catalytic performance, but Ru stabilizes the metal adsorbed hydrogen and enhances the ammonia production velocity as reported by Ranjit et al. [59]. Adding more to the survey, to achieve a better yield of NH_3 holes scavenger are used otherwise, these holes in the VB will react with the hydroxyl ion and get converted to hydroxyl radical which will oxidize NH_3 and decrease the production amount or lowers the AQY. Additionally, the N_2 sometimes reacts with hole and water to form NO with further oxidized to $^{-}NO_3$ by chemically interacting with molecular oxygen and H_2O [12]. Hence, it is very much demanding to tune the properties of the photocatalyst to achieve benchmark ammonia yield or high QY. The above requirements can be meant via modulating optical bandgap, crystal structure, morphology, and surface texture. In this context of boosting the catalytic efficiency of the material, various strategies were adopted that include doping, defect/vacancy creation, co-catalyst loading, facet engineering, forming a composite with carbonaceous materials, hybrid materials mimicking natural nitrogenase, and formation of heterojunction based catalytic systems [2,12,13,24]. Adding something extra to the survey, photocatalytic N_2 oxidation is another aspect that is gaining tremendous attention nowadays (as presented in Scheme 6). In this process, N_2 gets photo-oxidized to NO with the help of water and holes, while O_2 gets reduced to H_2O with the photo-excited electrons. Then ultimately, NO further oxidized to nitrate ($^{-}NO_3$) by reacting with water and molecular oxygen. Additionally, a new research trend is gathering full attention where the produced nitrate is photocatalytically reduced to ammonia with excellent selectivity in the presence of an electron donor (e.g. HCOOH) [12,84–88].

3. Quantification/detection of NH_3 through various methods

Detection and quantification of NH_3 produced from N_2 fixation in an accurate and reproducible manner is a challenging and essential task due to (i) low catalytic efficiency of catalyst, (ii) low ppm/ppb level of NH_3 formation rate, and (iii) interferant effect [12,18,89]. In this direction, various international standardized organization (APHA, ASTM, and US-EPA) approved testing methods are widely followed that includes (i) colorimetric (i.e. Nessler's reagent, phenolate, Kruse and Mellon colorimetric method, Trichloramine method, Salicylate-hypochlorite method and Indo-phenol blue method(IB)), (ii) Ion chromatography (IC)/ HPCL, (iii) Ion-selective electrode (ISE), (iv) titration technique, (v) fluorescence and (vi) H^1 NMR spectroscopy [3,5,12,18,89]. These methods as shown in Scheme 7 are technically sound and show a good precise result for ammonia in water type systems.

Nevertheless, the presence of certain ions, the chemical composition of the material, pH of the medium, nature of the sacrificial agent, and solvent in use play a vital part in the detection accuracy or precision of the followed method. This is because NH_3 production via N_2 photo-fixation process is of nano/micromolar level [89,90]. Therefore, it is indeed very essential to repeat or adopt other testing methods to get the concordant result or negligible error in data. As an example, NH_x-containing photocatalyst and sacrificial agent or their secondary products interact with the formed NH_3 that leads

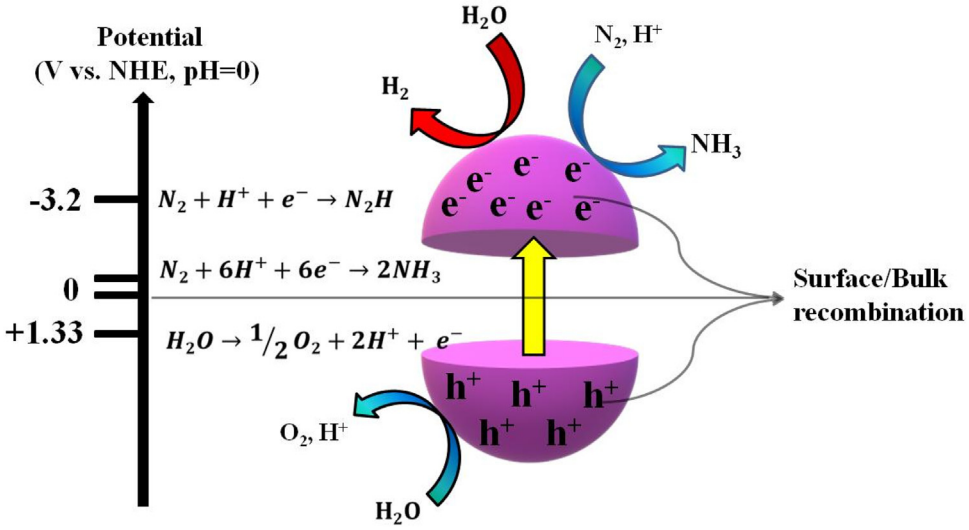

Scheme 5. Represents the photofixation of N_2 to NH_3 with associated side reaction.

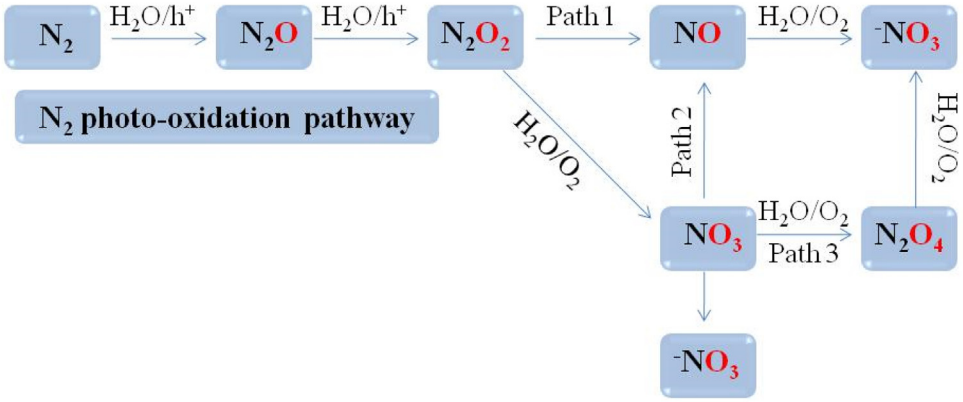

Scheme 6. Mechanism of N_2 oxidation via a photocatalytic pathway.

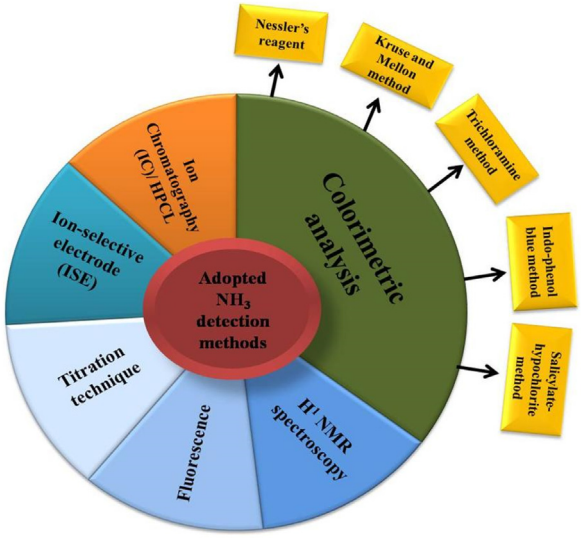

Scheme 7. Different ammonia detection methods followed.

to an erroneous result, hence these parameters should be taken care of to get accurate data [18,89]. In detail, sacrificial reagents (hole scavengers like methanol, humic acid, ascorbic acid, ethanol, isopropanol, etc) or its oxidized product are used to boost the production rate sometimes makes a complex with so formed ammonia and results in erratic data [90]. Further, the N-atom containing chemical species (HMT, oleyl amine, TAA, etc) used in the synthesis of photocatalysts may leach out or decompose into the experimenting solution and this impairs the quantification result, therefore a control experiment is done in presence of Ar or $^{15}N_2$ to avoid the error [18,89,91]. Additionally, the certain catalyst itself is composed of N-atom (g-C_3N_4, Boron nitride, etc) or catalyst functionalized with nitrogen (ammine/nitro functionalized MOF, etc) when examined for N_2-fixation depicts inaccuracy in NH_3 yield/concentration. Again, the solvents used during the fixation experiment if contain a trace of NH_3 from any other source viz. NH_3 readily dissolves in water so atmospheric ammonia may contaminate the aqueous medium in which the N_2 photoreduction is taking place and this leads to an overestimation of NH_3 concentration during analysis [89]. Further, isotopic leveling i.e. N^{15} testing method is another alternative for confirmation of NH_3 formation through N_2 photofixation and the product ($^{15}NH_3$) is analyzed via H^1-NMR or MS technique, also via enzymatic analysis ammonia formation can be ascertained and hence the error in quantification or detection can be avoided. In brief, $^{14}NH_4^+$ generated from ^{14}N shows a triplet within 6.8–7.05 ppm range of H^1-NMR spectra with a J-coupling of 52 Hz whereas ^{15}N isotope shows a doublet in the same ppm range but having a J-coupling of 73 Hz. For the ^{15}N isotope leveling market available $(^{15}NH_4)_2SO_4$ reagent is used to perform the experiment and NMR analysis. However, in the H^1-NMR spectra,

both ^{14}N and ^{15}N signals will be seen but the intensity of the ^{15}N isotope is more compared to ^{14}N [46,89,92,93]. It is very difficult to find the best quantification/testing method for NH_3 concentration at ppm and ppb standard including the effect of interferants. This problem is due to less database/information available about the interfering factors that affect NH_3 detection at nano/micromolar concentration. This section provides a short description of the frequently followed NH_3 detection/quantification techniques like Nessler's reagent method, the indophenol blue method, ISE, and ion chromatography method taking into account the effect of pH, ion presence, sacrificial agents, solvent used, and N-atom containing catalyst. Compared to spectroscopic methods i.e. Nessler's and Indo-phenol blue method, the IC technique is more reproducible and advantageous but is quite costlier and a bit complex from the instrumentation point of view [18,89]. However, the colorimetric pathway is cost-effective and facile. Yet, the IC method is far more superior because of the following features (i) durable/compatible, (ii) high selectivity/sensitivity,(iii) more reliable, and (iv) high efficiency/assured [18,22,94]. In details, Nessler's reagent (solution of K_2HgI_4 and KOH) method, NH_3 forms a reddish-brown colored complex with iodine and mercury under alkaline medium (in absence of interferants, Eqn-9) which shows optical absorbance at about 420 nm and the intensity of absorbance is directly proportional to the concentration of ammonia in the solution. Rochelle salt is sometimes added to the reagent during testing to reduce the effect of interfering ions [89,95].

$$2[HgI_4]^{2-} + NH_3 + 3OH^- \rightarrow Hg_2ONH_2I + 7I^- + 2H_2O \ldots\ldots \quad (9)$$

However, certain points are there which need to be taken care of while going for NH_3 detection (i) Nessler's agent can be stored for only three weeks, so should be used before time, (ii) Ultrapure water or NH_3 free solvent should be used for reagent preparation, (iii) The reagent should be handled with utmost safety as it contains toxic Hg and (iv) the analysis should be made within 10–30 min after the mixing of NH_3 containing solution and Nessler's chemical to get accurate data [89]. Further, side product/intermediates of N_2 fixation (urea, hydrazine, glycine, amine, etc) or the presence of certain ion that increases the turbidity of the medium may affect the detect process [96–98]. In the case of the Indophenol blue method ammonia forms a blue color compound in an alkaline medium by interacting with phenol and hypochlorite as shown in Eqn-10 (Bethelot reaction) [95].

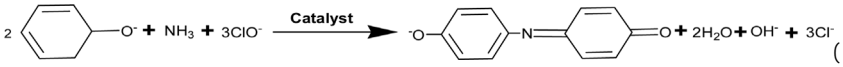

(10)

Here, sodium nitroprusside is used as a color intensifying agent and citrate buffer as a pH stabilizer. As reported by Zhang et al. IC, indophenol and Nessler's reagent detection method gives an accurate and acceptable result at lower NH_3 concentration i.e. within 0–500 μg/L whereas above this range IC and Nessler's methods are reliable and effective however indophenol process fails to provide the accurate result or in other words, gives erroneous/overestimated NH_3 concentration [89]. Further, a change in pH also affects the detection process and gives the wrong result. Nessler's method works over a wide range of pH i.e. from acid to alkaline via neutral with an error of 11 % (in acidic medium). That because, of the nature of the interaction between ammonia, iodine, and mercury in an acidic medium. Whereas via the indophenol blue method, the solution color changes from yellow (in neutral) to green (in acidic) with pH change which affects the quantification process. So, this method gives an erroneous concentration of ammonia in the acidic solution due to the instability of sodium hypochlorite. Hence, indophenol blue methods show the viable result in alkaline and neutral medium only with low error percentage but Nessler's reagent depicts accurate NH_3 concentration in all three mediums [89]. Further, the presence of certain ions also impacts the detect methods, let us discuss Nessler's process, ions which show their absorbance around 420 nm and chemically reacts with the reagent displays interference effect and therefore the obtained result shows error [22,89]. Likewise, sacrificial agents used in photocatalytic N_2 fixation and the oxidized product formed during the reaction along with their percentage in solution produces inaccuracy in concentration measure via the colorimetric method. Normal ammonia solution is yellow, but the presence of these agents (methanol, ethanol, DMF, DMSO, acetone, etc) and intermediates (formaldehyde, formic acid, etc) changes the color of solution e.g. through indophenol blue technique, in presence of formaldehyde the color appears to be pink while in formic acid it turns light yellow. Hence, the concentration obtained through Nessler's or indophenol blue method shows wrong or overestimated concentration. Hence, both the spectroscopic analysis techniques are not perfect for ammonia quantification in presence of organic sacrificial reagents; however, if measurements are done then under control condition and in sacrificial agent condition, the IC method is more preferred (as shown in Fig. 3) [89].

Additionally, the ISE detection technique is another widely adopted method due to its broad detection limit i.e. 30 ppb to 1000 ppm with high selectivity and more importantly less affected by interfering agents [22,95]. However, it operates at a very slow pace at ultra-low concentration and the operational condition is quite complex with instrumental drift. Further, the main primacies of ISE over colorimetric methods are (i) turbidity and color do not affect ammonia estimation, and (ii) it operates in a wide detection range (0.03–1400 NH_3-N mg L^{-1}) [16,99]. In summary, the chromatography method is a more reliable or assured technique as the components of the substrate get separated by column and IC is the most recommended one by the various international organization and scientific groups towards NH_3 quantification. Again, atomization of instruments with the attachment of the cation-exchange column and conductive detector widens up the range of NH_3 estimation and reduces the analysis time giving reproducible, precise, and accurate results [18,89]. Scheme 8 displays a suitable method for ammonia detection under specific conditions.

4. The strategy adopted to magnify the catalytic performance and overcome the connected limitations

To short-out, the associated deterrent with semiconductors/photocatalysts (as discussed in the previous section) that impede the industrial-scale production of NH_3 via light-driven dinitrogen fixation, the research institution across the globe used all their skill and potential towards designing various photocatalyst/material modification techniques that include, doping (metal/non-metal or both), noble-metal loading (semiconductor-metal), hetero/homo-junction formation (semiconductor-semiconductor), double or Z/S-scheme charge transfer dynamics, defect/vacancy chemistry, facet/edge engineering, amorphous engineering and tuning via carbon-allotropes (graphene, C-dot, CNT, etc) (semiconductor-carbons) to subside the associated bottlenecks with photon drove NRR (scheme.). In detail, vacancy or defect chemistry i.e. oxygen vacancies (OVs), nitrogen vacancies (NVs), and sulfur vacancies (SVs) are found to be promising techniques in the process of uplifting the NRR catalytic efficiency of the materials (as depicted in Scheme 9) [2–5]. The presence of different types of vacancies tunes the intrinsic features of the catalyst like adsorption, charge separation & migration, electronic structure, number of active site availability,

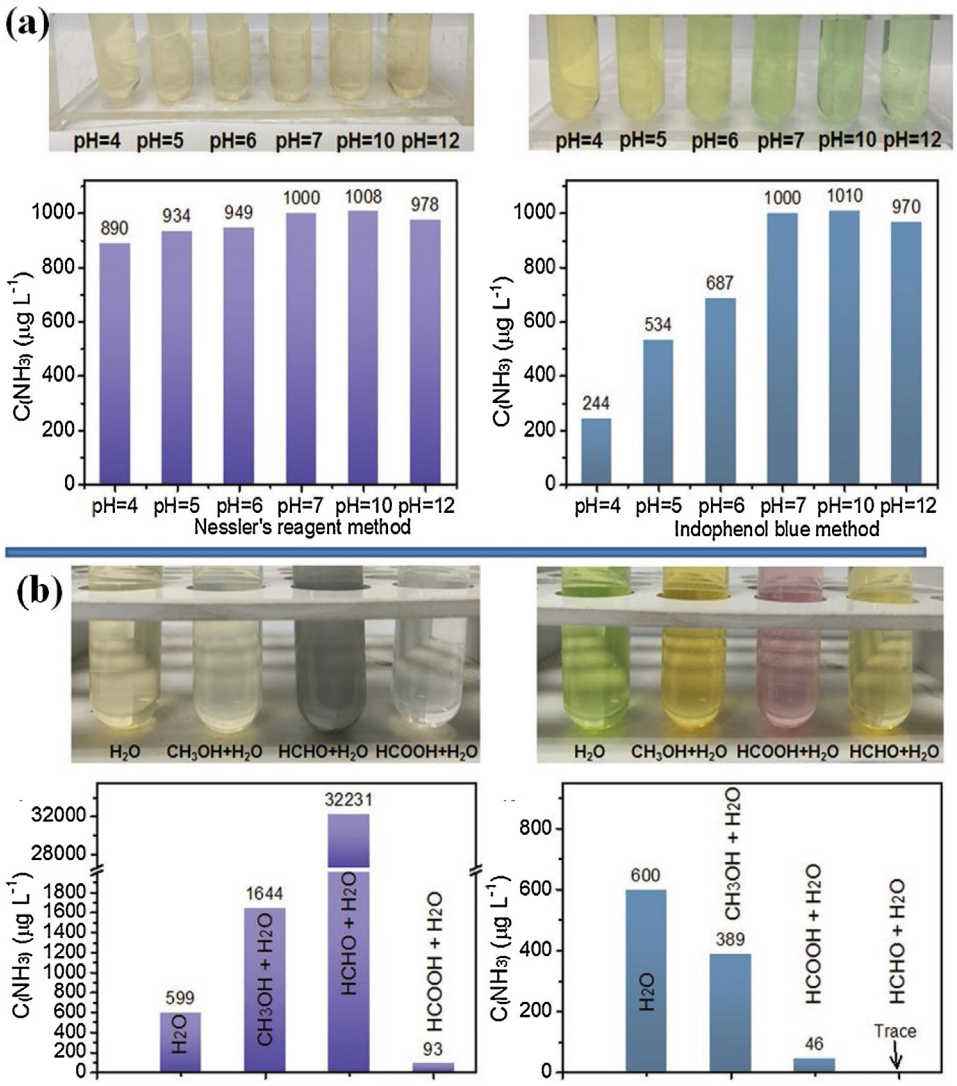

Fig. 3. (a) Photographs of ammonia solutions and corresponding concentrations of ammonia detected using each method, and (b) picture of NH_3 solutions and solution concentrations determined by Nessler's reagent method and the indophenol blue method in the presence of different oxidizing reagents. Reproduced with permission from reference [89].

and more importantly minimizes the activation energy hump that allows the smooth flow of the reaction [5–7]. These defect sites trap the photoexcited electron-hole pairs and hence reduce the recombination process. Further, N_2 gets adsorbed in these vacancies and through the back-donation concept, the strong triple bond in N_2 gets weakened and so the cleavage and protonation process becomes easier [3]. In another approach, doping of foreign or heteroatoms into the lattice framework of the catalyst results in altering the surface texture, electronic properties, chemical composition, adsorption/desorption behavior, and optical response. Doping of metal (transition elements) or non-metal (S, C, O, P, etc) leads to the formation of and impurity or sub energy band within the bandgap of the material that widens the light absorption range (redshift or decrease in the bandgap) and increases the charge transfer process [3,12,99,100]. Additionally, edge engineering is another method by which the catalytic performance of 2D based photocatalytic materials can be tuned up as it provides heterogeneity to edge site, electronic configuration, and functionalities of the specimen. It was observed that edge carbon atoms of graphene are catalytically more active than basal plane C-atoms as this region offers more active sites with high energy density, similar types of edge chemistry are also observed for 2D metal chalcogenides (eg.MoS_2) [3,13,4,101]. The computational study on MXene suggests that metal-containing terminal sites are more capable of activating N_2 and so depicts high NRR activity compared to the oxygen-functional group (directly linked to metal atoms) composing the terminal surface. Further, the basal plane shows low nitrogen reduction efficiency due to weak N_2 binding ability [14,102]. The Single-atom catalyst is also an interesting heterogeneous catalysis method where the cause of enhanced activity corresponds to the maximum availability of atomic sites. Here the metal atoms are bound to a support material resulting in unique physio-chemical features [3,103–105]. Facet engineering of crystals is drawing huge attention, as by this technique it is possible to introduce a specific facet or crystal plane at the atomic level (i.e. ordering of atoms on different lattice planes) that elevates the catalytic behavior of the material. Computational studies reveal that intermediates formed during NRR get strongly attached to step atoms than terrace ones because they provide more active sites for adsorption and activation [4,106]. For example, (001) plane of BiOCl NSs, (411) facet of Pt, (111) facets of octahedral Pd NPs, etc depict encouraging performance [107–109]. Extending the information, carbon derivatives like CNT, rGO, graphene, activated carbon, and carbon dots are frequently

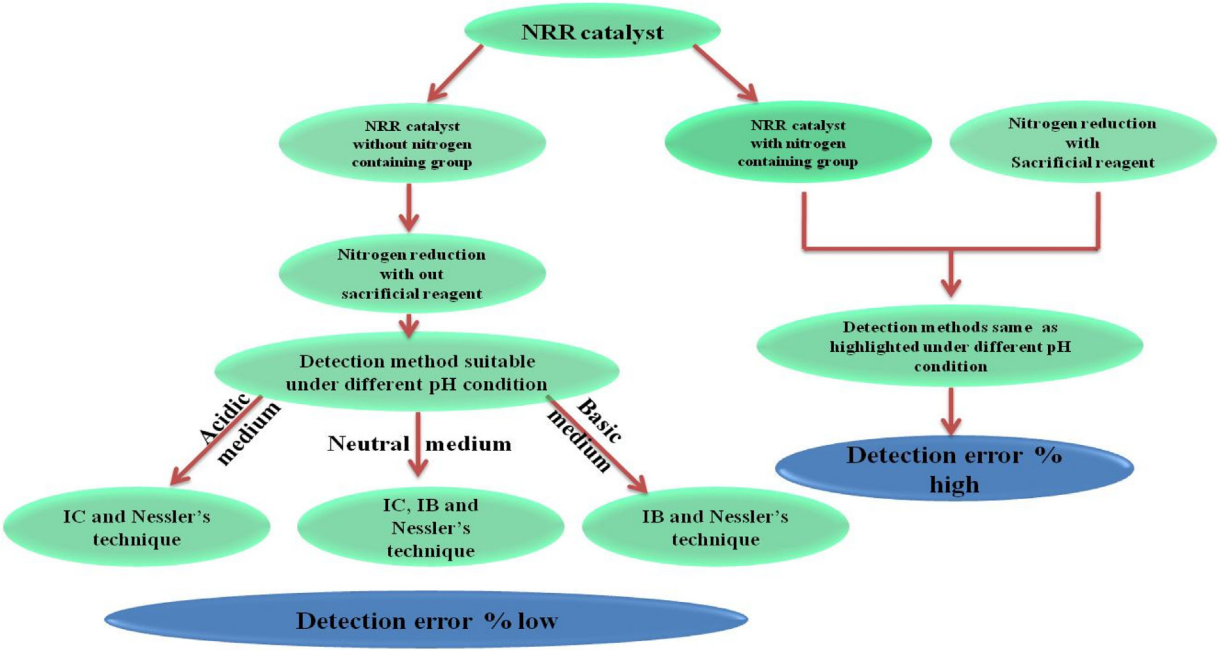

Scheme 8. Scheme representing a suitable method for ammonia detection.

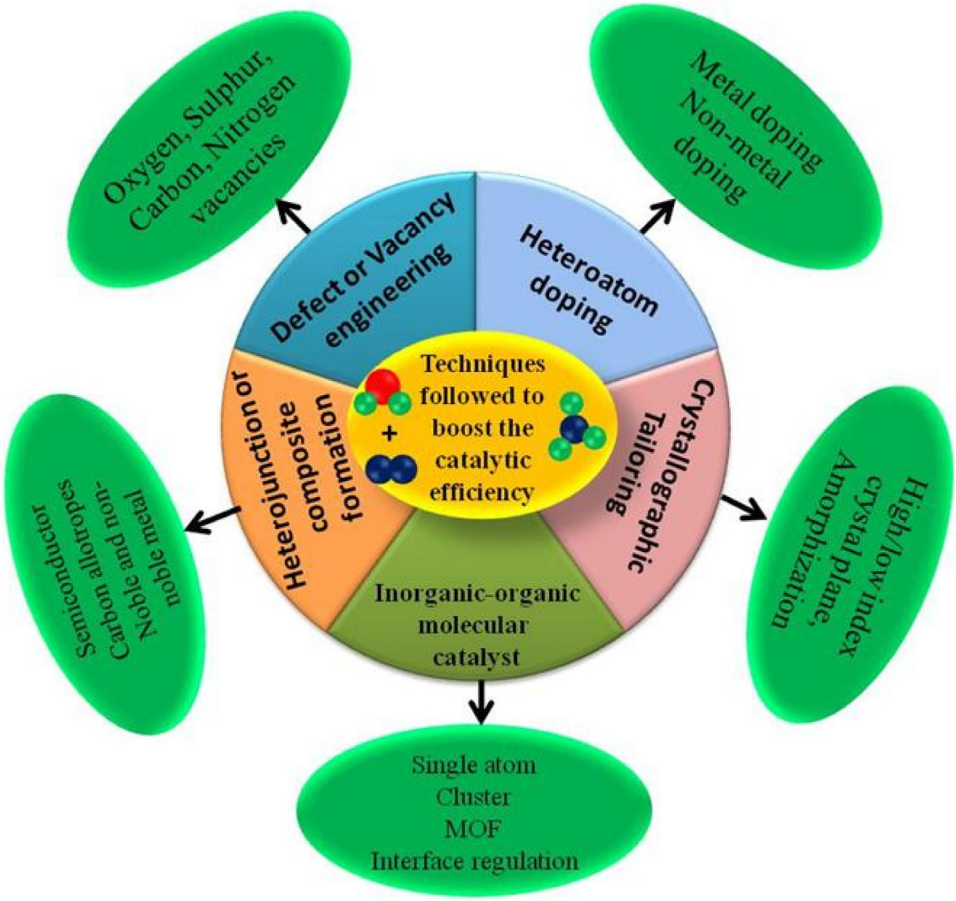

Scheme 9. Schematic representation of different catalyst modification techniques.

used to build carbon-semiconductor based photocatalytic systems that display high catalytic activity. Carbon is taken as a component in the heterojunction because of the following advantages (i) acts as an electron sink i.e. accepts and channelizes charge carriers, (ii) as support, (iii) prevent agglomeration of nanoparticles, (iv) adsorption of substrate for better interaction, (v) as a mediator

and (vii) also helps in tailoring the morphology of the material during preparation that brought about a change in adsorption and light absorption ability [13,18]. Bio-memetic nitrogenase type of catalytic systems i.e. cluster catalyst is also a fascinating strategy towards magnifying NRR performance [4,5,110]. Technically, cocatalyst (reduction, oxidation, and plasmonic type) loading over photocatalyst results in magnifying the catalytic response of the material many times compared to its neat part. This type of tactic is frequently used to increase the efficiency of semiconducting photocatalyst towards water splitting, CO_2 reduction, and N_2 fixation. Cocatalyst usually reduces the activation energy barrier, prohibits excitons recombination, and prevents photo-corrosion of the materials. These highlighting features make the cocatalyst special and hence its presence increases the catalytic potential of the system [7,111–113]. Adding more to it, constructing a semiconductor-semiconductor heterojunction (binary or multijunction) based photocatalytic system is another promising and feasible strategy to upgrade the catalytic efficiency of the photocatalysts towards NRR and other photocatalytic reactions. As we know, light absorption and charge carrier separation ability are the two most demanding properties for the photocatalyst and this can be best achieved by integrating two or more semiconducting material, where at the interface or junction point an internal electric field is generated that retards the recombination process and increases the charge carrier densities. The mechanism that operates within the heterojunction system resulting in superior catalytic efficiency may be classified as (i) double charge transfer (type 1 or 2) or (ii) Z-scheme (with or without mediator). In the former type, photoexcited electrons jump from the conduction band (CB) of one semiconductor(A) with more negative potential to the CB of other semiconductor(B) having less negative potential, at the same time holes migrates from the valency band (VB) of a semiconductor having the higher positive potential to the VB of other semiconductor with lower potential. Whereas in the case of Z or S scheme type charge migration pathway, electrons from the CB of one photocatalyst combines with the holes from the VB of other semiconductors via a mediator or without a mediator, therefore the photogenerated electrons are available in the CB of one catalyst to carry out reduction and holes in the VB of other to brought about oxidation [7,114,115]. Photoexcited electron-hole pairs were formed upon suitable light irradiation and due to strong interfacial contact and junction formation, charge carrier recombination is hindered leading to a longer lifespan of excitons and so the catalytic system shows improved catalysis. Another interesting modification technique that is gathering huge attention in NRR and other catalytic applications under ambient conditions is amorphous nanocatalyst. Such nanomaterials with irregular atomic ordering exhibit tremendous catalytic properties because of high concentration active center or in other words unsaturated coordination sites relating to dangling bonds in this phase [3,116]. The above-discussed modification techniques or methods are widely followed to develop an efficient NRR photocatalytic system that can reach the set benchmark and make the photon irradiated N_2 conversion to NH_3 reaction a commercial or industrial process.

5. Advance materials or photocatalytic systems were examined for photocatalytic NRR and their respective catalytic efficiency

From the literature survey made on this specific topic of light-oriented dinitrogen reduction to ammonia and the relationship between reported NRR activity and physio-chemical features, the following are few collected photocatalytic systems developed by different research groups around the planet with their corresponding catalytic efficiency.

5.1. Defect and doping engineering

The defects (oxygen, sulfur, and nitrogen) introduction into the photocatalyst is seen as a better approach for the fixation of dinitrogen as discussed above. To start with, Mi et al. fabricated oxygen vacancy (OVs) optimized TiO_2 by a solid phase reduction method in presence of $NaBH_4$ and the defect concentration is modulated by varying the reduction temperature between 310−360 °C. Controlled quantity of vacancy presence magnifying the activity by reducing the recombination process and when present in a large quantity, no doubt increases the adsorption of N_2 molecules but at the same time decreases the lifetime of charge carriers by acting as recombination center and so the net ammonia production pace declines greatly. The obtained IPCE measurement data at 300 nm shows that samples prepared at 340 °C (R-340) have high conversion efficiency i.e. 10.9 % whereas that of R-360 is 1.9 % only. These results suggest that OVs are optimized in R-340 sample which is nicely supported by the high ammonia production rate of 324.86 μmol/g/h and AQY of 1.1 % at 365 nm over R-340 catalyst compared to other prepared samples. Further, surface photovoltage and steady-state photoluminescence (PL) spectroscopy justified the effective charge separation in the case of R-340 catalyst. Based on the N_2-TDP analysis plot it can be concluded that the chemi-adsorbed N_2 molecules at the vacancy site get polarised by the transfer of an electron from these vacancy points of TiO_2 (containing electron-rich Ti^{3+}) to the anti-bonding orbital of N_2 that weaken the bond strength and increases the rate of conversion. Additionally, DFT calculation was also carried out to find the effect of oxygen vacancy presence and absence on the activation of dinitrogen on the (101) facet of prepared TiO_2 and the outcome indicates that OVs are highly essential in this activation process. Further, N_2-TPD analysis was carried out to investigate the details of the N_2 adsorption and activation process which is very essential in nitrogen fixation reaction. TiO_2 usually possesses a certain amount of OVs because of its low formation energy, high surface energy, and large exposed surface sites of TiO_2. The N_2-TPD data shows two N_2 desorption humps at 130 and 365 °C respectively corresponding to physisorbed and chemisorbed N_2 molecule. Interestingly, with an increase in OVs, the adsorption and activation process becomes more pronounced which indicates the important role of OVs in the performed N_2 photoreduction reaction. R-340 depicts good durability with almost no downfall in the N_2 reduction rate even after 360 min [117]. Through amine assisted hydrothermal method, J. Wang and the group synthesized hydrogen-treated defect-controlled tubular TiO_2 (TiO_2-H_2) from various amine precursor-like urea, dicyandiamide, and cyanamide respectively (as depicted in Fig. 4). However, dicyanamide-derived TiO_2-H_2 (TiO_2-H_2-DA) exhibits excellent stability with a very little decrease in the photocatalytic activity even after 7 continuous cycles. Further, TiO_2-H_2-DA shows a remarkable N_2 reduction rate of 1.2 μmol/L/h which is attributed to the optimal amount of Ti^{3+} or oxygen vacancies that aid the electron-hole separation process and also facilitates N_2 polarization. The presence of rectifying defects due to decomposition of the organic precursor is well characterized by XRD, Raman, XPS, and EPR analysis whereas low charge carrier recombination is comprehensively measured by TRPL, transient current, and impedance spectra [118].

Interesting work was performed by Shiraishi and team on surface oxygen vacancies optimized BiOCl (BiOCl-OVs) toward photocatalytic N_2 fixation in presence of chloride ion-containing water and sea-water (as shown in Fig. 5). The noble-metal free photocatalyst with oxygen vacancy (BiOCl-OVs) was prepared by the facile solvothermal method. Usually, BiOX with $[Bi_2O_2]^{2+}$ tetragonal matlockite layers intercalated by halogen anions double-layer undergoes self-degradation when irradiated in presence of water and becomes dysfunctional. This is due to its characteristic band

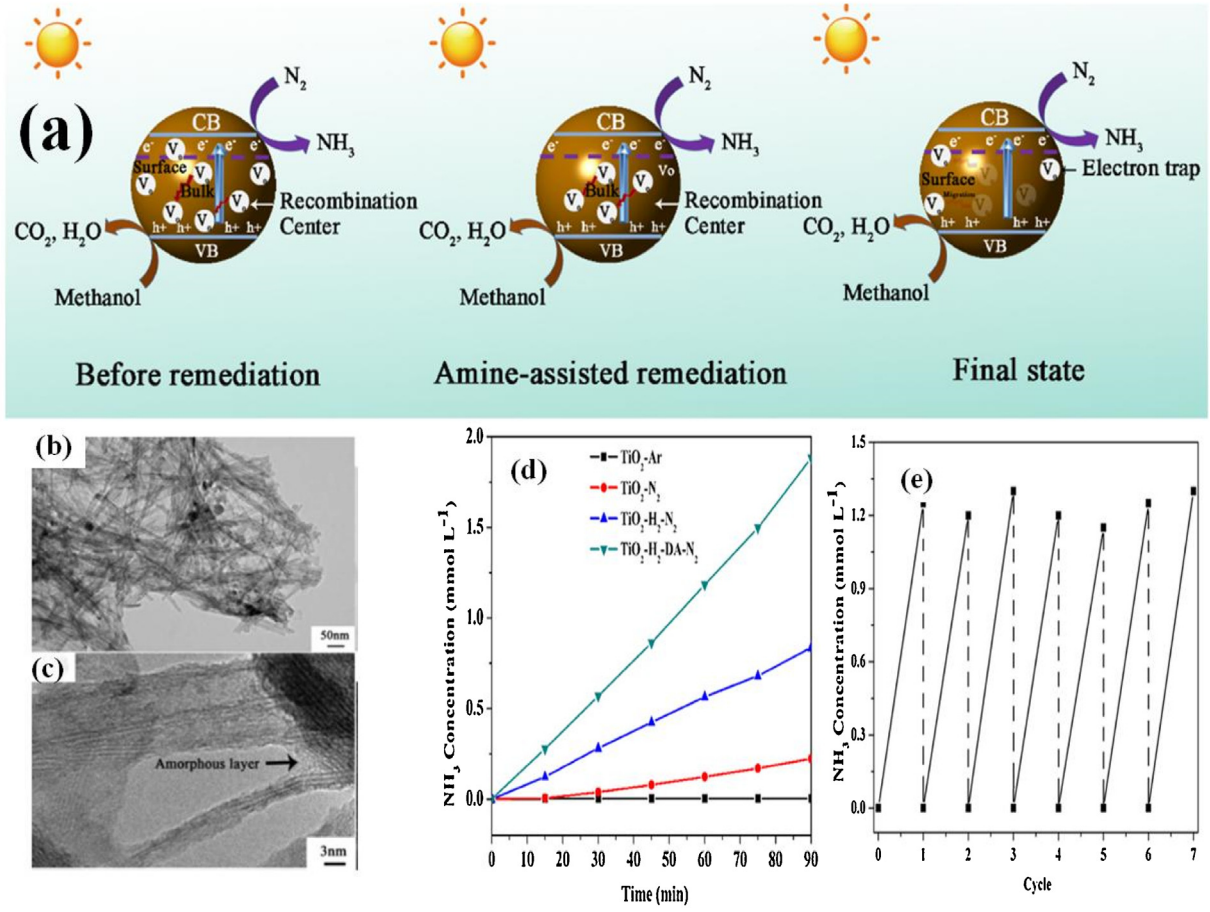

Fig. 4. (a) Represents the photocatalytic mechanism of N_2 fixation under different conditions. (b, c) TEM and HRTEM image of tubular TiO_2 with an amorphous layer of TiO_2-H_2 respectively. (d) Photocatalytic N_2 fixation by TiO_2, TiO_2-H_2, and TiO_2-H_2-DA, and (e) N_2 recycle test with TiO_2-H_2-DA. Reproduced with permission from reference [118].

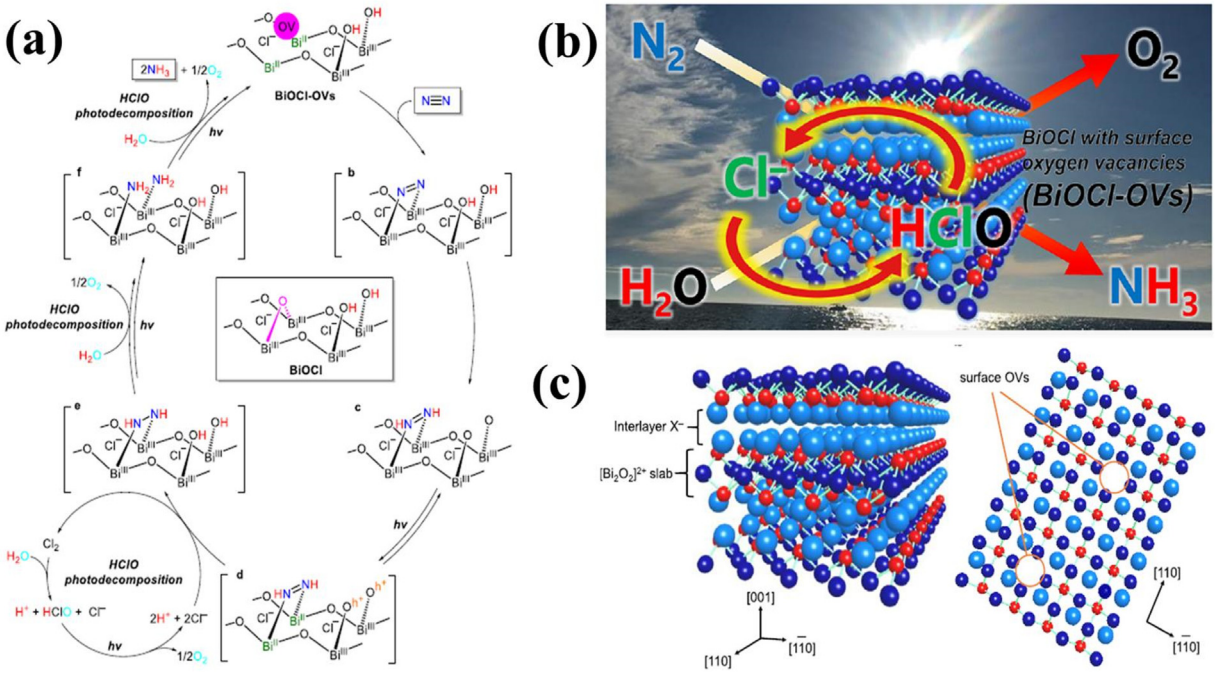

Fig. 5. (a) Proposed photocatalytic pathway for N_2 fixation over BiOCl-OVs in acidic medium, (b) Overall conversion of N_2 and H_2O to NH_3 and O_2 by BiOCl-OVs catalyst, and (c) Represents the crystal and surface structures of BiOX-OVs. Reproduced with permission from reference [119].

arrangement where the valance band that is mainly made of Cl 3p orbital specifically oxidizes intercalated Cl^- ions over water resulting in self-oxidation and self-reduction of lattice Bi^{3+}. But in this case, used hypochloric acid undergoes decomposition to produces chloride ions which refills the leach out interlayer Cl- anions and regenerates the catalytic activity. Further, the presence of oxygen defects stimulates the N_2 adsorption and activation process. In this reduction, process water acts as the electron donor and the BiOCl-OVs show a benchmark solar-to-chemical conversion efficiency of 0.05 % in artificial seawater under-stimulated solar light which is comparable to the average efficiency of natural photosynthesis of plant [119].

Further, the work of Zhang group i.e. sulfur vacancy constituted In_2S_3 hallow nanotube prepared from MIL-68 (In) precursor by self-templating and calcination method depicts a significant N_2 photoreduction activity of 52.49 mmol/h/g. Interestingly, the long hexagonal prism type morphology of the MIL-68 is retained in the formed hollow tubular In_2S_3 during the followed sulphidization process. The S-vacancies (characterized through EPR and XPS) play a major part in the process of chemisorption and polarization of N_2 towards a higher rate of NH_3 formation. Additionally, because of these vacancies, the material captures a wide range of photon and fosters the electron-hole separation ability [120]. The nitrogen-vacancy containing g-C_3N_4 fabricated by Wang et al. illustrates its spontaneity towards photocatalytic nitrogen fixation under various sacrificial electron donors (methanol) and is observed to display robust conversion efficiency. Methanol not only acts as a hole scavenger but also possessed a high solubility of N_2 and hence supplies proton for dinitrogen fixation, which ultimately contributes to an improved NH_3 evolution velocity of 3.632 mmol h^{-1} g^{-1} with a notable AQE of 21.5 % (~420 nm) on the K^+ grafted g-C_3N_4 [121]. In another investigation, electron-rich $Cu^{\delta+}$ and oxygen vacancy equipped ZnCr LDH nanosheets were prepared by Zhang and team through a simple co-precipitation method, shows a molecular nitrogen photoreduction of 110 μmol/g/h with excellent selectivity (92 %) and durability (8 cycles) without the support of co-catalyst and sacrificial agent. The electronegative difference between bonded atoms Cu(1.90), Zn(1.65), and Al(1.61) leads to the formation of electron-dense $Cu^{\delta+}$ in the LDH sheets. Further, the light to chemical conversion (LCC) efficiency of 5% Cu-ZnCr-LDH was found to be 0.0042 % under Xe lamp and 0.014 % for AM 1.5 G simulated solar light illumination. DFT, EPR, and XPS studies indicate that Cu introduction to LDH results in the formation of oxygen defect and electron-rich unsaturated $Cu^{\delta+}$ species within the nanosheets that readily favor the charge separation and transfer process, stimulating activation and multi-electron reduction of N_2 to NH_3 [122]. Recently, both the theoretical and experimental results of NRR have been made at ambient conditions by defect engineering of doping. It is found that heteroatom doping not only increases the vacancy states in the system but also constructively accelerates the dinitrogen long lifetime activation and corresponding reduction over the vacancy generated doped catalytic systems. Further, Fu et al. adopted the defect-dopant tactic and reported visible light-responsive hallow porous g-C_3N_4 with N-vacancy and oxygen doping from dicyan diamine via a two steps strategy i.e. low temperature hydrothermal followed by calcination method. The so-formed hollow-porous graphitic carbon nitride with spongy walls and a specific surface area of 220.16 m^2 g^{-1} depicts a high NH_3 production rate of 118.8 mg/L/h/g_{cat} when irradiated under a 500 W Xe lamp source. This enhanced activity is attributed to (i) hollow-loose porous structure, (ii) N-vacancy, and oxygen doping that effectively separates charge carriers and supports nitrogen activation via donor-acceptor chemistry, and (iii) More negative conduction band [123]. Similarly, Liang and co-workers prepared boron-doped g-C_3N_4 with N-defect (BNUCNx) via thermal decomposition of melamine and $NaBH_4$ (Fig. 6). The obtained visible photon active BNUCNx exhibits an improved ammonia generation pace i.e. 435.28 μmol/g/h under 300 W Xe light which is due to the presence of defects and doping that activates N_2 and prolongs the lifetime of electron-hole pairs. The above observation is well explained through the DFT study and catalytic results [124].

In another case, Yu et al. doped Fe into BiOBr lattice and introduced oxygen vacancies to the crystal by the solvothermal method. The author reports that Fe-BiOBr nanosheet produces NH_3 at the rate of 382.68 μmol/g/h (under 300 W Xe lamp), which is 8 times higher than neat BiOBr without any sacrificial agent. Fe doping produces electron-rich O-vacancies and the reduced Fe species transfers its 3d electrons to the π^* orbital (anti-bonding) of N_2 resulting in activation of adsorbed dinitrogen for enhanced NH_3 formation. The oxygen vacancy presence is well illustrated by theoretical calculation, EPR, and XPS measurements [125]. Besides, Zhang et al. doped Fe to $SrTiO_3$ crystal framework forming $Fe_xSr_{1-x}TiO_3$ solid solution ($0 \le x \le 0.20$) by hydrothermal followed by calcination at 700 °C and found that when Fe contained lies between 0.03 and 0.20, the catalyst depicts notable N_2 fixation. But among the doped $Fe_xSr_{1-x}TiO_3$ samples, $Fe_{0.10}Sr_{0.90}TiO_3$ catalyst gives the result i.e. 30.1 μmol g^{-1} h^{-1} of NH_3 formation which is 3.2 fold higher than neat $SrTiO_3$. When Fe concentration goes beyond 0.10, the doped $Fe_xSr_{1-x}TiO_3$ material gets converted to a binary composite of Fe doped $SrTiO_3$ and α-Fe_2O_3 which exhibits low catalytic activity as the haematite part supports charge recombination. Further, experiments disclose that surface Fe(III) doped center assist interfacial charge migration from doped catalyst to adsorbed dinitrogen promoting elementary N_2 reduction by a $6e^-$ reduction pathway. Further, to figure out N_2 chemisorption and activation mechanism over the designed photocatalysts, N_2-TPD analysis is carried out. The parent catalyst i.e. $SrTiO_3$ shows an intense N_2 desorption band at 79 °C without any TCD signal after 200 °C indicating loose binding of N_2 via physisorption. Whereas in the case of $Fe_xSr_{1-x}TiO_3$ catalysts (X = 0.05 to 0.10) a strong desorption peak is observed about 90 −95 °C along with two low intense signals at ~380 and ~450 °C which suggest different chemisorption of N_2 molecule. However, the $Fe_{0.10}Sr_{0.90}TiO_3$ sample depicts additional signals at 300 and 680 °C suggesting that surface Fe^{3+} doped sites facilitate N_2 chemisorption and successive activation which encourage the N_2 photofixation process. Adding more to this, $Fe_{0.10}Sr_{0.90}TiO_3$ shows extraordinary stability up to 3 recycles of 5 h each without any significant change in activity and structural framework as confirmed by XRD and XPS pattern of the sample before and after 15 h catalytic run [126]. Extending the research in the direction of vacancy chemistry, Xiao research group introduced both Fe and oxygen vacancy to BiOCl nanosheet lattice (as depicted in Fig. 7) and observed a great lift in ammonia production speed i.e. 1.022 mmol·g^{-1} h^{-1} with a TOF of 0.863 h^{-1} and AQY equal to 1.8 % at 420 nm for 5% Fe doped BiOCl system. The team found a volcanic type performance of the catalyst between NH_3 formation and the amount of Fe doped to BiOCl crystal. From XPS analysis the author observed that electron flows from Fe to Bi and N_2-TPD suggest that N_2 reduction occurs in the vacancy site. The group found that no appreciable change in activity and morphology of the best catalyst even after 5 conjunctive runs which reflects the ultra-stability of the photocatalyst [127].

In another work, Xiong et al. prepared a series of Bi_5O_7Br nanostructured NRR catalysts by low-temperature thermal method (20−100 °C). The 40 °C treated tubular Bi_5O_7Br sample shows the best nitrogen fixation rate among other prepared photocatalysts i.e. 12.27 mM·g^{-1} h^{-1} which corresponds to the low bandgap, high concentration of oxygen vacancies, better diffusion of charge carriers, and low charge transfer resistance. The effective adsorption and polarization of dinitrogen are further promoted by the presence of oxygen vacancies which is the vital step in nitrogen fixation reaction. This is well monitored by in situ infrared spectroscopy and

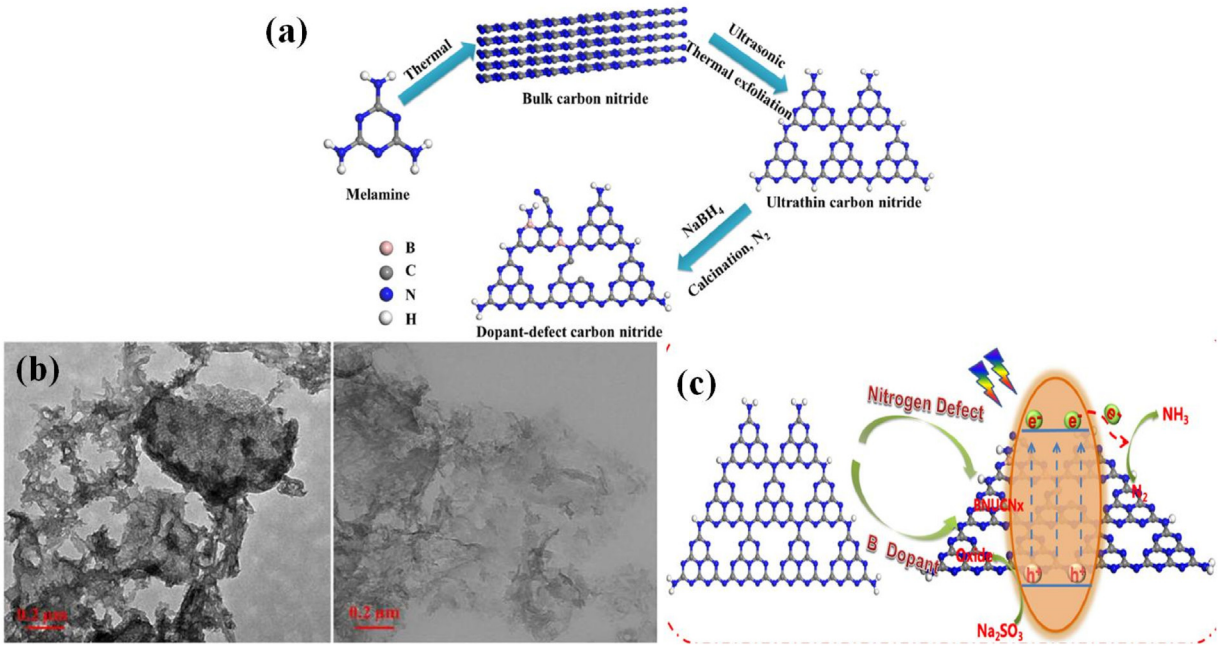

Fig. 6. (a) Synthesis protocol of BNUCNx. (b) TEM pictures of CN and BNUCNx sample and (c) Plausible mechanism for photocatalytic NH_3 generation by BNUCNx catalyst. Reproduced with permission from reference [124].

DFT study (Fig. 8). Further, the scavenger test suggests that oxygen vacancy and superoxide radicals play a primary part in nitrogen photoreduction reaction [128]. With the idea that refining defect states by doping technique are an effective tactic towards solving the associated problems with dinitrogen fixation i.e. polarization of strong triple bond and successful protonation, Xiong research team prepared Mo doped $W_{18}O_{49}$ ultrathin nanowires by solvothermal method. The low valence Mo doped $W_{18}O_{49}$ nanowires in which coordinatively unsaturated metal atoms (CUS) equipped with oxygen defect sites encourage polarization of attached N_2 via fast electron migration from CUS to dinitrogen (due to metal-oxygen covalency) resulting in easier N≡N bond fission by a proton coupling mechanism. The deep insight of the above concept is vividly described by the DFT study. Because of this Mo doping, the defect states move towards the Fermi level making the photoelectrons more powerful to successfully carry out the N_2 reduction process. Among the prepared photocatalysts 1% Mo doped $W_{18}O_{49}$ sample depicts the best performance of 195.5 $\mu mol\, h^{-1}\, g^{-1}$ with an AQY of 0.33 % at 400 nm and solar-to-ammonia efficiency of 0.028 % under-stimulated AM 1.5 G light illumination [50].

Adding more to the survey, the author's group has also explored the benefits of doping chemistry on nitrogen fixation, in which the team developed boron and sulfur-doped carbon modified TiO_2 (CT) catalyst by a facile one-pot method. Doping of non-metal (B or S-atoms) to the anatase TiO_2 lattice drives UV-TiO_2 to Vis-TiO_2 with oxygen vacancies as assisted by UV–vis spectroscopy and XPS analysis. Among the doped TiO_2 samples, B doped CT shows the best activity of 32.38 $\mu mol\, L^{-1}$ and an ACE equal to 0.076 % in 10 % methanol solution at low pH conditions. The observed boost in performance is attributed to oxygen defect and porous structure [64].

5.2. Nanostructure engineering

In the context of nanostructure engineering, crystallographic modification, amorphization technique, functionalization, development of particular crystal structures and exposed facets in metal oxides type of systems results in the creation of a large number of defect centers (due to extend of distortion in the atomic array) and dangling bonds (unsatisfied or uncoordinated atoms) in the catalyst which successfully captures inert or non-polar molecules like N_2 and reduces the activation barrier. Thinking of the promising outcomes of amorphization engineering, Chen and partner reported an amorphous-crystalline heterophase-oriented spherical CeO_2 catalyst with a controlled quantity of oxygen vacancy via reversing abnormal Ce (III) pyrolysis method from cerium based oxide-carbonate precursor at high temperature in an inert atmosphere. HRTEM image demonstrates the presence of both amorphous and crystalline character within the same material, whereas XPS and EPR analysis confirm the occurrence of oxygen defect. The observed high N_2 photoreduction ability of the A-$CeO_{X\text{-}4}$ sample (i.e. NH_3 production rate of 109 $\mu mol\, h^{-1}\, g^{-1}$ and AQY of 4.23 % at 425 nm) is attributed to the presence of oxygen vacancies that traps the photoelectrons and increases the concentration at the catalyst surface (supported by TRPL and transient current plot) which later get utilized in polarising and reducing the triple bond order of adsorbed nitrogen for protonation. From the temperature and pressure experiment, it was concluded that with an increase in temperature and pressure the rate of NH_3 formation increases. Reserving Ce (III) ions strategy by carbonates pyrolysis at inert condition is responsible for amorphization and oxygen vacancy in the CeO_2 matrix [129]. Additionally, facet-oriented materials are of great interest nowadays in N_2 reduction chemistry, based on the above idea Zhang et al. developed (001) facet engineered BiOBr nanosheet model catalyst with optimized oxygen vacancies and localized π electrons by solvothermal method. The characteristic (001) plane of the BiOBr sheet terminating with oxygen atoms of high density enables oxygen vacancy formation in normal conditions. The prepared UV–vis-photon-sensitive catalyst (BOB-001-OV) displays a high ammonia production rate of 223.3 $\mu mol\, h^{-1}\, g^{-1}$ (UV–vis light) and 104.2 $\mu mol\, h^{-1}\, g^{-1}$ (visible light) with an external quantum yield of 0.23 % at 420 nm without any scavenger and cocatalyst. The coordinated N_2 is activated by the back donation concept where d-electrons or the charge on the vacancy site (Ov) is transferred to the π antibonding orbital of N_2 causing elongation of the triple bond and hence easing the

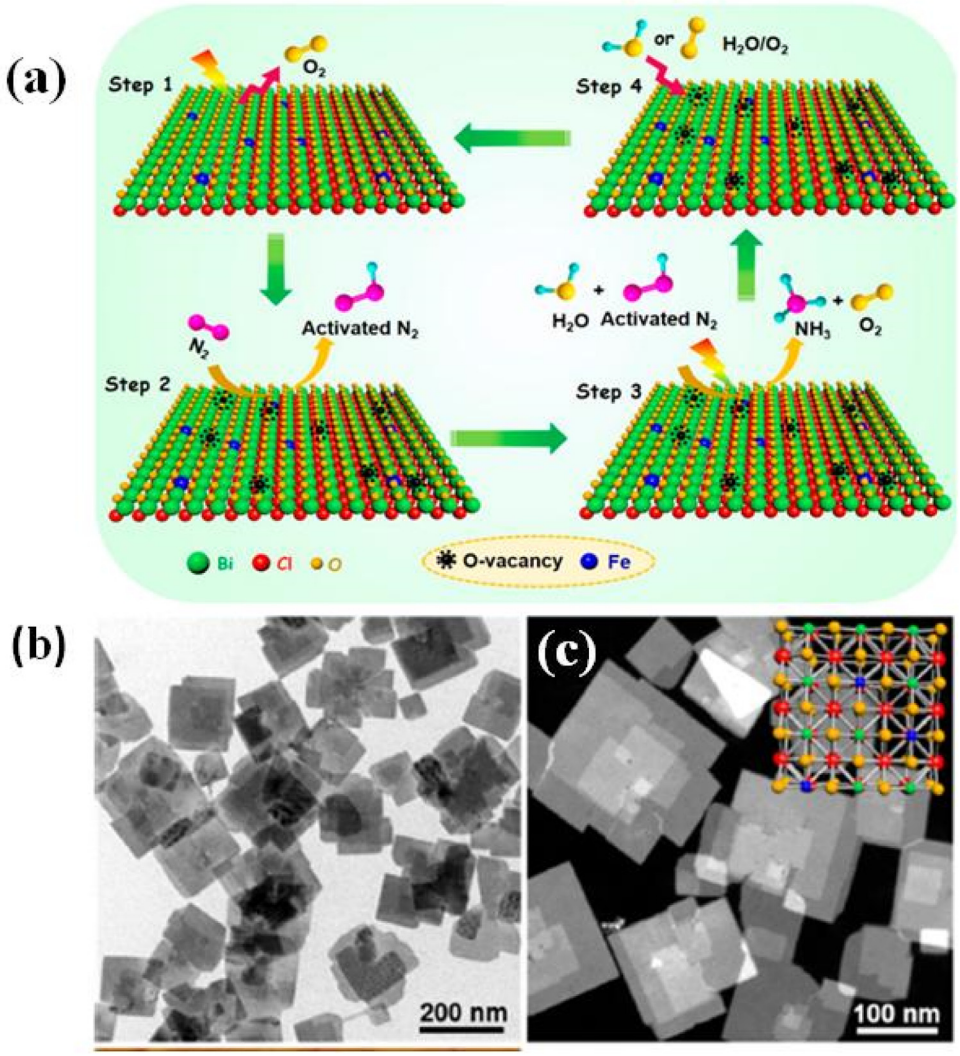

Fig. 7. (a) Represents a schematic model for photocatalytic N_2 fixation, and (b and c) TEM and HAADF-STEM pictures of 5% Fe-BiOCl NSs. Reproduced with permission from reference [127].

bond-breaking process. Usually, the conduction band potential of BiOBr is not at the right position for direct reduction N_2 or form solvated electrons but the presence of oxygen defect makes the process feasible as justified by computational study. The catalyst shows long-term stability of 8 consecutive cycles without any significant loss of catalytic activity. Further, to verify the N_2 fixation reaction at Ov site of (001) facet, N_2-TPD, and *in situ* diffuse reflectance, Fourier transform infrared analysis is carried out while the effective charge carrier separation dynamic induced by Ov is characterized with TRPL and room temperature steady-state and transient photocurrent measurements. Additionally, N_2 fixation is also associated with lots of by-product like N_2H_4, $^{-}NO_2$, and $^{-}NO_3$ but interestingly in the present investigation very negligible amount (2.4 % for N_2H_4, and 1.9 % for -NO_3) of such residual chemical species is reported which is due to the end-on type mechanism and less NH_3 oxidation possibility [48]. Again, Chen and the team designed a cyano-group modified g-C_3N_4 catalyst (detail shown in Fig. 9) by heating prepared g-C_3N_4, melamine, and LiCl/KCl salt together at 550 °C in an alumina boat. The formed CG—CN photocatalyst shows an NH_3 production rate of 442.92 $\mu g/h/g_{cat}$ in absence of sacrificial chemical and noble metal-based co-catalyst. The introduction of cyano group by molten salt calcination method is found to be effective as it helps in reducing the charge recombination process and also promotes the activation of adsorbed dinitrogen due to its electron-withdrawing effect, which was confirmed through *in situ* Fourier transform infrared and Nitrogen temperature-programmed desorption analysis (N_2-TPD). To justify that ammonia is generated from the supplied N_2 and water without destroying the catalyst, IC and Proton-NMR measurements are performed. Theoretical study reveals that N-atom directly bonds to cyano moiety have higher Lewis acidic character (lower charge density) compared to C≡N group (higher charge density), which further suggests that the cyano group increases the activation of N_2 towards NH_3. Additionally, the best photocatalyst shows tremendous durability with no obvious change in catalytic performance even after 4 consecutive cycles [130].

5.3. Inorganic-organic molecular catalyst type

On the theme of the molecular catalyst concept, the Haung research team fabricated a series of functionalized Ti-MOF (NH_2-MIL-125, CH_3-MIL-125, and OH-MIL-125) hydrothermally by ligand substitution method in MIL-125 (Ti) and then subjected to photoreduction of N_2 to NH_3 under an ambient condition in absence of sacrificial reagent. It was reported that out of all, NH_2-MIL-125 displays the best NH_3 yield of 12.3 μmol/g/h, and AQY of 0.26 % is attributed to the creation of Ti^{3+} species via electron transfer from ligand to metal charge (LMCT) mechanism. The Ti_8 defect sites con-

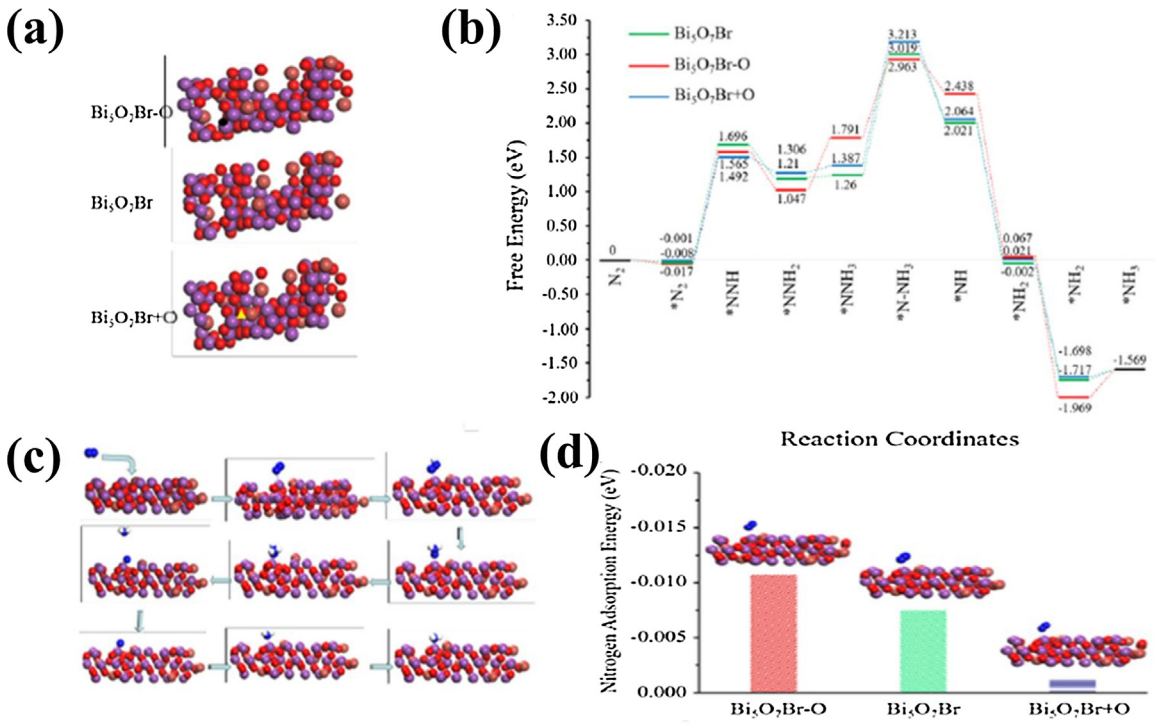

Fig. 8. (a) Structural models of anoxic Bi_5O_7Br-O, pristine Bi_5O_7Br, and oxygen-enriched Bi_5O_7Br $Bi_5O_7Br + O$ along with defect and rich oxygen (b) Reaction energy diagram of nitrogen fixation catalyzed by Bi_5O_7Br-O, Bi_5O_7Br, and $Bi_5O_7Br + O$. (c) Illustration of nitrogen fixation pathway, and (d) Nitrogen adsorption energy (eV) on the surfaces of Bi_5O_7Br-O, Bi_5O_7Br, and $Bi_5O_7Br + O$. Reproduced with permission from reference [128].

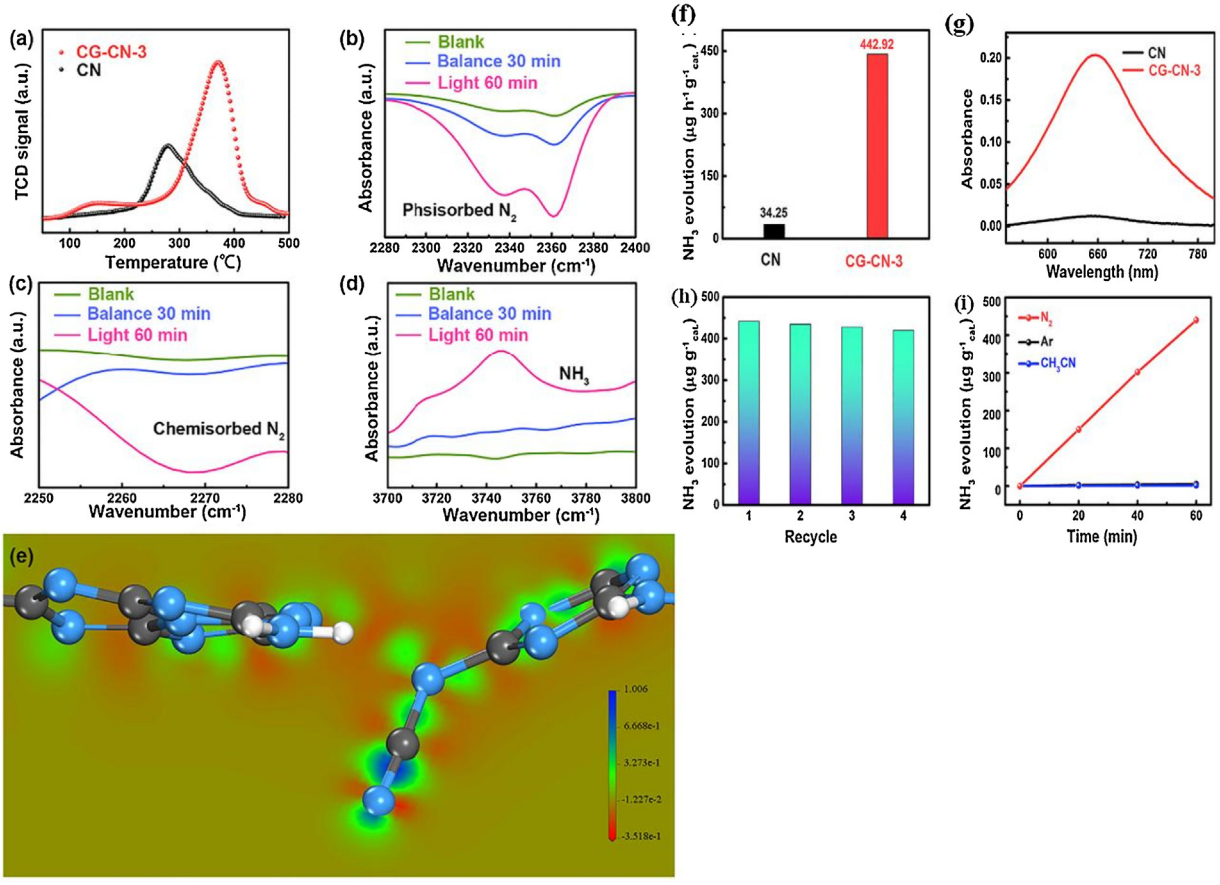

Fig. 9. (a) N_2-TPD of CN and CG-CN-3, (b-d) In situ FT-IR spectra on CG-CN-3, (e) Charge density difference of CG-CN-3, (f) Nitrogen fixation rate of CN and CG-CN-3,(g) Absorbance spectra of the solution containing NH_3 and indophenol indicator, (h) Cycling experimental performance of CG-CN-3 and (i) Photofixation of N_2 in different condition. Reproduced with permission from reference [130].

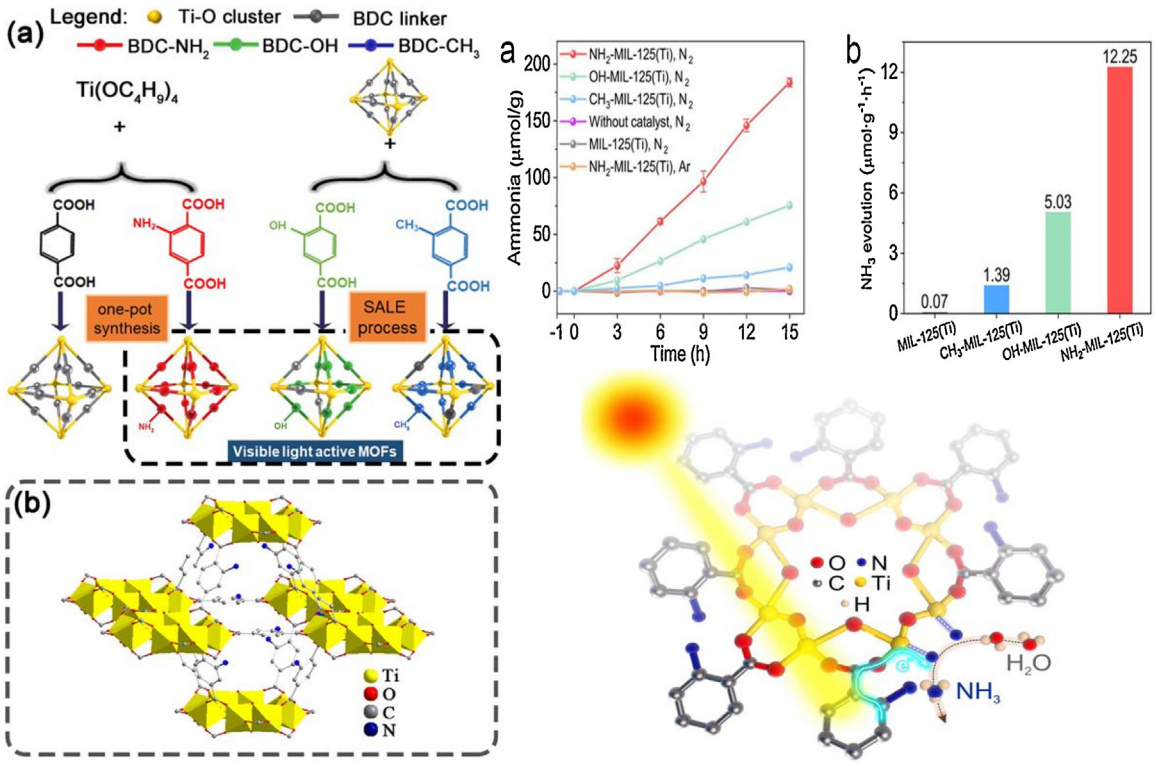

Fig. 10. (a) Scheme representing different visible active MOFs for N_2 photofixation,(b) Schematic picture of ammine functionalized MIL-125(Ti), (c) Amount of ammonia formation over different prepared MIL-125 catalyst, (d) Rate of NH3 yield over different photocatalyst for 15 h and (d) Proposed mechanism of NH_3 production by MIL-125(Ti). Reproduced with permission from reference [131].

taining Ti(III) bring about the activation of attached N_2 by donating an electron to the antibonding orbital of nitrogen molecule resulting in weakening of the triple bond and itself transferring back to Ti^{4+} that makes the reduction of adsorbed N_2 to ammonia easier. This electron migration from Ti^{3+} to N_2 is well confirmed through the TRPL study (Fig. 10) [131].

In another work, to improve the aqueous phase dinitrogen photo-fixation to ammonia under an ambient condition in absence of sacrificial agents, Zhong et al. reported highly stable single-atom anchored ultrathin co-valent triazine framework nanosheets (CTF) with Pt-N_3 as the active sites (Pt-SACs/CTF) by photo-deposition technique (Fig. 11). The deposition of Pt over the surface of 2D-CTF-PDDA-TPDH is diagnosed by XPS and HADDF-STEM characterization whereas the partial charge transfer from Pt to CTF is analyzed via DFT and XANES study. The fitting EXAFS curves suggest that Pt is bonded to three N-atom of CFT sheets which is again supported by the DFT study. Further, the computational calculation data implies an alternative reaction pathway for N_2 photoreduction over the Pt-N_3 site of Pt-SACs/CTF catalyst. The empty sp^3 hybrid orbital of Pt in the Pt-N_3 framework interacts with nitrogen molecules and activates it for reduction to NH_3. Again, Pt loading to the stable 2D-CTF-PDDA-TPDH nanosheets encourages separation of photogenerated electron-hole pairs resulting in an increment in NH_3 production rate i.e. 171.40 μmol/g/h and an AQY of 1.4 % under monochromatic light irradiation [132].

Yang-Guang Li and group prepared inorganic polynuclear metal-oxygen cluster (polyoxometalates: POMs) i.e. a Keggin type highly stable zeolitic imidazolate framework-67(ZIF-67) catalyst with self-healing property. POMs integrated composites are regarded as highly efficient photoelectric N_2 reduction specimens because of the following properties associated with the polyoxometalates, (i) POMs retains their structure even after cascade multielectron and reversible N_2 reduction reaction where redox sites exist simultaneously, (ii) certain POMs absorbs a broad range of light via d-d inter-valency transition and are electron surplus species helping the transfer and storage of electrons, (iii) POMs get reduces by LMCT mechanism in presence of light and sacrificial agents and hence provides sufficient amount of photoelectrons for N_2 fixation,(iv) decreases the recombination process resulting low charge transfer impedance and (v) the reduced POMs retrieves to its original form through oxidation, generating a recyclable N_2 photo-fixation catalytic system. Further, the porous structure of ZIF-67 adds more advantages to the developed ZIF-67@POMs catalyst. The so-formed ZIF-67@$K_{11}[PMo_4V_8O_{40}]$ displays dinitrogen fixation velocity of 149 μmol/L/h with solar to ammonia (STA) efficiency and TOF of 0.032 % and 94 mmol M^{-1} h^{-1} respectively (as shown in Fig. 12). Additionally, the best photocatalyst (ZIF-67@POMs) shows appreciable durability up to 5 cycles with a small decrease in performance i.e. 10 % and this extraordinary stability is well supported by XRD and IR analysis of the sample after the reusability test [133].

5.4. Co-catalyst and composite/heterojunction construction

Adding more to the text, plasmonic Bi-metal deposited $InVO_4$ nanosheets with mesoporous framework synthesized (hydrothermally) by Zheng and group observed that 5% Bi/$InVO_4$ shows an ammonia generation of 626 μmol/g/h. The cause of such improved activity corresponds to the surface plasmonic effect produced by Bi-metal and the developed Schottky barrier at the interface of metallic Bi and $InVO_4$ leading to better separation charge carriers [134]. The developed Au nanocrystal loaded TiO_2 nanotube with a porous framework by Xu et al. via electrospun-photoreduction technique (Au@TiO_2) completely outperform commercial P25 in the performed N_2 photofixation reaction (Fig. 13). The decorated Au nanocrystals improve the electron-hole separation process in

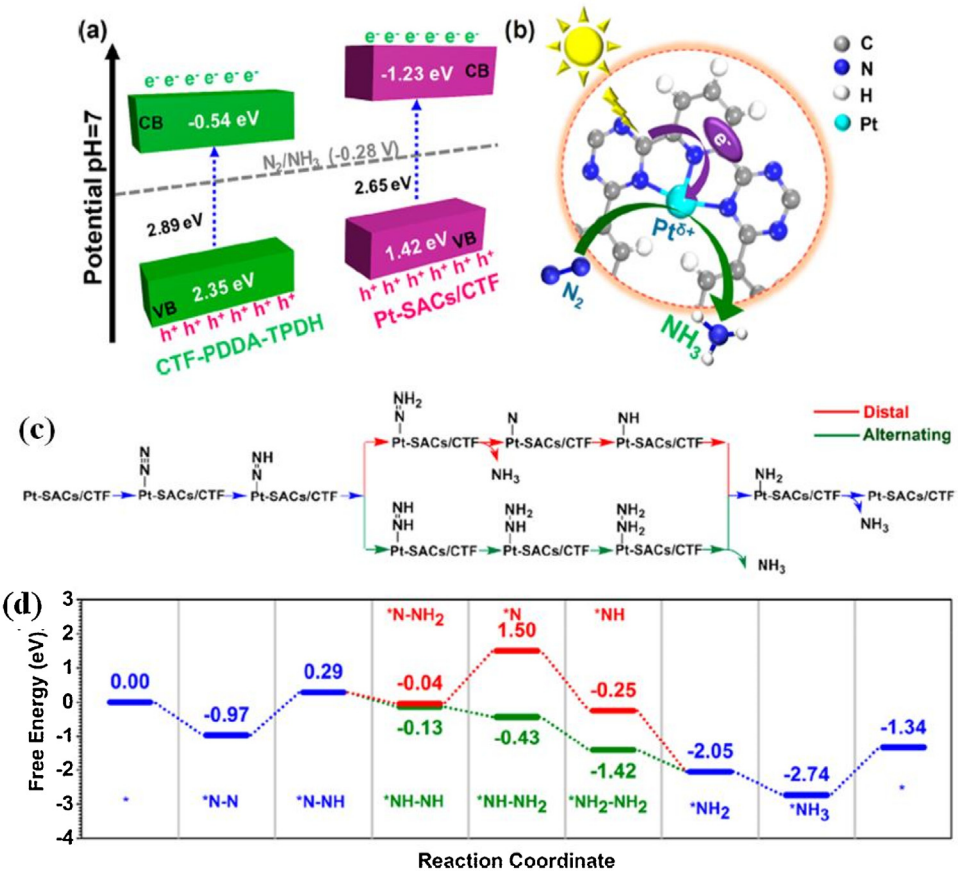

Fig. 11. (a) Represents the band energy diagram of CTF-PDDA-TPDH and the Pt-SACs/CTF catalysts. (b) Photocatalytic mechanism of N_2 fixation over Pt-SACs/CTF catalyst and (c, d) Schematic representation with energy profiles of distal and alternating mechanisms for the nitrogen reduction process on the Pt-SACs/CTF catalyst respectively. Reproduced with permission from reference [132].

the porous TiO_2 NT by an amplified near-field electromagnetic field and resonant photon scattering mechanism. Further, the light absorption range is shifted to the visible region due to the plasmon effect of Au in Au@TiO_2 NT. Additionally, the increase in oxygen vacancy concentration in TiO_2 NT during Au loaded is attributed to an increase of donor levels of TiO_2 during Au deposition because donors are in equilibrium with formed vacancies or increase in oxygen vacancy in TiO_2 is because of charge compensation chemistry. The presence of oxygen vacancies is well characterized by Raman and EPR scans and the delay recombination process through TRPL, LSV, and Pl measurements. Again, oxygen vacancy contained in Au@TiO_2 NT facilitates productive N_2 chemisorption and activation capacity resulting in an AQY of 0.101 % under-stimulated light irradiation (at 350 ± 20 nm). The reusability plot confirms the photostability of the material with a little decrease in activity even after 3 cycles of 5 h each [135].

Further, extending the chemistry of plasmonic catalysis, Wang et al. fabricated a cost-effective porous CuFe plasmon-assisted NRR catalyst from $Cu_{21}Fe_{79}$ powders by sulphuric acid (1.83 M) etching method. In this Cu-based photocatalyst, N_2 gets adsorbed and polarised at the Fe site whereas Cu end generates hot-electron via surface plasmon resonance (SPR) mechanism that ultimately reduces the attached dinitrogen to ammonia. Benefiting from the porous framework and SPR effect, the $Cu_{96}Fe_4$ sample displays distinct ammonia generation velocity of 342 μmol h^{-1} g^{-1} and an STA efficiency of 0.055 % under 250 mW cm^{-2} Xe lamp and retains a 100 % catalytic activity even after ten consecutive cycles. Also, the DFT study indicates an increase in valance state and coordination of Fe atom in $Cu_{96}Fe_4$ plasmonic material during the reaction, which implies the formation of the nitrogen-based complex at the surface and efficacious activation of N_2 over Fe atoms by distal pathway. Besides hot electrons (525 nm), the d-to-s inter-band electronic excitation (365 nm and 420 nm) in the Cu nanocrystal plays a critical part in triggering the catalytic performance of the porous bimetallic NRR catalyst [136]. Extending the surface plasmon concept further, Xiong and the group prepared AuRu core-antenna nanostructure N_2 reducing photocatalyst with benchmark activity under mild reaction conditions without the assistance of any sacrificial agent (as shown in Fig. 14). In this study, the team reported that in the bimetallic alloy, Ru acts as the N_2 reducing site whereas Au supplies necessary electrons to Ru via a plasmon mechanism to carry out the N_2 fixation process. Further, the obtained catalytic results are highlighted in Table 1 [137].

Additionally, He and the group fabricated Ag/$KNbO_3$ nanocomposite via a combination of hydrothermal and photodeposition technique. Highly crystalline $KNbO_3$ nanorods are prepared from Nb_2O_5 precursor in low KOH concentration under a high hydrothermal temperature of 260 °C, whereas Ag nanoparticles are loaded over the nanorods by photodeposition method. The high crystallinity of $KNbO_3$ NRs speeds up the bulk charge separation while deposited Ag particles trap these excited electrons and improve the surface charge carrier separation efficiency in the Ag/$KNbO_3$ composite. Further, due to the SPR effect of Ag nanoparticles, the metal-semiconductor photocatalyst shows visible light capturing ability. Because of all the above mentioned beneficial features, the composite displays a remarkable N_2 photoreduction rate of 385 μmol L^{-1} h^{-1} g^{-1} under-stimulated solar light, 95.3 μmol L^{-1} h^{-1} g^{-1} in visible light, and 526 μmol L^{-1} h^{-1} g^{-1}

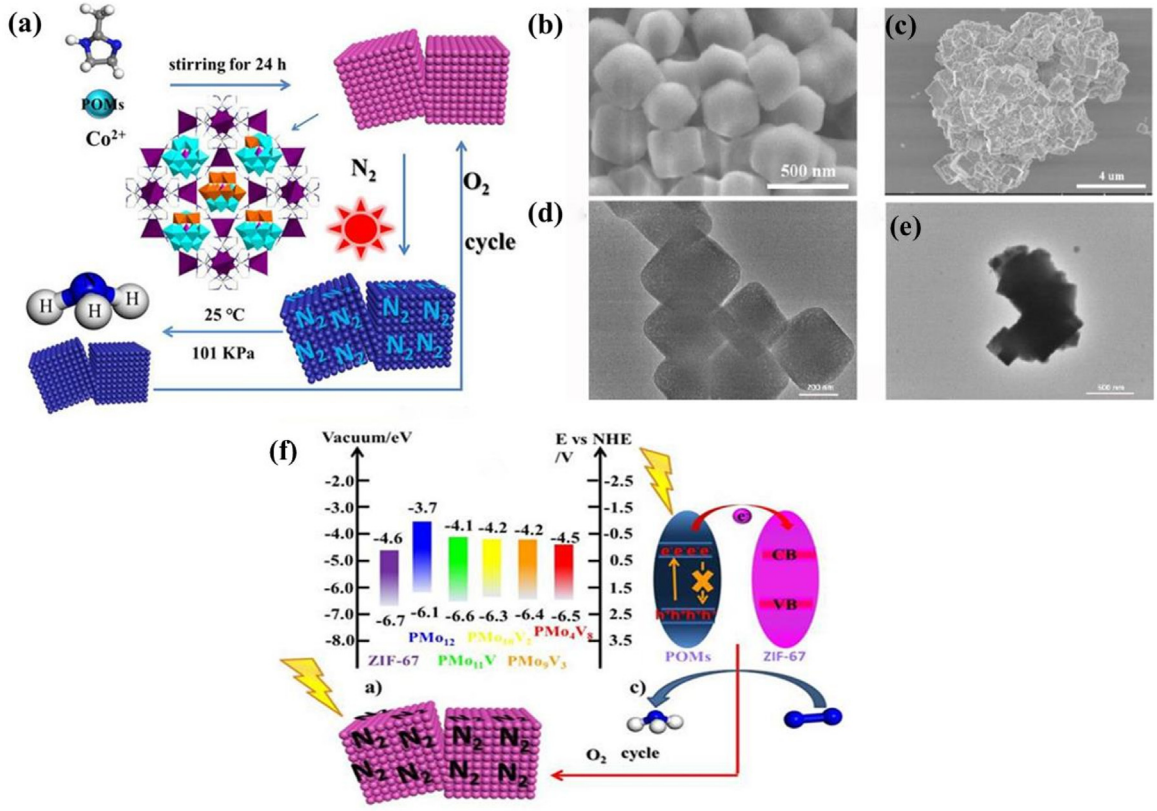

Fig. 12. (a) Schematic representation for the synthesis of ZIF-67 and POMs composite, and (b, c, d, e) SEM and TEM pictures of ZIF-67 and ZIF-67@$PMo_4V_8O_{40}$ respectively, and (f) Mechanism of N_2 fixation over ZIF-67@$PMo_4V_8O_{40}$. Reproduced with permission from reference [133].

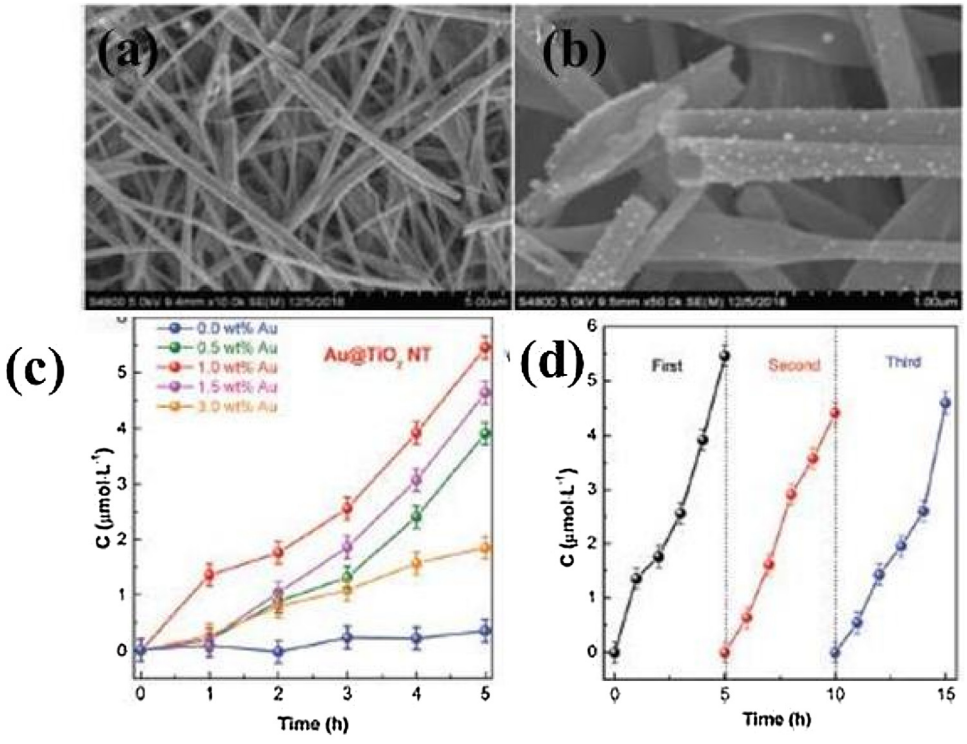

Fig. 13. (a and b) FESEM images of Au nanocrystal decorated TiO_2 nanotube,(c) Photocatalytic ammonia generation over different wt % Au loaded TiO_2 catalysts, and (d) Reusability test of 10 % wt Au@TiO_2. Reproduced with permission from reference [135].

Table 1
Summary of reported photocatalysts for photo-fixation of N_2 to NH_3 under ambient conditions.

Sl.No.	Sample Notation	Conditions	Sacrificial Reagent and Co-catalyst	Irradiation source (wavelength)	Catalytic efficiency	Rate of NH_3 formation	Durability	Estimation technique	ReferenceNo.
1	F-Vo-TiO_2	0.5 g catalyst + 500 mL of DI water	Both Absent	300 W Xe lamp	AQE = 0.38 % at 420 nm	206 μmol h^{-1} g^{-1}	25 h	Ion chromatography	[7]
2	Edge-rich black phosphorus nanoflakes (eBP NFs)	0.5 mg catalyst+ ultrapure water saturated with N_2	Na_2SO_3 no co-catalyst	420 nm LED lamp	Data not available	2.37 mmol/g/h	8 h	Nessler's reagent method	[34]
3	CdS:nitrogenase MoFe protein biohybrid	0.5 mg mL^{-1} catalyst + 500 mM HEPES (aq)	500 mM HEPES (aq), no co-catalyst	405 nm (~3.5 mW cm^{-2})	QY = 3.3 % TOF=75 min^{-1}	315 ± 55 nmol (mg MoFe protein)$^{-1}$ min^{-1}	Data not available	colorimetric ammonia assay kit (BioVision)	[39]
4	Sb_>3.0k_CF	1mg catalyst + 5 mL of water containing 20 % methanol	methanol, no co-catalyst	300 W Xenon lamp	TOF = 0.16 h^{-1}	388.5 μgNH_3 h^{-1} $gcat^{-1}$	5 h	Indophenol blue method/ Ion chromatograms	[44]
5	2D MXene-derived Nb_2O_5/C/Nb_2C/g-C_3N_4 heterojunctions	50 mg catalyst + 50 mL of methanol-double distilled water solution (20 %, v/v)	Methanol, no co-catalyst	300 W Xe lamp	Data not available	0.365 mmol/h /g (neutral) and 0.927 mmol/h /g (pH 9)	10 h	Nessler's reagent method	[74]
6	AuRu core antenna Nanostructures (shown in Fig. 14)	0.2 mg catalyst + 3 mL of DI water	Both Absent	300 W Xe lamp 400 mW cm^{-2}	AQY = 0.21 % (350 nm) and 0.17 % at 550 nm	101.4 μmol g^{-1} h^{-1}	24 h	Ion chromatography	[137]
7	$Co_{0.5}Fe_{0.5}In_2S_4$ ultrathin nanoflowers	40 mg catalyst +100 mL N_2 saturated aqueous solution	Both Absent	Xe lamp with an AM 1.5 Filter (100 mW cm^{-2})	AQY = 1.65 % at 350 nm,1.09 % at 400 nm and 0.12 % at 450 nm	85.8 μmol/g/h	12 h	Indophenol blue method and Nessler's reagent method	[149]
8	Alkali etched ZnCr-LDH nanosheets	30 mg catalyst +150 mL N_2 saturated ultrapure water	Both Absent	300 W Xe lamp(5.0 W/cm^2)	QE = 0.95 % at 380, 0.34 % at 420 and 0.11 % at 550 nm	33.19 μmol/g/h	5 h	Ion chromatography	[150]
9	Au@In_2O_3 HS	50 mg catalyst +90 mL N_2 saturated aqueous solution	No scavenger but Au as co-catalyst	500 W Hg lamp	Data not available	0.605 mol/g/h (normalized)	6 h	Indophenol blue method and Ion chromatography	[151]
10	N-MoS_2 microsphere	30 mg catalyst +45 mL water +5 mL methanol saturated with N_2	Methanol, no co-catalyst	300 W Xe lamp	Data not available	101.2 μ mol/g(cat)/h	20 h	Nessler's reagent method	[152]
11	g-C_3N_4 nanosheets/Bi_2MoO_6 photocatalysts	40 mg catalyst +2 mL water +40 mL ethanol(0.789 g/L) saturated with N_2	Ethanol, no co-catalyst	500 W Xe lamp (100 W/cm^2)	Data not available	3271 mmol/L /g	4 h	Nessler's reagent method	[153]
12	Defective $Bi_2O_2CO_3$ (BOC – X)	30 mg catalyst + 50 mL of methanol-water solution (5%, v/v)	Methanol, no co-catalyst	UV light (<365 nm, 42.51 mW cm^{-2}), visible-near infrared light (>420 nm, 13.25 mW cm^{-2}) and simulated sunlight (14.73 mW cm^{-2})	AQY = 1.02 % at 420 nm	957 μmol L^{-1}	20 h	Nessler's reagent method	[154]
13	1.5% BPNS/CdS	60 mg catalyst + 250 mL of methanol-water solution (1%, v/v)	Methanol, no co-catalyst	300 W Xe lamp	Data not available	240.17 μmol g^{-1} · h^{-1}	16 h	Nessler's reagent method	[155]

Table 1 (*Continued*)

Sl.No.	Sample Notation	Conditions	Sacrificial Reagent and Co-catalyst	Irradiation source (wavelength)	Catalytic efficiency	Rate of NH_3 formation	Durability	Estimation technique	ReferenceNo.
14	Au nanoparticle-embedded hollow mesoporous carbon nitride spheres (HCNSs)-NV	50 mg catalyst + 80 mL of methanol-water solution	Methanol, Au co-catalyst	300-W Xe lamp	Solar-to-ammonia conversion efficiency of 0.032 % and AQY of 0.64 % at 550 nm	783.4 μmol h^{-1} $gcat^{-1}$	4 h	Nessler's reagent method	[156]
15	Ti_3C_2 MXenes–P25	50 mg catalyst + 70 mL of methanol-water solution	Methanol, no co-catalyst	300 W Xe lamp	Data not available	43.44 μmol/g	3 h	Para-(dimethylamino) benzaldehyde method	[157]
16	In-built bionic "MoFe-cofactor" in Fe-doped two-dimensional $MoTe_2$ nanosheets (Fe-doped $MoTe_2$)	10 mg catalyst + 80 mL of Milli Q water	Both Absent	300 W Xe lamp (400 nm W cm^{-2})	Data not available	129.08 μmolg^{-1} h^{-1}	8 h	Nessler's reagent method	[158]
17	B-doping in g-C_3N_4 nanosheets (BCN)	20 mg +40 mL N_2-saturated 1.0×10^{-3} M Na_2SO_3 solution	Na_2SO_3, no co-catalyst	250 W Xe lamp (0.5 W cm^{-2})	QE = 0.64 % at 420 nm.	313.9 μmolg^{-1} h^{-1}	5 h	Nessler's reagent method	[159]
18	MoS_2 nano-flowers stacked by ultrathin sheets were *in situ* grown on oxygen self-doped porous biochar (MoS_2/OPC)	20 mg catalyst + 100 mL of DI water	Both Absent	300 W Xe lamp	Data not available	37.878 μmol g^{-1}·h^{-1}	20 h	Indophenol blue Method/ Nessler's reagent	[160]
19	MOF-76(Ce)	50 mg catalyst + 100 mL of DI water	Both Absent	300 W full-spectrum light source	Data not available	34 μmol$^{\bullet}$ g^{-1}·h^{-1}	8 h	Indophenol blue Method	[161]
20	Plasmonic MoO_{3-x} nanosheets	50 mg catalyst + 100 mL of pure water	Both Absent	300-W Xe lamp	AQY = 0.31 % (808 nm) and 0.22 % at 905 nm	251.1 μM g^{-1} h^{-1} (λ > 580 nm) 328 μM g^{-1} h^{-1} (full spectrum)	4 h run under different condition.	Ion chromatography and Nessler's reagent method	[162]
21	$Fe_1/C-PPh_3/NaI$	10 mg catalyst + 10 mL pure water +10 mL acetonitrile	Both Absent	Xe lamp of full-spectrum (250 mW cm^{-2})	AQY = 0.05 % at 490 nm	98 μmol$^{\bullet}$ g^{-1}·h^{-1}	100 % production rate for 4h	Ion chromatography	[163]
22	SL g-C_3N_4/$ZnFe_2O_4$ composited	100 mg catalyst + 200 mL of water	Both Absent		Data not available	122.3 μmol/L within 120 min	700 min	Nessler's reagent method	[164]
23	Ultralow-temperature synthesis of small Ag doped carbon nitride	0.1 g catalyst + 200 mL of water containing 5% alcohol	5% Ethanol, Au co-catalyst	300 W Xe lamp	Data not available	1.45 mmol/L/h/gcat	16 h	Nessler's reagent method	[165]

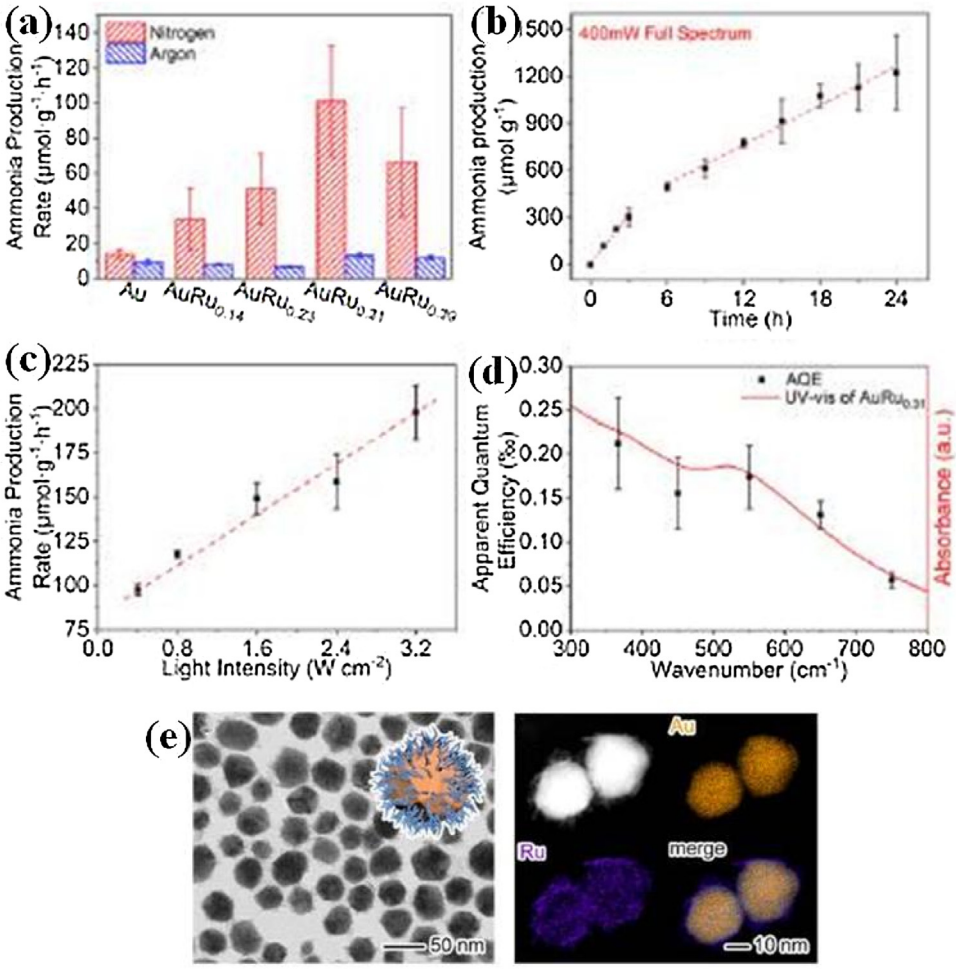

Fig. 14. (a-b) NH_3 production rate of different prepared catalysts, durability test, ammonia production rate by $AuRu_{0.31}$ catalyst in the first 2 h under different light intensity and calculated AQY over $AuRu_{0.31}$ under broad light irradiation, and (e) TEM image of $AuRu_{0.31}$ sample and color EDX mapping image of $AuRu_{0.31}$ catalyst. Reproduced with permission from reference [137].

under UV–vis photon irradiation along with a long term catalytic stability of 30 h without any noticeable change of production rate. Interestingly, the electron tapping type charge separation mechanism is followed over the photosensitized type under-stimulated solar by Ag nanoparticles. Furthermore, the productive excitons separation in 0.5 % $Ag/KNbO_3$ sample that leads to exceptional photocatalytic reduction pace is well confirmed by the observed low overpotential (-0.23 V) and small Tafel slope (144 mV/dec) [138]. To resolve the issues encountered in the above $Ag/KNbO_3$ catalytic system (i.e. cost and performance), Xing et al. modified $KNbO_3$ nanorods with cost-effective NiO co-catalyst forming a $NiO/KnbO_3$ p-n heterojunction composite by simple photodeposition method. The optimum composite ($NiO/KNbO_3$-30) shows an NH_3 production speed of 469.5 $\mu mol\, L^{-1}\, h^{-1}\, g^{-1}$ which further increases to 603.8 $\mu mol\, L^{-1}\, h^{-1}\, g^{-1}$ with more bubbling of N_2 gas under-stimulated sunlight. The reason behind such excellent activity is attributed to (i) effective charge carrier separation via double charge transfer mechanism due to built-in electric field at the interface (supported by impedance and transient current), (ii) low overpotential (-0.26 V), and (iii) minimum Tafel slope value (153 mV/dec) respectively [139]. Combining the characteristic features of MoO_2 (i.e. high conductivity, durability, and electron sink) and BiOCl (i.e. Л-back donation, oxygen defect, and empty 6d orbital), Wang and partner synthesized MoO_2/BiOCl sheet-plate nanocomposite via mechanical mixing procedure which produces ammonia at the rate of 35 μmol/g/h upon Xe lamp irradiation (intensity=500 mW cm^{-2}) in pure water and absence of hole trapping reagents. The high surface electron density and a large number of active site availability on MoO_2 co-catalyst in the composite facilitate effective charge carrier migration and increase the adsorption-activation process of N_2. The formed Mo-O-Bi bond at the junction operates as a mediator and promotes excitons transfer and polarization of N_2. Further, computational and experimental studies confirm that N_2 activation takes place over the Mo horizon in binary-hybrid [140]. In the context of composite and heterojunction system for dinitrogen fixation, extensive research work has been carried out by combining defect oriented single component with the binary or ternary composites. For example, Ma and co-worker reported an elementary NRR catalyst i.e. an *in situ* carbon modified nano-sized crystalline red phosphorous through sublimation-deposition method using SiO_2 nanospheres as a template. The designed photocatalyst (SiO_2/C—RP) shows an NH_3 formation velocity of 0.73 $\mu mol\, h^{-1}$ (4.4 times higher than bulk red phosphorous (BP)) under a Xe lamp source of intensity 320 $mWcm^{-2}$ without scavenger and co-catalyst. The reason behind such substantially increased activity is credited to the large active surface area, broad-spectrum absorption (Vis-NIR), good water dispersibility, and better charge carrier separation. The low water contact angle value *ca* 30° for SiO_2/C—RP suggest that the surface of the material is more hydrophilic in nature compare to bulk RP, favoring effective mass transfer, and wide photon absorption. Further, the obtained transient photocurrent and Nyquist plot confirm

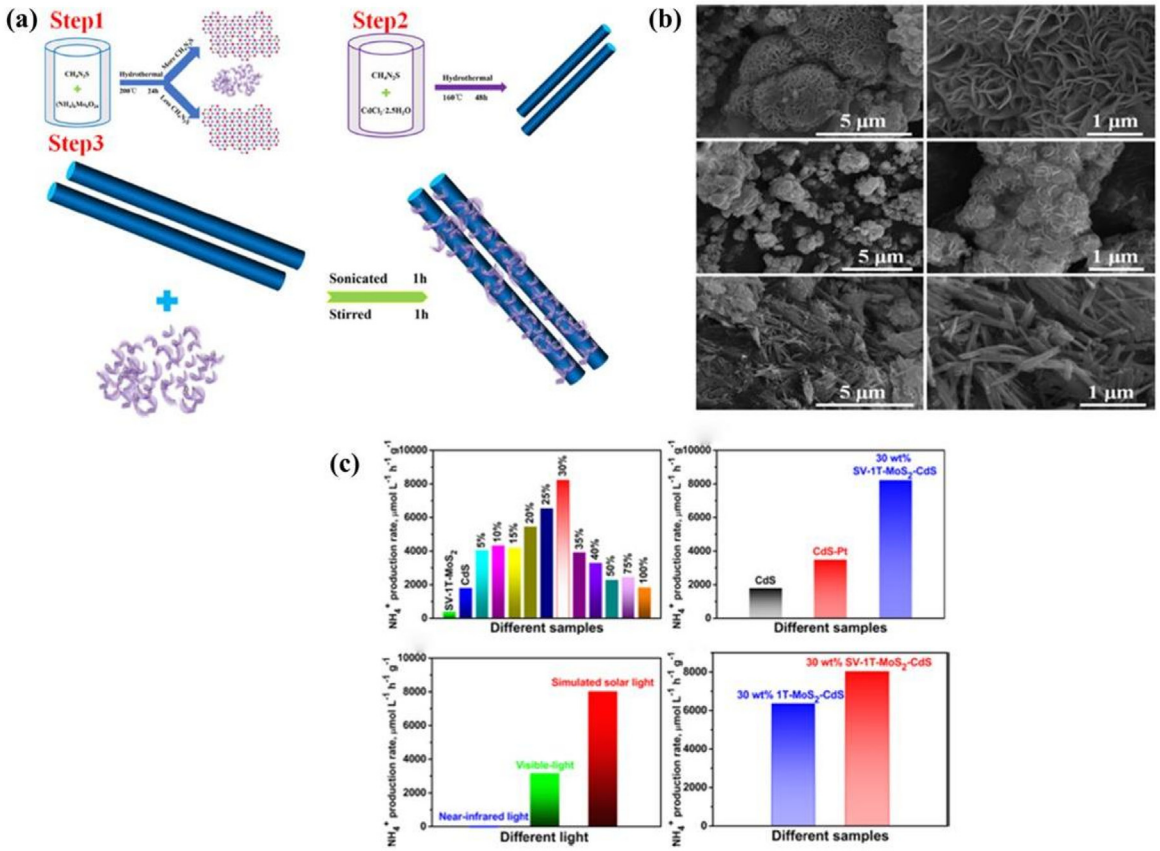

Fig. 15. (a) Schematic representation of the synthesis of 1T-MoS_2/CdS photocatalytic composites. (b) SEM images of SV-1T-MoS_2, 1T-MoS_2, and CdS nanorods and (c) Photocatalytic NH_4^+ production rates by different samples and light irradiation. Reproduced with permission from reference [144].

a low recombination rate. The catalyst also shows tremendous photostability i.e. up to 4 cycles (2 h run each) with a little decrease in ammonia production rate (13 %) [141]. Z-scheme-oriented photocatalytic systems are gathering huge attention because in a single component we can have the benefit of both the combining component. So, the Z or S-scheme oriented (particle-sheet) AgBr/$Bi_4O_5Br_2$ nanocomposite developed by He et al. following hydrothermal and ion exchange technique reports a notable dinitrogen fixation rate of 174.4 μmol/L/h under-stimulated solar light and a photostability of 25 h. The formed heterojunction (i.e. AgBr/$Bi_4O_5Br_2$) exists as Ag/AgBr/$Bi_4O_5Br_2$ (a ternary type hybrid), where metallic nano-silver is formed by the *in-situ* decomposition of AgBr. Importantly, XPS analysis ascertains that an ion-exchange mechanism operates within Ag^+ and $Bi_4O_5Br_2$ which results in the formation of a ternary hybrid i.e. presence of metallic Ag in the AgBr/$Bi_4O_5Br_2$ composite (surface-enhanced Raman scattering). Further, the metallic Ag nanoparticle plays a pivotal role in magnifying the catalytic molecular nitrogen photoreduction process due to (i) acts as a mediator or bridge between AgBr and $Bi_4O_5Br_2$ causing effective charge carrier separation via the Z-scheme pathway and (ii) through surface plasmon effect broaden the light absorption range. Better excitons separation shows a good correlation with LSV, EIS, and transient current measurements. The heterojunction-based catalyst (AgBr/$Bi_4O_5Br_2$) shows a faster rate of N_2 reduction compared to neat samples which is better explained through low overpotential (-0.55 V) and smaller Tafel slope (134 mV/dec) value. The performed scavenger test using isopropyl alcohol and benzoquinone clarifies the detrimental effect of O_2 in dinitrogen fixation reaction [142]. As we know, low solubility and lazy diffusion rate of dinitrogen in water are the reason behind the observed low catalytic conversion efficiency of N_2 to NH_3.To address these drawbacks, Tan et al. performed molecular nitrogen photo-fixation in an aqueous medium over a catalyst having water-attracting-repelling type morphology with triphase (gas-liquid-solid) reaction interface mechanism. The so-formed binary composite ($Bi_4O_5Br_2$/ZIF-8), $Bi_4O_5Br_2$ acts as the hydrophilic part, and ZIF-8 as the hydrophobic end. The water-repelling MOF unit (ZIF-8) catches the surrounding air when comes in touch with the liquid phase resulting in the formation of gas-liquid-solid triphase at the micro or nano range. The hydrophobic and hydrophilic nature of the combining units is fully characterized by contact angle measurements. In this triphase type reaction, the supplied nitrogen gas directly interacts with the catalyst interface without going through the liquid phase triggering systematic and productive absorption of photogenerated electrons, thereupon accelerating the photoinduced activation and reduction process. The binary photocatalyst ($Bi_4O_5Br_2$/ZIF-8(30 %)) with excellent triphase contact displays an elevated ammonia formation velocity of 327.338 μmol L^{-1} h^{-1} g^{-1} which is nearly 3.6-fold higher than neat $Bi_4O_5Br_2$ [143]. The prepared ultra-stable sulfur vacancy concentrated oxygen doped 1T-MoS_2 nanosheet decorated with CdS nanorods by Tian et al. (30 wt% SV-1T-MoS_2-CdS composites) manifest benchmark N_2 photoreduction ability of 8220.83 μmol L^{-1} h^{-1} g^{-1} and AQY of 4.42 % under-stimulated solar light (Fig. 15). CdS and SV-1T-MoS_2 were synthesized via the hydrothermal method and later mixed and evaporated to give the final product i.e. SV-1T-MoS_2-CdS composites. The concentration of S-vacancies and phase ratio within the sample is maintained by controlling the number of Mo and S precursors. Excess thiourea that is attached to the primary crystallites, preventing directional or particular plane-oriented nucleation of crystals results in S-vacancy formation. SV-1T-MoS_2 acts as a co-catalyst in the binary SV-1T-MoS_2-CdS composites and surpasses the activity of Pt co-catalyst

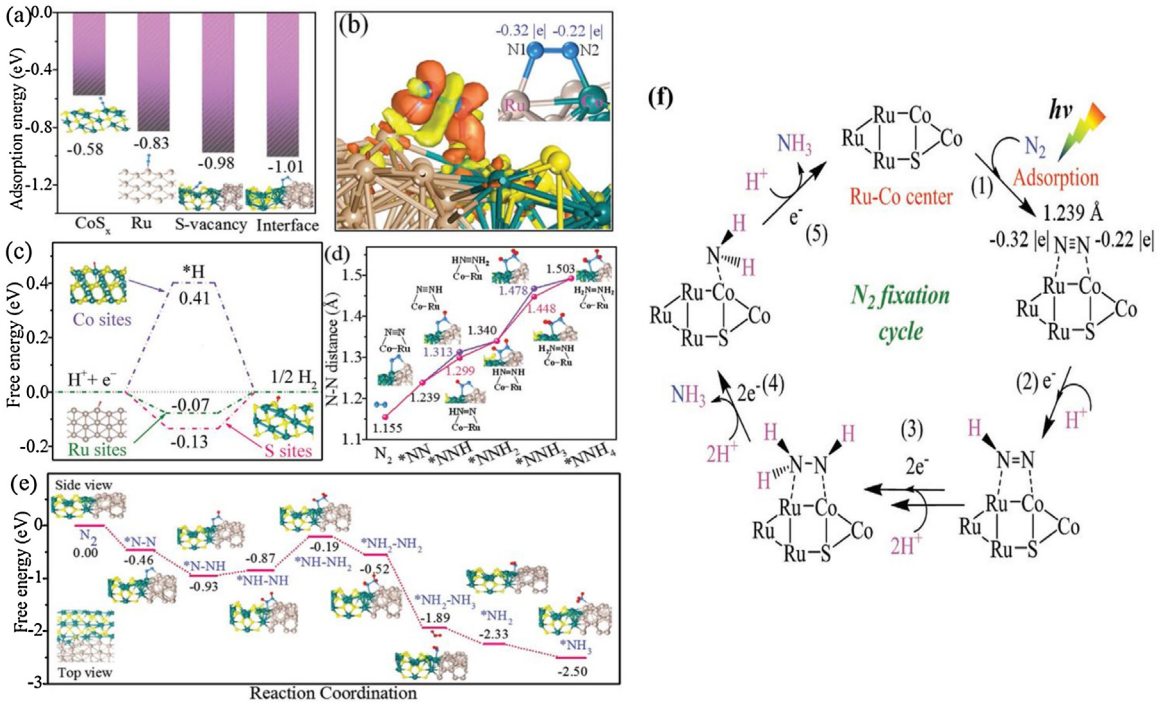

Fig. 16. Represents the theoretical calculations (a) Adsorption energy of N_2 on single site of Ru, Co (or S-vacancy) in CoSx and Ru/CoSx interface, (b) Differential charge density in Ru/CoSx interface, (c) Free energy of HERs on Ru and Co in CoSx, (d) N–N distances of free N_2 and intermediates during hydrogenation, (e) N_2RR pathway on Ru (001)/CoSx(101) interface and (f) Mechanism of N_2 fixation over Ru/CoSx surface. Reproduced with permission from reference [146].

towards photocatalytic nitrogen reduction. Further, deposited SV-1T-MoS_2 not only magnifies the catalytic efficiency of CdS but also protects CdS from photocorrosion which is an interesting finding. The S-vacancy in the SV-1T-MoS_2-CdS composite is responsible for effective charge carrier separation and activation of adsorbed N_2 molecule. The presence of vacancy in the prepared sample was examined by the author XPS and EPR analysis whereas the lifetime of the charge carrier is monitored by TRPL and steady-state PL spectra [144].

The prepared p-n heterojunction based photocatalytic system (TiO_2/$ZnFe_2O_4$) by Wu et al. integrating p-type $ZnFe_2O_4$ and n-type mesoporous TiO_2 sphere through a solvothermal-calcination procedure endows improved N_2 photofixation ability compared to few reported materials and the neat combining entity. The mesoporous structure of TiO_2 and intimate contact between TiO_2 and $ZnFe_2O_4$ resulting in Z-scheme-oriented p-n composite (MT/ZFO) is due to the varying calcination temperature. The obtained binary hybrid (MT/ZFO) at 400 °C shows an optimum ammonia generation velocity of 1.48 μmol L^{-1} min^{-1} in the ambient atmosphere and sustains the same rate up to 600 min justifying the extraordinary photostability of the material. The high negative reduction potential value of ZFO conduction band electrons in the composite hastens the N_2 reduction to NH_3 under 250 W Xe lamp illuminations. Further, the observed impressive catalytic performance of the p-n hybrid corresponds to restricted electron-hole recombination via the proposed mediator free all-solid-state Z-scheme type charge shuttling mechanism and mesoporous framework [145]. To realize sustainable N_2 fixation under mild condition, Jin and team prepared a p-n heterojunction based photocatalyst (Bi_2MoO_6/OV-BiOBr) by solution-phase method, in which Bi_2MoO_6 nanorods behaves like n-type semiconductor and oxygen vacancy dense BiOBr nanosheets as p-type material respectively. The generated p-n junction due to proper band alignment at the interface of Bi_2MoO_6 and OV-BiOBr results in wide spectrum utilization and better electron-hole pair separation. Moreover, the hierarchical geometry with controlled oxygen vacancies in the binary hybrid (Bi_2MoO_6/OV-BiOBr) develops large numbers of the active site and electron trapping centers for constructive N_2 adsorption and polarization which later makes the reduction reaction smooth. The synergistic effect of both oxygen vacancy and p-n junction that operates in the composite proves to be very beneficial in increasing the NH_3 generation rate i.e. 90.7 μmol g^{-1} h^{-1} without the assistance of any co-catalyst or hole scavengers [146]. Another heterojunction composite with Ru-Co bimetallic center at the interface was constructed by Liu et al. in which sulfur vacancy induced Ru-CoSx is fused with g-C_3N_4 forming Ru-Vs-CoS/CN photocatalyst (Fig. 16). The designed ternary catalytic specimen shows an eye-catching N_2 photoreduction capacity i.e. 0.438 mmol·g^{-1} h^{-1} of NH_3 with AQY of 1.43 % at 400 nm and solar to the ammonia conversion efficiency of 0.042 % in pure water under-stimulated sunlight. Each N-atom of N_2 is bonded to the bimetallic Ru-Co center of the Ru-CoSx unit in a side-on bridge fashion as both the Ru and Co atoms are the interface of Ru/CoSx are under coordination. Further, because of the asymmetric electron flow from both the metal center to the adsorbed dinitrogen, the N≡N gets polarised and the bond order decreases. Besides, the plasmonic electric-filed-enhancement effect of Ru at the Ru/CoSx surface further widens the visible light absorption ability and facilitates the production of more amounts of energetic photoelectrons. Again, the originated Schottky barrier at the Ru/CoSx interface boost the productive charge separation and transfer from CoSx to Ru. The N-atom attached to Ru end is hydrogenated first as it possesses high electron density compared to Co-atom which results in weakening the triple bond and faster photoreduction N_2 as illustrated by computational calculation [147].

In both the above discussed doped photocatalytic systems the observed enhanced N_2 reduction mainly corresponds to defect formation that supports adsorption, activation, and delay electron-hole pair recombination. A Fascinating investigation was made by Feng et al. where the group developed a $LnCO_3OH$/g-C_3N_4 (Ln-CN, Ln = La, or Pr) heterojunction composite by *in situ* solvothermal method. The partial decomposition of a g-C_3N_4 moiety (known as self-sacrificing) producing carbonate and hydroxyl ion which

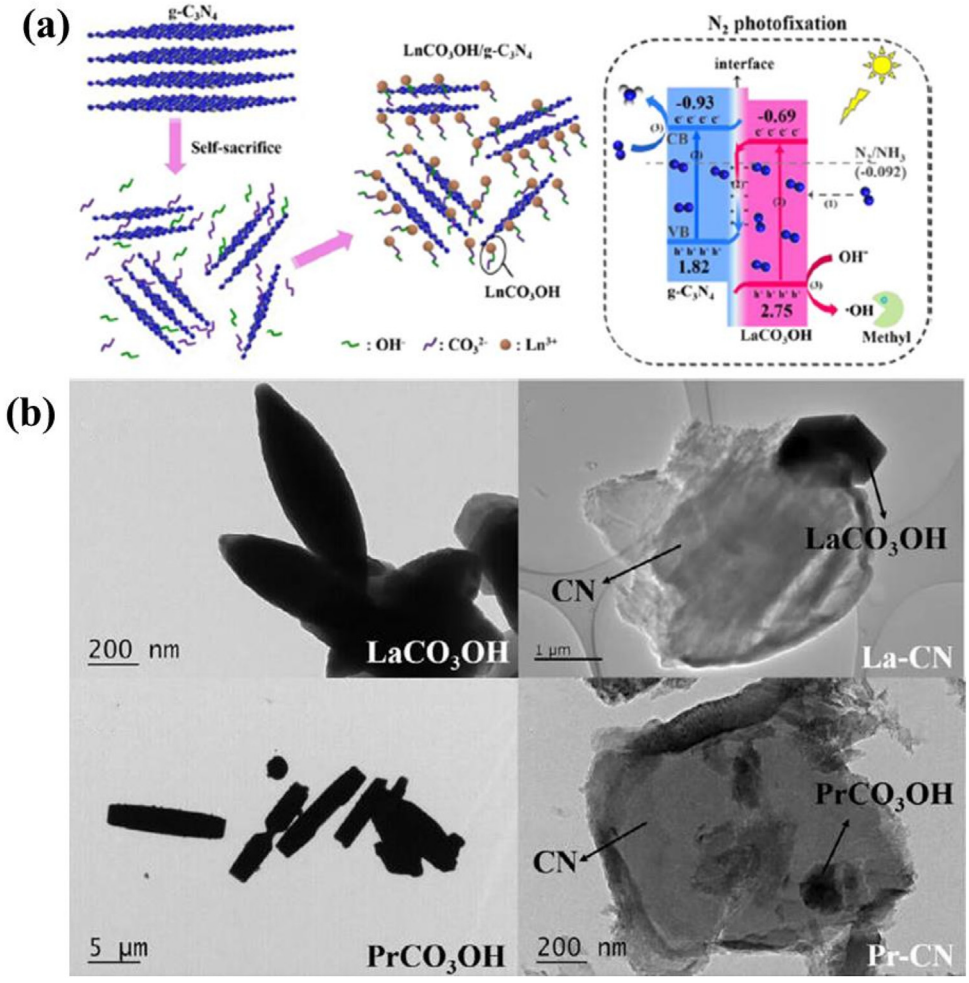

Fig. 17. (a) Schematic representation of synthesis and mechanism of N_2 photofixation, and (b) TEM image of $LnCO_3OH$ (Ln = Pr, La) and corresponding composites with g-C_3N_4(Ln-CN).

further under specific conditions reacts with Ln^{+3} cation generating Ln-CN heterojunction composite. The observed N_2 conversion rate is 8.20 mM g^{-1} h^{-1} and 8.91 mM g^{-1} h^{-1} for La-CN and Pa-CN respectively. The effective charge separation in the composite goes via Z-scheme type charge migration and N_2 is reduced by the photoexcited electrons on the conduction band of g-C_3N_4 (as shown in Fig. 17) [148].

In this context of dinitrogen photoconversion to ammonia over heterojunction based photocatalytic systems, Parida and group have made significant progress by designing promising photocatalytic composites that illustrate the rewarding features of heterojunction chemistry towards successful production of ammonia from dinitrogen under room conduction. In the first attempt, the team fabricated oxygen vacancy induced FeS_2-FeP-CeO_2NS ternary heterojunction based nanocomposite by a combination of hydrothermal and sulfidation–phosphatization technique (Fig. 18 a). This phosphide guarded ternary hybrid (CPS3) exhibits the best ammonia evolution velocity i.e. 5.6 mmol h^{-1} g^{-1} (conversion efficiency = 0.59 %) which is about 8.2 and 10.18 fold higher than CeO_2–FeS_2 and CeO_2–FeP catalyst respectively in acidic medium. At lower pH (acidic), the kinetic energy barrier for N_2 reduction decreases, and the concentration of H^+ ions in the solution increases which fastens the conversion process. Furthermore, the presence of oxygen vacancies/Ce^{+3} and Fe-P facilitate the adsorption and polarization of nitrogen molecules and also assist the effective separation and transfer of excitons to the catalyst surface to carry out the reduction process. Further, the kinetic data suggest that the photofixation reaction proceeds by a two electron-proton couple pathway. Again, the photocatalyst shows incredible stability due to the presence of P-atoms which restricts the photo-oxidation of Fe and sulfur atoms of the nanohybrid as supported by XPS analysis. The presence of Ce^{+3}/OVs and charge separation efficiency is well confirmed by XPS, EPS, and EIS characterization [61]. In the next approach, the group designed a 2D-2D p-n heterojunction composite of p-MoS_2/n-$MgIn_2S_4$ having a marigold flower-like structure by hydrothermal method. The strong interfacial contact between both the 2D components of the p-n monohybrid favors the effective charge carrier separation and transfer to the catalyst surface via the p-n heterojunction for selective reduction of N_2 molecules without forming any energy-intensive intermediates (Fig. 18 b). The optimum NH_3 formation rate over the binary hybrid i.e. 5% MoS_2/MIS shows 0.81 mg/L in absence of hole scavengers and 1.54 mg/L in the methanol/water system takes place through a two-step four-electron multiphoton coupled process. The observed rise in photocatalytic N_2 fixation in the 2D-2D composite is due to a large number of exposed active sites via edge sulfur linkage and productive electron-hole pair separation by the built-in electric field at the junction point or the interfacial contact region. From the performed experiments it was concluded that MoS_2 framed NRR catalytic systems display superior activity in

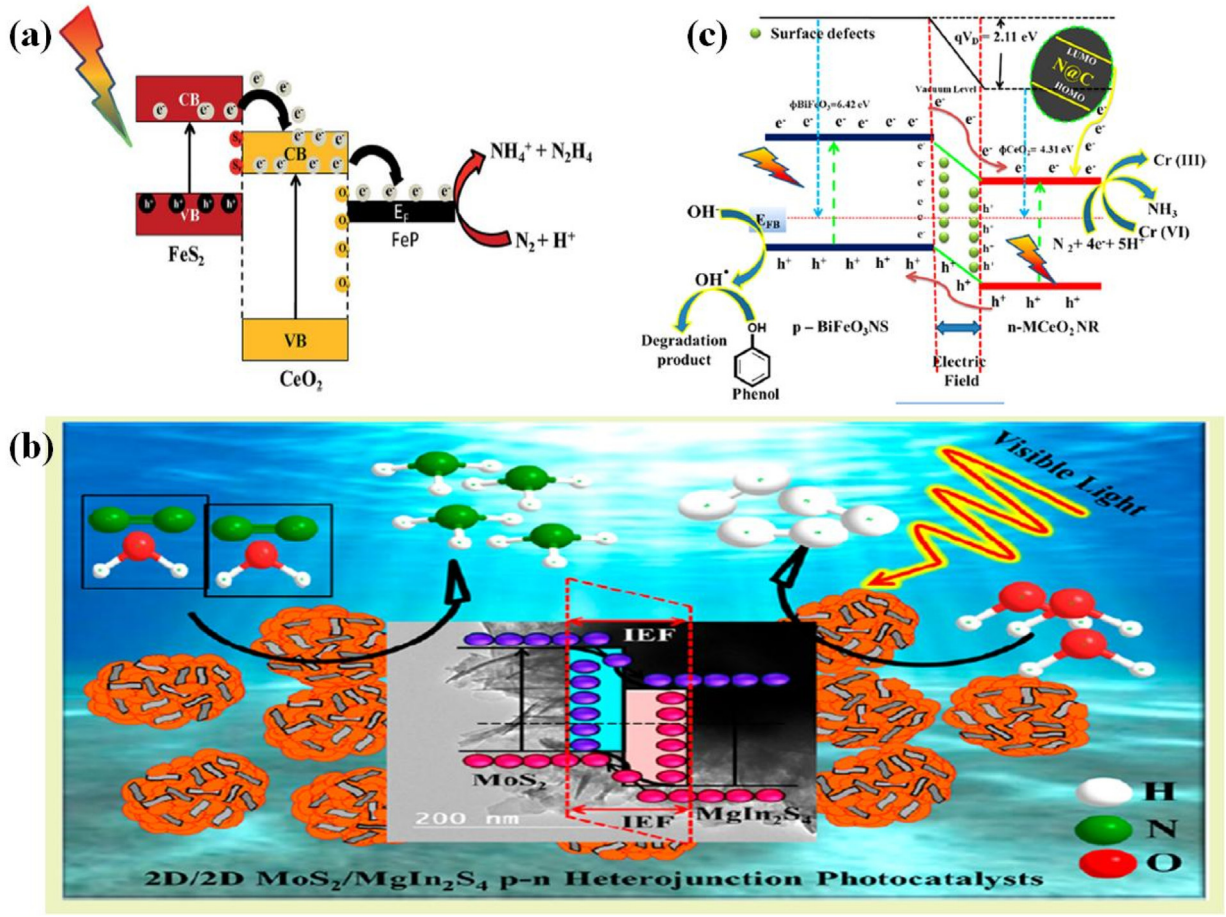

Fig. 18. Represents the photocatalytic N_2 fixation mechanism of (a) FeS_2-FeP-CeO_2NS ternary catalyst. (b) 2D-2D p-MoS_2/n-$MgIn_2S_4$ and (c) carbon sensitized $MCeO_2$–BFO p-n junction.

low acidic and neutral pH conditions because, in strong acidic pH, water reduction reaction subjugates. Further, it was proposed that methanol not just acts as a sacrificial electron donor but also forms -CO_2^* an oxidized product, that accelerated the dinitrogen reduction process. Additionally, the formed p-n heterojunction between p-MoS_2 and n-$MgIn_2S_4$ in the binary hybrid is proved by Mott-Schottky measurements [62]. Further, extending the chemistry of p-n heterojunction, the team designed the third NRR catalytic system i.e. by uniting 1D $BiFeO_3$ nanorod (n-type) with 2D CeO_2 sheet (p-type) via hydrothermal method. Proper band edge alignment resulting p-n heterojunction (Mott-Schottky analysis) along with built-in electric field at the junction region encourages double charge transfer dynamic which leads to better charge separation and the oxygen defect sites help in proper adsorption and activation of supplied nitrogen molecules that finally amplifies the N_2 reduction reaction (Fig. 18 c). The formed defect engineered (Ce^{+3}/OVs) and carbon sensitized $MCeO_2$–BFO p-n junction composite exhibits a high ammonia production rate of 117.77 $\mu mol\ h^{-1}\ g^{-1}$ (apparent conversion efficiency (ACE) = 0.018 %) via a four-electron/five proton-coupled reduction mechanism. XPS and EPR characterization supports defect content however PL, EIS, and Bode phase plot ascertains the slow recombination of charge carriers in the binary hybrid [63]. Yet, we are far behind the set benchmark of NRR catalyst efficiency; hence the group effort or sprit in targeting the most promising photocatalyst for dinitrogen fixation under the ambient condition that can reach the set target is in full swing.

6. Resent reported state of art materials

To relay the progress made in photon-driven dinitrogen reduction, several reports are summarized in Table 1 which demonstrates the constituent of the catalytic system, reaction condition, catalytic efficiency, durability, and light source.

7. Conclusion and perspective

In conclusion, the review summarized the fundamental findings of dinitrogen fixation especially via photocatalysis, explains the detail starting from adsorption of N_2 to activation to reduction i.e. the mechanistic pathway, various followed quantification methods along with the limitation connected with those methods, different catalyst modification techniques alongside the chemistry of those techniques resulting significant improvement in efficiency and lastly recent state of art materials developed towards achieving benchmark NRR activity under operational condition. In brief, the fixation of dinitrogen under ambient environments is a challenging assignment for both fundamental research and industrial applications, as this investigation theme is closely concomitant with energy disaster and environmental catastrophe. Particularly, photocatalytic dinitrogen reduction has evoked prodigious research insight and can be considered as the greener and promising route to surrogate the energy-intensive HB method. Photocatalytic NRR provides some distinct opportunities over the established HB process such as (i) N_2 and H_2O used as basic material for NH_3 synthesis,

which is budget-friendly and surfeit in the environment; (ii) NRR with zero-carbon release can assuage the environmental problems; (iii) requires photons to trigger the fixation reaction and (iv) it can lead a potential way to store clean and renewable energy. However, fixing N_2 in a photocatalytic way is not that easy as thought by the scientific community.

Based on the above-discussed recapitulation on photocatalytic dinitrogen fixation, here we have put forward some related limitation; scientific outlook, and future perspective on how to further beef up the activity of photon driven NRR systems:

(i) Intrinsic inertia or non-polar nature of nitrogen molecules, multi-electron/proton involvement, and weak binding of the molecules over catalysts horizon are some of the connected imperfections of photocatalytic NH_3 synthesis. Additionally, the production of molecular hydrogen and hydrazine is being accompanied by ammonia production which is a diminution aspect, ultimately results in very low NH_3 selectivity and yield. Furthermore, assessing the photocatalytic NRR reactions faces substantial scientific and practical heat. For example, ammonia is present everywhere i.e. in air, experimental consumables, N-atom containing catalyst, and even in human breathe, therefore it is hard to conclude that the quantified ammonia is generated from NRR reactions or stemmed from exogenous contaminations. Again, the capping agents used for catalysts syntheses such as thioacetamide (TAA) and hexamethylenetetramine (HMTA) decomposes easily upon irradiation and hence leads to error in NH_3 detection. Therefore, the indispensable blank/control experiments, e.g. in the $Ar/^{15}N$ streams, are enjoined to certify that the detected NH_3 is produced from the supplied N_2 gas reduction.

(ii) Further, there are several ways for ammonia quantification, out of which spectrophotometric assay, ion-chromatography, ion-selective electrode, and NMR spectroscopic techniques are frequently used. Spectrophotometrically, ammonia is quantified by the use of Nessler's reagents and indo-phenol blue techniques. The pH, ionic strength, and sacrificial agents may interfere with the accuracy of spectrometric quantification of ammonia. Ion-chromatography and NMR technique mostly provides accurate ammonia results.

(iii) Moreover, it is very essential to unveil the fundamental mechanism of molecular nitrogen conversion to ammonia. NRR is a complicated multi-step electron-proton coupled reaction and as a result, the scientific groups from different corners of the globe were unable to predict and explain a proper mechanistic pathway for N_2 photo-reduction, which needs to be uncovering properly. Therefore, a combination of theoretical exploration and experimental data is an authoritative tactic to find out the appropriate underlying mechanism and pathways for NRR. In this topic, prior attention should be given to building models that are nearer to the actual reaction mechanisms.

(iv) For achieving commendable NRR performance there is a need of creating chemical bond channels between nitrogen molecules and the catalyst surface. Hence, there is a necessity to design and develop new technologies for the material synthesis of different compositions and morphologies. It is being believed that morphological oriented nanomaterials have a synergistic effect in enhancing the photocatalytic N_2 fixation. Besides, surface engineering, defect creation, composite formation, crystallographic tailoring, and chemical alternation, and so on are found to be competent strategies for enhancing the N_2 photoreduction. Specifically, a defective photocatalyst exhibits better NRR results compared to that of bulk materials. Similarly, the introduction of dopants and vacancies in the catalysts leads to good NRR activity by increasing the catalyst adsorption and activation ability for inert N_2 resulting in diminishing the N—N triple bond order by electron back donation to the anti-bonding orbital of nitrogen. Another way for enhancing the NRR reaction is the utilization of a co-catalyst. But due to competition between two-electron for HER and six-electron for NRR, the metal and non-metal based co-catalysts are being preferred for N_2 photoreduction over noble metal-rooted co-catalyst. It has been also visualized that a combination of defective co-catalyst and engineered heterojunction could help to magnify the ammonia production rate. Because of the high activity of single metal atoms, designing a heterogeneous single-atom catalyst could be an important aspect of promoting NRR. For example, the Ru-single atom catalyst shows enhanced ammonia yield and selectivity. Furthermore, a single-atom catalyst can be derived from metal-organic frameworks or complexes.

(v) The active sites, reaction intermediates along with interactions with catalysts in NRR, and changes in textural properties on the surface of the catalyst were monitored by advanced characterization techniques such as spherical aberration-corrected transmission electron microscopy (ACTEM), *in-situ* synchrotron radiation (SR) techniques, *in-situ* X-ray photoelectron spectroscopy (XPS), *in-situ* diffuse reflectance Fourier transform infrared spectroscopy (DRFTIRS), and *in-situ* electron paramagnetic resonance spectroscopy (EPR). The more advanced characterization tool such as surface-enhanced infrared spectroscopy (SEIRS) and high-resolution electron energy loss spectroscopy (HREELS) are also being used to gather depth understanding and knowledge of the NRR mechanism.

Although several catalyst modification methods, detection techniques, advanced instrumentation, and computation studies are followed to touch the set NRR efficiency benchmark we are yet to report the best NRR photocatalyst that can replace the traditional HB process, and hence their still exist many possibilities for boosting their dinitrogen photofixation abilities. We hope that all of the above-discussed dinitrogen fixation fundamentals and reported articles own illimitable potential and possibilities, which need to be meticulously studied and cherished. The group also believes that this review will be endowing valuable information to the readers who are quite fascinated by N_2 photofixation reaction, material science, and nanotechnology.

Declaration of Competing Interest

There are no conflicts to declare.

Acknowledgments

The authors are very much obliged to S'O'A (Deemed to be University) management for their support and encouragement.

References

[1] H.P. Jia, E.A. Quadrelli, Mechanistic aspects of dinitrogen cleavage and hydrogenation to produce ammonia in catalysis and organometallic chemistry: relevance of metal hydride bonds and dihydrogen, Chem. Soc. Rev. 43 (2) (2014) 547–564.
[2] X. Xue, R. Chen, C. Yan, P. Zhao, Y. Hu, W. Zhang, S. Yang, Z. Jin, Review on photocatalytic and electrocatalytic artificial nitrogen fixation for ammonia synthesis at mild conditions: advances, challenges and perspectives, Nano Res. (2019) 1229–1249.
[3] V. Rosca, M. Duca, M.T. de Groot, M.T. Koper, Nitrogen cycle electrocatalysis, Chem. Rev. 109 (6) (2009) 2209–2244.
[4] D.E. Canfield, A.N. Glazer, P.G. Falkowski, The evolution and future of Earth's nitrogen cycle, science 330 (6001) (2010) 192–196.
[5] A.E. Shilov, Catalytic reduction of molecular nitrogen in solutions, Russ. Chem. Bull. 52 (12) (2003) 2555–2562.
[6] C.G. Zhan, J.A. Nichols, D.A. Dixon, Ionization potential, electron affinity, electronegativity, hardness, and electron excitation energy: molecular properties from density functional theory orbital energies, J. Phys. Chem. A 107 (20) (2003) 4184–4195.

[7] R. Guan, D. Wang, Y. Zhang, C. Liu, W. Xu, J. Wang, Z. Zhao, M. Feng, Q. Shang, Z. Sun, Enhanced photocatalytic N_2 fixation via defective and fluoride modified TiO_2 surface, Appl. Catal. B (2020) 119580.
[8] B. Thamdrup, New pathways and processes in the global nitrogen cycle, Annu. Rev. Ecol. Evol. Syst. 43 (2012) 407–428.
[9] T.A. Bazhenova, A.E. Shilov, Nitrogen fixation in solution, Coordn. Chem. Rev. 144 (1995) 69–145.
[10] R.F. Service, Liquid sunshine, Science 361 (2018) 120.
[11] K. Wang, D. Smith, Y. Zheng, Electron-driven heterogeneous catalytic synthesis of ammonia: current states and perspective, Carbon Resour. Convers. 1 (1) (2018) 2–31.
[12] L. Shi, Y. Yin, S. Wang, H. Sun, Rational catalyst design for N_2 reduction under ambient conditions: strategies towards enhanced conversion efficiency, ACS Catal. 10 (2020) 6870–6899.
[13] C. Guo, J. Ran, A. Vasileff, S.Z. Qiao, Rational design of electrocatalysts and photo (electro) catalysts for nitrogen reduction to ammonia (NH_3) under ambient conditions, Energy Environ. Sci. 11 (1) (2018) 45–56.
[14] M.J.F. Appl, 1999. NH3 principles and industrial practice. 245, 12.
[15] J. John, D.K. Lee, U. Sim, Photocatalytic and electrocatalytic approaches towards atmospheric nitrogen reduction to ammonia under ambient conditions, Nano Converg. 6 (1) (2019) 15.
[16] B.K. Burgess, D.J. Lowe, Mechanism of molybdenum nitrogenase, Chem. Rev. 96 (7) (1996) 2983–3012.
[17] X. Chen, N. Li, Z. Kong, W.J. Ong, X. Zhao, Photocatalytic fixation of nitrogen to ammonia: state-of-the-art advancements and future prospects, Mater. Horiz. 5 (1) (2018) 9–27.
[18] H. Liu, Ammonia synthesis catalyst 100 years: practice, enlightenment and challenge, Chinese J. Catal. 35 (10) (2014) 1619–1640.
[19] R.F. Service, New Recipe Produces Ammonia From Air, Water, and Sunlight, 2014.
[20] R. Shi, X. Zhang, G.I. Waterhouse, Y. Zhao, T. Zhang, The journey toward low temperature, low pressure catalytic nitrogen fixation, Adv. Energy Mater. 10 (19) (2020) 2000659.
[21] M.H. Vu, M. Sakar, S.A. Hassanzadeh-Tabrizi, T.O. Do, Photo (electro) catalytic nitrogen fixation: problems and possibilities, Adv. Mater. Interfaces 6 (12) (2019) 1900091.
[22] R. Manjunatha, A. Karajić, M. Liu, et al., A review of Composite/Hybrid electrocatalysts and photocatalysts for nitrogen reduction reactions: advanced materials, mechanisms, challenges and perspectives, Electrochem. Energy Rev. 3 (2020) 506–540.
[23] J.W. Erisman, M.A. Sutton, J. Galloway, Z. Klimont, W. Winiwarter, How a century of ammonia synthesis changed the world, Nat. Geosci. 1 (10) (2008) 636–639.
[24] M. Li, H. Huang, J. Low, C. Gao, R. Long, Y. Xiong, Recent progress on electrocatalyst and photocatalyst design for nitrogen reduction, Small Methods 3 (6) (2019) 1800388.
[25] B.M. Hoffman, D. Lukoyanov, Z.Y. Yang, D.R. Dean, L.C. Seefeldt, Mechanism of nitrogen fixation by nitrogenase: the next stage, Chem. Rev. 114 (8) (2014) 4041–4062.
[26] G.N. Schrauzer, T.D. Guth, Photolysis of water and photoreduction of nitrogen on titanium dioxide, J. Am. Chem. Soc. 99 (22) (2002) 7189–7193.
[27] O. Rusina, O. Linnik, A. Eremenko, H. Kisch, Nitrogen photofixation on nanostructured iron titanate films, Chem. Eur. J. 9 (2) (2003) 561–565.
[28] H. Hirakawa, M. Hashimoto, Y. Shiraishi, T. Hirai, Photocatalytic conversion of nitrogen to ammonia with water on surface oxygen vacancies of titanium dioxide, J. Am. Chem. Soc. 139 (31) (2017) 10929–10936.
[29] K.A. Brown, D.F. Harris, M.B. Wilker, A. Rasmussen, N. Khadka, H. Hamby, S. Keable, G. Dukovic, J.W. Peters, L.C. Seefeldt, P.W. King, Light-driven dinitrogen reduction catalyzed by a CdS: nitrogenase MoFe protein biohybrid, Science 352 (6284) (2016) 448–450.
[30] H. Ma, Z. Shi, Q. Li, S. Li, Preparation of graphitic carbon nitride with large specific surface area and outstanding N_2 photofixation ability via a dissolve-regrowth process, J. Phys. Chem. Solids 99 (2016) 51–58.
[31] Y. Cao, S. Hu, F. Li, Z. Fan, J. Bai, G. Lu, Q. Wang, Photofixation of atmospheric nitrogen to ammonia with a novel ternary metal sulfide catalyst under visible light, RSC Adv. 6 (55) (2016) 49862–49867.
[32] C.M. Janet, S. Navaladian, B. Viswanathan, T.K. Varadarajan, R.P. Viswanath, Heterogeneous wet chemical synthesis of superlattice-type hierarchical ZnO architectures for concurrent H_2 production and N_2 reduction, J. Phys. Chem. C 114 (6) (2010) 2622–2632.
[33] H. Miyama, N. Fujii, Y. Nagae, Heterogeneous photocatalytic synthesis of ammonia from water and nitrogen, Chem. Phys. Lett. 74 (3) (1980) 523–524.
[34] S. Bian, M. Wen, J. Wang, N. Yang, P.K. Chu, X.F. Yu, Edge-rich black phosphorus for photocatalytic nitrogen fixation, J. Phys. Chem. Lett. 11 (3) (2020) 1052–1058.
[35] S. Cao, N. Zhou, F. Gao, H. Chen, F. Jiang, All-solid-state Z-scheme 3, 4-dihydroxybenzaldehyde-functionalized Ga_2O_3/graphitic carbon nitride photocatalyst with aromatic rings as electron mediators for visible-light photocatalytic nitrogen fixation, Appl. Catal. B 218 (2017) 600–610.
[36] H. Li, J. Shang, J. Shi, K. Zhao, L. Zhang, Facet-dependent solar ammonia synthesis of BiOCl nanosheets via a proton-assisted electron transfer pathway, Nanoscale 8 (4) (2016) 1986–1993.
[37] S. Sun, X. Li, W. Wang, L. Zhang, X. Sun, Photocatalytic robust solar energy reduction of dinitrogen to ammonia on ultrathin MoS_2, Appl. Catal. B 200 (2017) 323–329.
[38] K. Tennakone, J.M.S. Bandara, C.T.K. Thaminimulla, W.D.W. Jayatilake, U.S. Ketipearachchi, O.A. Ileperuma, M.K.A. Priyadarshana, Photoreduction of dinitrogen to ammonia by ultrafine particles of iron hydroxide oxide (Fe(O)OH) formed by photohydrolysis of iron (II) bicarbonate, Langmuir 7 (10) (1991) 2166–2168.
[39] A. Banerjee, B.D. Yuhas, E.A. Margulies, Y. Zhang, Y. Shim, M.R. Wasielewski, M.G. Kanatzidis, Photochemical nitrogen conversion to ammonia in ambient conditions with FeMoS-chalcogels, J. Am. Chem. Soc. 137 (5) (2015) 2030–2034.
[40] L. Li, Y. Wang, S. Vanka, X. Mu, Z. Mi, C.J. Li, Nitrogen photofixation over III-Nitride nanowires assisted by ruthenium clusters of low atomicity, Angew. Chemie Int. Ed. 56 (30) (2017) 8701–8705.
[41] K. Tennakone, C.T.K. Thaminimulla, W.C.B. Kiridena, Nitrogen photoreduction by coprecipitated hydrous oxides of samarium (III) and vanadium (III), Langmuir 9 (3) (1993) 723–726.
[42] Z. Zhao, S. Hong, C. Yan, C. Choi, Y. Jung, Y. Liu, S. Liu, X. Li, J. Qiu, Z. Sun, Efficient visible-light driven N_2 fixation over two-dimensional Sb/TiO_2 composites, Chem. Commun. 55 (50) (2019) 7171–7174.
[43] C. Xiao, H. Hu, X. Zhang, D.R. MacFarlane, Nanostructured gold/bismutite hybrid heterocatalysts for plasmon-enhanced photosynthesis of ammonia, ACS Sustain. Chem. Eng. 5 (11) (2017) 10858–10863.
[44] Z. Zhao, C. Choi, S. Hong, H. Shen, C. Yan, J. Masa, Y. Jung, J. Qiu, Z. Sun, Surface-engineered oxidized two-dimensional Sb for efficient visible light-driven N_2 fixation, Nano Energy (2020) 105368.
[45] Y. Yang, T. Zhang, Z. Ge, Y. Lu, H. Chang, P. Xiao, R. Zhao, Y. Ma, Y. Chen, Highly enhanced stability and efficiency for atmospheric ammonia photocatalysis by hot electrons from a graphene composite catalyst with Al_2O_3, Carbon 124 (2017) 72–78.
[46] M. Nazemi, M.A. El-Sayed, Plasmon-enhanced photo (electro) chemical nitrogen fixation under ambient conditions using visible light responsive hybrid hollow Au-Ag_2O nanocages, Nano Energy 63 (2019) 103886.
[47] C. Xiao, L. Zhang, K. Wang, H. Wang, Y. Zhou, W. Wang, A new approach to enhance photocatalytic nitrogen fixation performance via phosphate-bridge: a case study of SiW_{12}/K-C_3N_4, Appl. Catal. B 239 (2018) 260–267.
[48] S. Wang, X. Hai, X. Ding, K. Chang, Y. Xiang, X. Meng, Z. Yang, H. Chen, J. Ye, Light-switchable oxygen vacancies in ultrafine Bi_5O_7Br nanotubes for boosting solar-driven nitrogen fixation in pure water, Adv. Mater. 29 (31) (2017) 1701774.
[49] H. Li, J. Shang, Z. Ai, L. Zhang, Efficient visible light nitrogen fixation with BiOBr nanosheets of oxygen vacancies on the exposed {001} facets, J. Am. Chem. Soc. 137 (19) (2015) 6393–6399.
[50] N. Zhang, A. Jalil, D. Wu, S. Chen, Y. Liu, C. Gao, W. Ye, Z. Qi, H. Ju, C. Wang, X. Wu, Refining defect states in $W_{18}O_{49}$ by Mo doping: a strategy for tuning N_2 activation towards solar-driven nitrogen fixation, J. Am. Chem. Soc. 140 (30) (2018) 9434–9443.
[51] X. Li, W. Wang, D. Jiang, S. Sun, L. Zhang, X. Sun, Efficient solar-driven nitrogen fixation over carbon-tungstic-acid hybrids, Chemistry: a European Journal. 22 (39) (2016) 13819–13822.
[52] S. Sun, Q. An, W. Wang, L. Zhang, J. Liu, W.A. Goddard III, Efficient photocatalytic reduction of dinitrogen to ammonia on bismuth monoxide quantum dots, J. Mater. Chem. A 5 (1) (2017) 201–209.
[53] Q. Liu, L. Ai, J. Jiang, MXene-derived TiO_2@C/gC_3N_4 heterojunctions for highly efficient nitrogen photofixation, J. Mater. Chem. A 6 (9) (2018) 4102–4110.
[54] K. Hoshino, R. Kuchii, T. Ogawa, Dinitrogen photofixation properties of different titanium oxides in conducting polymer/titanium oxide hybrid systems, Appl. Catal. B 79 (1) (2008) 81–88.
[55] Y. Zhao, Y. Zhao, G.I. Waterhouse, L. Zheng, X. Cao, F. Teng, L.Z. Wu, C.H. Tung, D. O'Hare, T. Zhang, Layered-double-hydroxide nanosheets as efficient visible-light-driven photocatalysts for dinitrogen fixation, Adv. Mater. 29 (42) (2017) 1703828.
[56] L. Ye, C. Han, Z. Ma, Y. Leng, J. Li, X. Ji, D. Bi, H. Xie, Z. Huang, Ni_2P loading on $Cd_{0.5}Zn_{0.5}S$ solid solution for exceptional photocatalytic nitrogen fixation under visible light, Chem. Eng. J. 307 (2017) 311–318.
[57] J. Yang, Y. Guo, R. Jiang, F. Qin, H. Zhang, W. Lu, J. Wang, J.C. Yu, High-efficiency "working-in-tandem" nitrogen photofixation achieved by assembling plasmonic gold nanocrystals on ultrathin titania nanosheets, J. Am. Chem. Soc. 140 (27) (2018) 8497–8508.
[58] T. Hou, R. Guo, L. Chen, Y. Xie, J. Guo, W. Zhang, X. Zheng, W. Zhu, X. Tan, L. Wang, Atomic-level insights in tuning defective structures for nitrogen photofixation over amorphous SmOCl nanosheets, Nano Energy 65 (2019) 104003.
[59] K.T. Ranjit, T.K. Varadarajan, B. Viswanathan, Photocatalytic reduction of dinitrogen to ammonia over noble-metal-loaded TiO_2, J. Photochem. Photobiol. A: Chem. 96 (1-3) (1996) 181–185.
[60] N.N. Rao, S. Dube, P. Natarajan, Photocatalytic reduction of nitrogen over (Fe, Ru or Os)/TiO_2 catalysts, Appl. Catal. B 5 (1-2) (1994) 33–42.
[61] S. Sultana, S. Mansingh, K.M. Parida, Phosphide protected FeS_2 anchored oxygen defect oriented CeO_2 NS based ternary hybrid for electrocatalytic and photocatalytic N_2 reduction to NH_3, J. Mater. Chem. A 7 (15) (2019) 9145–9153.
[62] G. Swain, S. Sultana, K. Parida, Constructing a novel surfactant-free MoS_2 nanosheet modified $MgIn_2S_4$ marigold microflower: an efficient visible-light driven 2D-2D p-n heterojunction photocatalyst toward HER and pH regulated NRR, ACS Sustain. Chem. Eng. 8 (12) (2020) 4848–4862.

[63] S. Mansingh, S. Sultana, R. Acharya, M.K. Ghosh, K.M. Parida, Efficient photon conversion via double charge dynamics CeO_2–$BiFeO_3$ p–n heterojunction photocatalyst promising toward N_2 fixation and phenol–Cr (VI) detoxification, Inorg. Chem. 59 (6) (2020) 3856–3873.
[64] S. Mansingh, K.K. Das, A. Behera, S. Subudhi, S. Sultana, K. Parida, Bandgap engineering via boron and sulphur doped carbon modified anatase TiO2: a visible light stimulated photocatalyst for photo-fixation of N2 and TCH degradation, Nanoscale Advances 2 (5) (2020) 2004–2017.
[65] C.F. Fu, X. Wu, J. Yang, Material design for photocatalytic water splitting from a theoretical perspective, Adv. Mater. 30 (48) (2018) 1802106.
[66] Y. Zhao, S. Zhang, R. Shi, G.I. Waterhouse, J. Tang, T. Zhang, Two-dimensional photocatalyst design: a critical review of recent experimental and computational advances, Mater. Today 34 (2020) 78–91.
[67] L.M. Duman, W.S. Farrell, P.Y. Zavalij, L.R. Sita, Steric switching from photochemical to thermal reaction pathways for enhanced efficiency in metal-mediated nitrogen fixation, J. Am. Chem. Soc. 138 (45) (2016) 14856–14859.
[68] X. Cui, C. Tang, Q. Zhang, A review of electrocatalytic reduction of dinitrogen to ammonia under ambient conditions, Adv. Energy Mater. 8 (22) (2018) 1800369.
[69] L.M. Azofra, N. Li, D.R. MacFarlane, C. Sun, Promising prospects for 2D d2–d4 M_3C_2 transition metal carbides (MXenes) in N_2 capture and conversion into ammonia, Energy Environ. Sci. 9 (8) (2016) 2545–2549.
[70] G. Ertl, Primary steps in catalytic synthesis of ammonia, J. Vac. Sci. Technol. A Vac. Surf. Films 1 (2) (1983) 1247–1253.
[71] C.D. Zeinalipour-Yazdi, J.S. Hargreaves, C.R.A. Catlow, DFT-D3 study of molecular N_2 and H_2 activation on Co_3Mo_3N surfaces, J. Phys. Chem. C 120 (38) (2016) 21390–21398.
[72] Y. Abghoui, A.L. Garden, J.G. Howalt, T. Vegge, E. Skúlason, Electroreduction of N2 to ammonia at ambient conditions on mononitrides of Zr, Nb, Cr, and V: a DFT guide for experiments, ACS Catal. 6 (2) (2016) 635–646.
[73] Y. Yao, S. Zhu, H. Wang, H. Li, M. Shao, A spectroscopic study on the nitrogen electrochemical reduction reaction on gold and platinum surfaces, J. Am. Chem. Soc. 140 (4) (2018) 1496–1501.
[74] H. Jiang, C. Zang, Y. Zhang, W. Wang, C. Yang, B. Sun, Y. Shen, F. Bian, 2D MXene-derived Nb_2O_5/C/Nb_2C/g-C_3N_4 heterojunctions for efficient nitrogen photofixation, Catal. Sci. Technol. 2020 (10) (2020) 5964–5972.
[75] J. Soria, J.C. Conesa, V. Augugliaro, L. Palmisano, M. Schiavello, A. Sclafani, Dinitrogen photoreduction to ammonia over titanium dioxide powders doped with ferric ions, J. Phys. Chem. 95 (1) (1991) 274–282.
[76] S. Bourgeois, D. Diakite, M. Perdereau, A study of TiO_2 powders as a support for the photochemical synthesis of ammonia, React. Solids 6 (1) (1988) 95–104.
[77] P.P. Radford, C.G. Francis, Photoreduction of nitrogen by metal doped titanium dioxide powders: a novel use for metal vapour techniques, J. Chem. Soc. Chem. Commun. 24 (1983) 1520–1521.
[78] W. Zhao, J. Zhang, X. Zhu, M. Zhang, J. Tang, M. Tan, Y. Wang, Enhanced nitrogen photofixation on Fe-doped TiO_2 with highly exposed (1 0 1) facets in the presence of ethanol as scavenger, Appl. Catal. B 144 (2014) 468–477.
[79] D. Zhu, L. Zhang, R.E. Ruther, R.J. Hamers, Photo-illuminated diamond as a solid-state source of solvated electrons in water for nitrogen reduction, Nat. Mater. 12 (9) (2013) 836–841.
[80] J.A. Bandy, D. Zhu, R.J. Hamers, Photocatalytic reduction of nitrogen to ammonia on diamond thin films grown on metallic substrates, Diam. Relat. Mater. 64 (2016) 34–41.
[81] J.R. Christianson, D. Zhu, R.J. Hamers, J.R. Schmidt, Mechanism of N_2 reduction to NH_3 by aqueous solvated electrons, J. Phys. Chem. B 118 (1) (2014) 195–203.
[82] A.R. Singh, B.A. Rohr, J.A. Schwalbe, M. Cargnello, K. Chan, T.F. Jaramillo, I. Chorkendorff, J.K. Nørskov, Electrochemical Ammonia synthesis-The selectivity challenge, ACS Catal. 7 (1) (2017) 706–709.
[83] K.R. Schubert, H.J. Evans, Hydrogen evolution: a major factor affecting the efficiency of nitrogen fixation in nodulated symbionts, Proc. Natl. Acad. Sci. 73 (4) (1976) 1207–1211.
[84] Y. Liu, M. Cheng, Z. He, B. Gu, C. Xiao, T. Zhou, Z. Guo, J. Liu, H. He, B. Ye, B. Pan, Pothole-rich ultrathin WO3 nanosheets that trigger N≡ N bond activation of nitrogen for direct nitrate photosynthesis, Angew. Chemie Int. Ed. 58 (3) (2019) 731–735.
[85] S.J. Yuan, J.J. Chen, Z.Q. Lin, W.W. Li, G.P. Sheng, H.Q. Yu, Nitrate formation from atmospheric nitrogen and oxygen photocatalysed by nano-sized titanium dioxide, Nat. Commun. 4 (1) (2013) 1–7.
[86] M. Cheng, C. Xiao, Y. Xie, Photocatalytic nitrogen fixation: the role of defects in photocatalysts, J. Mater. Chem. A 7 (34) (2019) 19616–19633.
[87] N. Tong, Y. Wang, Y. Liu, M. Li, Z. Zhang, H. Huang, T. Sun, J. Yang, F. Li, X. Wang, PdSn/NiO/$NaTaO_3$: La for photocatalytic ammonia synthesis by reduction of NO_3^- with formic acid in aqueous solution, J. Catal. 361 (2018) 303–312.
[88] H. Hirakawa, M. Hashimoto, Y. Shiraishi, T. Hirai, Selective nitrate-to-ammonia transformation on surface defects of titanium dioxide photocatalysts, ACS Catal. 7 (5) (2017) 3713–3720.
[89] Y. Zhao, R. Shi, X. Bian, C. Zhou, Y. Zhao, S. Zhang, F. Wu, G.I. Waterhouse, L.Z. Wu, C.H. Tung, T. Zhang, Ammonia detection methods in photocatalytic and electrocatalytic experiments: how to improve the reliability of NH_3 production rates? Adv. Sci. 6 (8) (2019) 1802109.
[90] X. Gao, Y. Wen, D. Qu, L. An, S. Luan, W. Jiang, X. Zong, X. Liu, Z. Sun, Interference effect of alcohol on Nessler's reagent in photocatalytic nitrogen fixation, ACS Sustain. Chem. Eng. 6 (4) (2018) 5342–5348.
[91] A.C. Nielander, J.M. McEnaney, J.A. Schwalbe, J.G. Baker, S.J. Blair, L. Wang, J.G. Pelton, S.Z. Andersen, K. Enemark-Rasmussen, V. Colic, S. Yang, A versatile method for ammonia detection in a range of relevant electrolytes via direct nuclear magnetic resonance techniques, ACS Catal. 9 (7) (2019) 5797–5802.
[92] L.F. Greenlee, J.N. Renner, S.L. Foster, The Use of Controls for Consistent and Accurate Measurements of Electrocatalytic Ammonia Synthesis From Dinitrogen, 2018.
[93] D.L. Boucher, J.A. Davies, J.G. Edwards, A. Mennad, An investigation of the putative photosynthesis of ammonia on iron-doped titania and other metal oxides, J. Photochem. Photobiol. A: Chem. 88 (1) (1995) 53–64.
[94] R. Michalski, Ion chromatography applications in wastewater analysis, Separations 5 (1) (2018) 16.
[95] L. Zhou, C.E. Boyd, Comparison of Nessler, phenate, salicylate and ion selective electrode procedures for determination of total ammonia nitrogen in aquaculture, Aquaculture 450 (2016) 187–193.
[96] X. Gao, Y. Wen, D. Qu, L. An, S. Luan, W. Jiang, X. Zong, X. Liu, Z. Sun, Interference effect of alcohol on Nessler's reagent in photocatalytic nitrogen fixation, ACS Sustain. Chem. Eng. 6 (4) (2018) 5342–5348.
[97] R. Chen, C. Yang, W. Cai, H.Y. Wang, J. Miao, L. Zhang, S. Chen, B. Liu, Use of platinum as the counter electrode to study the activity of non precious metal catalysts for the hydrogen evolution reaction, ACS Energy Lett. 2 (5) (2017) 1070–1075.
[98] S.H. Yuen, A.G. Pollard, Determination of nitrogen in agricultural materials by the nessler reagent. II.—Micro-determinations in Plant Tissue and in Soil Extracts, J. Sci. Food Agric. 5 (8) (1954) 364–369.
[99] A. Le Duy, R. Samson, Testing of an ammonia ion selective electrode for ammonia nitrogen measurement in the methanogenic sludge, Biotechnol. Lett. 4 (5) (1982) 303–306.
[100] C. Mao, J. Wang, Y. Zou, H. Li, G. Zhan, J. Li, J. Zhao, G. Zhan, Anion (O, N, C, and S) vacancies promoted photocatalytic nitrogen fixation, Green Chem. 21 (11) (2019) 2852–2867.
[101] J. Kibsgaard, Z. Chen, B.N. Reinecke, T.F. Jaramillo, Engineering the surface structure of MoS_2 to preferentially expose active edge sites for electrocatalysis, Nat. Mater. 11 (11) (2012) 963–969.
[102] Y. Luo, G.F. Chen, L. Ding, X. Chen, L.X. Ding, H. Wang, Efficient electrocatalytic N_2 fixation with MXene under ambient conditions, Joule 3 (1) (2019) 279–289.
[103] H. Zhang, G. Liu, L. Shi, J. Ye, Single-atom catalysts: emerging multifunctional materials in heterogeneous catalysis, Adv. Energy Mater. 8 (1) (2018) 1701343.
[104] Y. Wang, Y.J. Tang, K. Zhou, Self-adjusting activity induced by intrinsic reaction intermediate in Fe–N–C single-atom catalysts, J. Am. Chem. Soc. 141 (36) (2019) 14115–14119.
[105] W. Zhao, L. Zhang, Q. Luo, Z. Hu, W. Zhang, S. Smith, J. Yang, Single Mo1 (Cr1) atom on nitrogen-doped graphene enables highly selective electroreduction of nitrogen into ammonia, ACS Catal. 9 (4) (2019) 3419–3425.
[106] K. Zhou, Y. Li, Catalysis based on nanocrystals with well-defined facets, Angew. Chemie Int. Ed. 51 (3) (2012) 602–613.
[107] J. Jiang, K. Zhao, X. Xiao, L. Zhang, Synthesis and facet-dependent photoreactivity of BiOCl single-crystalline nanosheets, J. Am. Chem. Soc. 134 (10) (2012) 4473–4476.
[108] X. Huang, Z. Zhao, J. Fan, Y. Tan, N. Zheng, Amine-assisted synthesis of concave polyhedral platinum nanocrystals having {411} high-index facets, J. Am. Chem. Soc. 133 (13) (2011) 4718–4721.
[109] W. Zhu, S. Kattel, F. Jiao, J.G. Chen, Shape-controlled CO_2 electrochemical reduction on nanosized Pd hydride cubes and octahedra, Adv. Energy Mater. 9 (9) (2019) 1802840.
[110] S.L. Foster, S.I.P. Bakovic, R.D. Duda, S. Maheshwari, R.D. Milton, S.D. Minteer, M.J. Janik, J.N. Renner, L.F. Greenlee, Catalysts for nitrogen reduction to ammonia, Nat. Catal. 1 (7) (2018) 490–500.
[111] J. Ran, J. Zhang, J. Yu, M. Jaroniec, S.Z. Qiao, Earth-abundant cocatalysts for semiconductor-based photocatalytic water splitting, Chem. Soc. Rev. 43 (22) (2014) 7787–7812.
[112] M. Liu, Y. Chen, J. Su, J. Shi, X. Wang, L. Guo, Photocatalytic hydrogen production using twinned nanocrystals and an unanchored NiSx co-catalyst, Nat. Energy 1 (11) (2016) 1–8.
[113] Y. Xie, T.T. Wang, X.H. Liu, K. Zou, W.Q. Deng, Capture and conversion of CO_2 at ambient conditions by a conjugated microporous polymer, Nat. Commun. 4 (1) (2013) 1–7.
[114] Y. Ohko, T. Tatsuma, T. Fujii, K. Naoi, C. Niwa, Y. Kubota, A. Fujishima, Multicolour photochromism of TiO2 films loaded with silver nanoparticles, Nat. Mater. 2 (1) (2003) 29–31.
[115] J.S. Steckel, J.P. Zimmer, S. Coe-Sullivan, N.E. Stott, V. Bulović, M.G. Bawendi, Blue luminescence from (CdS) ZnS core–shell nanocrystals, Angew. Chemie 116 (16) (2004) 2206–2210.
[116] C. Li, T. Wang, Z.J. Zhao, W. Yang, J.F. Li, A. Li, Z. Yang, G.A. Ozin, J. Gong, Promoted fixation of molecular nitrogen with surface oxygen vacancies on plasmon-enhanced TiO_2 photoelectrodes, Angew. Chemie Int. Ed. 57 (19) (2018) 5278–5282.
[117] G. Zhang, X. Yang, C. He, P. Zhang, H. Mi, Constructing a tunable defect structure in TiO_2 for photocatalytic nitrogen fixation, J. Mater. Chem. A 8 (1) (2020) 334–341.

[118] J. Wang, W. Lin, Y. Ran, J. Cui, L. Wang, X. Yu, Y. Zhang, Nanotubular TiO2 with remedied defects for photocatalytic nitrogen fixation, J. Phys. Chem. C 124 (2) (2019) 1253–1259.
[119] Y. Shiraishi, M. Hashimoto, K. Chishiro, K. Moriyama, S. Tanaka, T. Hirai, Photocatalytic dinitrogen fixation with water on bismuth oxychloride in chloride solutions for solar-to-Chemical energy conversion, J. Am. Chem. Soc. 142 (16) (2020) 7574–7583.
[120] Z. He, Y. Wang, X. Dong, N. Zheng, H. Ma, X. Zhang, Indium sulfide nanotubes with sulfur vacancies as an efficient photocatalyst for nitrogen fixation, RSC Adv. 9 (38) (2019) 21646–21652.
[121] X. Li, X. Sun, L. Zhang, S. Sun, W. Wang, Efficient photocatalytic fixation of N_2 by KOH-treated g C_3N_4, J. Mater. Chem. A 6 (7) (2018) 3005–3011.
[122] S. Zhang, Y. Zhao, R. Shi, C. Zhou, G.I. Waterhouse, L.Z. Wu, C.H. Tung, T. Zhang, Efficient Photocatalytic Nitrogen Fixation over Cuδ+-Modified Defective ZnAl-Layered Double Hydroxide Nanosheets, Adv. Energy Mater. 10 (8) (2020) 1901973.
[123] T. Huang, S. Pan, L. Shi, A. Yu, X. Wang, Y. Fu, Hollow porous prismatic graphitic carbon nitride with nitrogen vacancies and oxygen doping: a high-performance visible light-driven catalyst for nitrogen fixation, Nanoscale 12 (3) (2020) 1833–1841.
[124] C. Liang, H.Y. Niu, H. Guo, C.G. Niu, D.W. Huang, Y.Y. Yang, H.Y. Liu, B.B. Shao, H.P. Feng, Insight into photocatalytic nitrogen fixation on graphitic carbon nitride: defect-dopant strategy of nitrogen defect and boron dopant, Chem. Eng. J. 396 (2020) 125395.
[125] Y. Liu, Z. Hu, J.C. Yu, Fe enhanced visible-light-Driven nitrogen fixation on BiOBr nanosheets, Chem. Mater. 32 (4) (2020) 1488–1494.
[126] Z. Ying, S. Chen, T. Peng, R. Li, J. Zhang, Fabrication of an Fe-Doped $SrTiO_3$ photocatalyst with enhanced dinitrogen photofixation performance, Eur. J. Inorg. Chem. 2019 (16) (2019) 2182–2192.
[127] N. Zhang, L. Li, Q. Shao, T. Zhu, X. Huang, X. Xiao, Fe-doped BiOCl nanosheets with light-switchable oxygen vacancies for photocatalytic nitrogen fixation, Acs Appl. Energy Mater. 2 (12) (2019) 8394–8398.
[128] P. Li, Z. Zhou, Q. Wang, M. Guo, S. Chen, J. Low, R. Long, W. Liu, P. Ding, Y. Wu, Y. Xiong, Visible-light-Driven nitrogen fixation catalyzed by Bi_5O_7Br nanostructures: enhanced performance by oxygen vacancies, J. Am. Chem. Soc. 142 (28) (2020) 12430–12439.
[129] C. Zhang, Y. Xu, C. Lv, L. Bai, J. Liao, Y. Zhai, H. Zhang, G. Chen, Amorphous engineered cerium oxides photocatalyst for efficient nitrogen fixation, Appl. Catal. B 264 (2020) 118416.
[130] Y. Kong, C. Lv, C. Zhang, G. Chen, Cyano group modified g-C_3N_4: molten salt method achievement and promoted photocatalytic nitrogen fixation activity, Appl. Surf. Sci. (2020) 146009.
[131] H. Huang, X.S. Wang, D. Philo, F. Ichihara, H. Song, Y. Li, D. Li, T. Qiu, S. Wang, J. Ye, Toward visible-light-assisted photocatalytic nitrogen fixation: a titanium metal organic framework with functionalized ligands, Appl. Catal. B 267 (2020) 118686.
[132] J. Li, P. Liu, Y. Tang, H. Huang, H. Cui, D. Mei, C. Zhong, Single-atom Pt–N3 sites on the stable covalent triazine framework nanosheets for photocatalytic N_2 fixation, ACS Catal. 10 (4) (2020) 2431–2442.
[133] W. Chen, X.H. Li, P. He, T. Wang, X.W. Zhang, Y.G. Li, New applications of old inorganic oxygen clusters: keggin-type polyoxometalates PMo12-XVX (X=0, 1, 2, 3, 8) based ZIF-67 for enhanced photocatalytic nitrogen fixation, ChemSusChem 13 (10) (2020) 2769–2778.
[134] J. Wang, C. Hua, X. Dong, Y. Wang, N. Zheng, Synthesis of plasmonic bismuth metal deposited InVO4 nanosheets for enhancing solar light-driven photocatalytic nitrogen fixation, Sustain. Energy Fuels 4 (4) (2020) 1855–1862.
[135] S. Chang, X. Xu, Au nanocrystals decorated TiO_2 nanotubes for photocatalytic nitrogen fixation into ammonia, Inorg. Chem. Front. 7 (3) (2020) 620–624.
[136] T. Hou, L. Chen, Y. Xin, W. Zhu, C. Zhang, W. Zhang, S. Liang, L. Wang, Porous CuFe for plasmon-assisted N_2 photofixation, ACS Energy Lett. 5 (7) (2020) 2444–2451.
[137] C. Hu, X. Chen, J. Jin, Y. Han, S. Chen, H. Ju, J. Cai, Y. Qiu, C. Gao, C. Wang, Z. Qi, Surface plasmon enabling nitrogen fixation in pure water through a dissociative mechanism under mild conditions, J. Am. Chem. Soc. 141 (19) (2019) 7807–7814.
[138] P. Xing, S. Wu, Y. Chen, P. Chen, X. Hu, H. Lin, L. Zhao, Y. He, New application and excellent performance of Ag/$KNbO_3$ nanocomposite in photocatalytic NH3 synthesis, ACS Sustain. Chem. Eng. 7 (14) (2019) 12408–12418.
[139] P. Xing, W. Zhang, L. Chen, X. Dai, J. Zhang, L. Zhao, Y. He, Preparation of a NiO/KNbO3 nanocomposite via a photodeposition method and its superior performance in photocatalytic N_2 fixation, Sustain. Energy Fuels 4 (3) (2020) 1112–1117.
[140] C. Xiao, H. Wang, L. Zhang, S. Sun, W. Wang, Enhanced photocatalytic nitrogen fixation on MoO_2/BiOCl composite, ChemCatChem 11 (24) (2019) 6467–6472.
[141] L. Lin, Q. Zhu, A. Cheng, L. Ma, Efficient solar-driven nitrogen fixation over an elemental phosphorus photocatalyst, Catal. Sci. Technol. 10 (12) (2020) 4119–4125.
[142] Y. Chen, C. Zhao, S. Ma, P. Xing, X. Hu, Y. Wu, Y. He, Fabrication of a Z-scheme AgBr/$Bi_4O_5Br_2$ nanocomposite and its high efficiency in photocatalytic N_2 fixation and dye degradation, Inorg. Chem. Front. 6 (11) (2019) 3083–3092.
[143] J. Liu, R. Li, X. Zu, X. Zhang, Y. Wang, Y. Wang, C. Fan, Photocatalytic conversion of nitrogen to ammonia with water on triphase interfaces of hydrophilic-hydrophobic composite $Bi_4O_5Br_2$/ZIF-8, Chem. Eng. J. 371 (2019) 796–803.
[144] B. Sun, Z. Liang, Y. Qian, X. Xu, Y. Han, J. Tian, Sulfur vacancy-rich O-doped 1T-MoS_2 nanosheets for exceptional photocatalytic nitrogen fixation over CdS, ACS Appl. Mater. Interfaces 12 (6) (2020) 7257–7269.
[145] X. Rong, H. Chen, J. Rong, X. Zhang, J. Wei, S. Liu, X. Zhou, J. Xu, F. Qiu, Z. Wu, An all-solid-state Z-scheme TiO_2/$ZnFe_2O_4$ photocatalytic system for the N_2 photofixation enhancement, Chem. Eng. J. 371 (2019) 286–293.
[146] X. Xue, R. Chen, C. Yan, Y. Hu, W. Zhang, S. Yang, L. Ma, G. Zhu, Z. Jin, Efficient photocatalytic nitrogen fixation under ambient conditions enabled by the heterojunctions of n-type Bi_2MoO_6 and oxygen-vacancy-rich p-type BiOBr, Nanoscale 11 (21) (2019) 10439–10445.
[147] J. Yuan, X. Yi, Y. Tang, M. Liu, C. Liu, Efficient photocatalytic nitrogen fixation: enhanced polarization, activation, and cleavage by asymmetrical Electron donation to N≡ N bond, Adv. Funct. Mater. 30 (4) (2020) 1906983.
[148] X. Feng, H. Chen, F. Jiang, X. Wang, In-situ self-sacrificial fabrication of lanthanide hydroxycarbonates/graphitic carbon nitride heterojunctions: nitrogen photofixation under simulated solar light irradiation, Chem. Eng. J. 347 (2018) 849–859.
[149] Q. Wu, G. Zhou, T. Li, J. Guo, L. Liu, Spatiotemporal Coupling Dual-photocatalytic Integration in Atomic-hybridized $Co_{0.5}Fe_{0.5}In_2S_4$ Nanoflowers for High Efficiency Nitrogen Reduction, 2020, http://dx.doi.org/10.21203/rs.3.rs-41091/v1.
[150] Y. Zhao, L. Zheng, R. Shi, S. Zhang, X. Bian, F. Wu, X. Cao, G.I. Waterhouse, T. Zhang, Alkali etching of layered double hydroxide nanosheets for enhanced photocatalytic N_2 reduction to NH_3, Adv. Energy Mater. (2020) 2002199.
[151] R. Han, S. Chang, X. Xu, Gold nanocrystal anchored In_2O_3 hollow nanospheres for N_2 photofixation to ammonia, Inorg. Chem. Front. 7 (15) (2020) 2778–2782.
[152] A. Abulizi, H. Maimaitizi, D. Talifu, Y. Tursun, In situ synthesis of hierarchical nitrogen-doped MoS_2 microsphere with an excellent visible light-driven photocatalytic nitrogen fixation ability, Funct. Mater. Lett. 13 (05) (2020) 2051031.
[153] E. Vesali-Kermani, A. Habibi-Yangjeh, H. Diarmand-Khalilabad, S. Ghosh, Nitrogen photofixation ability of g-C_3N_4 nanosheets/Bi_2MoO_6 heterojunction photocatalyst under visible-light illumination, J. Colloid Interface Sci. 563 (2020) 81–91.
[154] C. Xu, P. Qiu, L. Li, H. Chen, F. Jiang, X. Wang, Bismuth subcarbonate with designer defects for broad-spectrum photocatalytic nitrogen fixation, ACS Appl. Mater. Interfaces 10 (30) (2018) 25321–25328.
[155] Z.K. Shen, Y.J. Yuan, P. Wang, W. Bai, L. Pei, S. Wu, Z.T. Yu, Z. Zou, Few-layer black phosphorus nanosheets: a metal-free cocatalyst for photocatalytic nitrogen fixation, ACS Appl. Mater. Interfaces 12 (15) (2020) 17343–17352.
[156] Y. Guo, J. Yang, D. Wu, H. Bai, Z. Yang, J. Wang, B.C. Yang, Au nanoparticle-embedded, nitrogen-deficient hollow mesoporous carbon nitride spheres for nitrogen photofixation, J. Mater. Chem. A Mater. Energy Sustain. 8 (32) (2020) 16218–16231.
[157] Y. Liao, J. Qian, G. Xie, Q. Han, W. Dang, Y. Wang, L. Lv, S. Zhao, L. Luo, W. Zhang, H.Y. Jiang, 2D-layered Ti_3C_2 MXenes for promoted synthesis of NH_3 on P25 photocatalysts, Appl. Catal. B (2020) 119054.
[158] H. Li, S. Gu, Z. Sun, F. Guo, Y. Xie, B. Tao, X. He, W. Zhang, H. Chang, In-built bionic “MoFe-cofactor” in Fe-doped two-dimensional $MoTe_2$ nanosheets for boosting the photocatalytic nitrogen reduction performance, J. Mater. Chem. A Mater. Energy Sustain. 8 (2020) 13038–13048.
[159] W. Wang, H. Zhou, Y. Liu, S. Zhang, Y. Zhang, G. Wang, H. Zhang, H. Zhao, Formation of B-N- C coordination to stabilize the exposed active nitrogen atoms in g-C_3N_4 for dramatically enhanced photocatalytic Ammonia synthesis performance, Small 16 (13) (2020) 1906880.
[160] B. Liu, J. Qin, H. Yang, X. Hu, W. Zhao, Z. Zhang, MoS_2 nano-flowers stacked by ultrathin sheets coupling with oxygen self-doped porous biochar for efficient photocatalytic N_2 fixation, ChemCatChem (2020), http://dx.doi.org/10.1002/cctc.202000992.
[161] C. Zhang, Y. Xu, C. Lv, X. Zhou, Y. Wang, W. Xing, Q. Meng, Y. Kong, G. Chen, Mimicking π backdonation in Ce-MOFs for solar-driven Ammonia synthesis, ACS Appl. Mater. Interfaces 11 (33) (2019) 29917–29923.
[162] H. Wu, X. Li, Y. Cheng, Y. Xiao, R. Li, Q. Wu, H. Lin, J. Xu, G. Wang, C. Lin, X. Chen, Plasmon-driven N_2 photofixation in pure water over MoO_{3-x} nanosheets under visible to NIR excitation, J. Mater. Chem. A 8 (5) (2020) 2827–2835.
[163] T. Hou, H. Peng, Y. Xin, S. Wang, W. Zhu, L. Chen, Y. Yao, W. Zhang, S. Liang, L. Wang, Fe single-atom catalyst for visible-light-Driven photofixation of nitrogen sensitized by Triphenylphosphine and sodium iodide, ACS Catal. 10 (10) (2020) 5502–5510.
[164] X. Rong, S. Liu, M. Xie, Z. Liu, Z. Wu, X. Zhou, X. Qiu, J. Wei, N_2 photofixation by Z-scheme single-layer g-C_3N_4/$ZnFe_2O_4$for cleaner ammonia production, Mater. Res. Bull. 127 (2020) 110853.
[165] Y. Wang, R. Zhao, F. Wang, Y. Liu, X. Yu, L. Chen, Y. Yao, S. Lu, X. Liao, Ultralow-temperature synthesis of small Ag doped carbon nitride for the Nitrogen photofixation, Catal. Sci. Technol. (2020), http://dx.doi.org/10.1039/D0CY01532F.